Asymptotic and Adaptive Approaches to Thin Body Problems in Elasticity

Otso Ovaskainen

Helsinki University of Technology
Institute of Mathematics
Research Reports A399

October 1998

ASYMPTOTIC AND ADAPTIVE APPROACHES TO THIN BODY PROBLEMS IN ELASTICITY

Otso Ovaskainen

Helsinki University of Technology
Institute of Mathematics
Research Reports A399

Dissertation for the degree of Doctor of Technology to be presented with due permission for public examination and depate in Auditorium D at Helsinki University of Technology (Espoo, Finland) on the 12th of November, 1998, at 12 o'clock noon.

Acknowledgments

This thesis is based on the work done at the Institute of Mathematics at Helsinki University of Technology. I want to express my gratitude to Professor Juhani Pitkäranta, the supervisor of this work, for introducing me to the subject and for his collaboration and constructive support. I also want to thank my colleagues at the Institute of Mathematics for their support.

I thank Professor Juha Paavola and Professor Rolf Stenberg for reviewing the manuscript and for their invaluable comments and criticism.

Espoo, October 1998

Otso Ovaskainen

Espoo, Finland
1998

Otso Ovaskainen: Asymptotic and Adaptive Approaches to Thin Body Problems in Elasticity, Helsinki University of Technology, Institute of Mathematics, Research Reports A399 (1998).

Abstract. *The thesis considers various themes related to numerical analysis of thin bodies. On one hand we discuss topics related to dimension reduction and asymptotics, on the other hand adaptive approaches including a posteriori error estimation. In addition to the discussion on more general level, we discuss in more detail two special domains, the elastic strip and the cylindrical shell. For these domains we also give numerical results illustrating the theorems derived in the thesis.*

AMS Subject Classification. 73C02, 73C20, 73K15

Key words and phrases: linear elasticity, shells, finite elements, adaptivity

ISBN 951-22-4263-X
ISSN 0784-3143
Libella Painopalvelu Oy, Espoo 1998

Institute of Mathematics
Helsinki University of Technology
P.O.Box 1100
FIN-02015 HUT, Finland
E-mail: math@hut.fi

Publications

The thesis consists of the following four papers.

[I] PITKÄRANTA, J., LEINO, Y., OVASKAINEN, O. AND PIILA, J., *Shell Deformation States and the Finite Element Method: A Benchmark Study of Cylindrical Shells*, Comp. Meth. in Appl. Mech. and Engrg. 128 (1995) 81-121.

[II] OVASKAINEN, O. AND PITKÄRANTA, J., *An Energy Method Approach to the Problem of Elastic Strip*, Preprint Helsinki University of Technology, Research Reports A328 (1994). To appear in SIAM Journal on Applied Mathematics.

[III] OVASKAINEN, O. AND PITKÄRANTA, J., *An h-p-n Adaptive Finite Element Scheme for Shell Problems*, Advances in Engrg. Software, 26 No. 3 (1996), 201-208.

[IV] OVASKAINEN, O. *Local A Posteriori Error Estimation on Thin Domains of Linear Elasticity: Theory and an Example*, Preprint Helsinki University of Technology, Research Reports A375 (1997). Submitted to M^3AS.

In [I], the author is responsible primarily for Chapter 6 (and the related Appendix). In [II] and [III], the author carried out the main part of the calculations involved in the analysis.

1 Introduction

The special class of geometries consisting of beams, arches, plates and shells is of major importance in the theory of elasticity. A characteristic feature of such problems is that at least one dimension of the body is small with respect to the others, i.e. the body is thin. This property makes the character of the problem essentially different and often more difficult than in thick body cases. In the thesis we study how the thickness property affects several aspects in analyzing elasticity problems.

The papers [I] and [II] are devoted to the study of two closely related topics: asymptotics and dimension reduction. In [III] and [IV] we study themes more straightly related to numerical solving of elasticity problems: adaptivity and a posteriori error estimation.

The main problem in asymptotics is to find the behavior of the deformation field as the thickness of the body tends to zero with the problem otherwise fixed. On the other hand, the idea of dimension reduction is to transform the original n dimensional problem into a simpler $n-1$ dimensional one in such a way that the solution to the new problem approximates the solution to the original problem with reasonable accuracy.

Before the last few decades dimensional reduction was seen mainly as a theoretical tool. The ultimate goal was typically to obtain analytic solutions, e.g. as Fourier expansions, in special cases. The classical plate and shell models served then as simpler models than the original 3D for such purposes. More recently, the development of computers has changed the point of view from asymptotic analysis to the direction of numerical analysis. One is no more so interested in getting analytic solutions for some special cases but rather in developing methods for effective and accurate solution of larger groups of problems. This is also reflected in the role of asymptotic analysis. In addition to the direct information it gives about the behavior of thin bodies, it may also be utilized e.g. as a tool for deriving estimates for the dimension reduction error. Such estimates are important especially when tracing and balancing various error components in the overall numerical approximation models. Typically these models are based on further finite element approximation within dimension reduction models.

The principal idea of adaptivity in numerical modelling is to first solve a problem with some initial set of degrees of freedom and then to use the solution itself to give information where to add d.o.f:s in order to most effectively improve the accuracy. A posteriori error estimation is then used in the adaptive procedure to indicate whether the current solution has achieved the desired level of accuracy.

The literature on adaptive finite element methods is wide, but so far little attention has been devoted to the design and to the actual behavior of adaptive algorithms for thin-domain elastic problems. We take some initial steps in this direction in the thesis.

2 Outline of the Work

In the thesis we consider linear elasticity on thin bodies. The body is assumed to occupy a domain $\Omega \subset \mathbf{R}^n$, where $n = 2, 3$, and Ω is given (in some coordinate system) as $\Omega = \omega \times (-h/2, h/2)$. Here ω represents the midsurface of the body and t the thickness of the body, which is assumed to be small as compared to the dimensions of ω.

The main emphasis is given to the study of two special problems, namely to the problem $\mathcal{P}_s$ of elastic strip (papers [II] and [IV]) and to the problem $\mathcal{P}_c$ of cylindrical shell (papers [I] and [III]). The domains Ω_s and Ω_c in these problems are given as

$$\begin{aligned} \Omega_s &= \{(x, z) | -H < x < H, -h/2 < z < h/2\}, \\ \Omega_c &= \{(x, \alpha, z) | -H < x < H, 0 \leq \alpha < 2\pi, -h/2 < z < h/2\}, \end{aligned}$$

where the former one is given in a cartesian and the latter one in a cylindrical coordinate system. The domains Ω_s and Ω_c are illustrated in Figures 1 and 2.

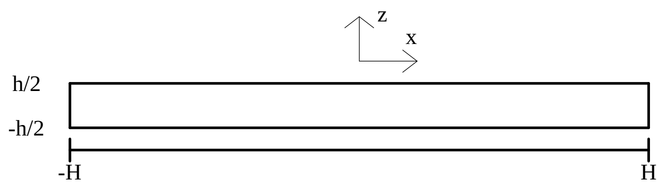

Figure 1: The domain Ω_s of elastic strip

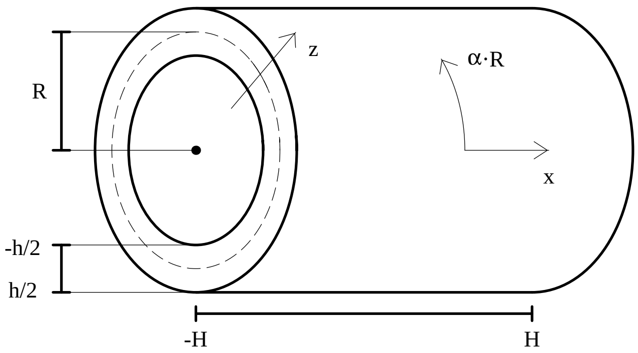

Figure 2: The domain Ω_c of cylindrical shell

In problem $\mathcal{P}_s$ we assume an external load f acting on the long sides of the strip ($z = \pm h/2$), and in addition any legal combination of stress and displacement boundary conditions at the ends of the strip ($x = \pm H$). In problem $\mathcal{P}_c$ we assume an external load of the form $f = P(x)\cos k\alpha$ acting on the outer surface of the shell ($z = h/2$) and three different kinds of kinematical boundary conditions at the ends of the shell ($x = \pm H$): clamped ends, free ends and weakly supported ends (referred to as simple sliding support). The trigonometrical distribution of the load f in the α-direction may be interpreted as to considering one Fourier-component of the load at a time. Due to this assumption, the shape of the solution in the α-direction may be solved explicitly and the problem is thus reduced to a two dimensional one in the (x, z)-space, k appearing in the problem only as a parameter.

In what follows, we will use dimensionless variables choosing $R = H$ for the length unit. The thickness h will thus be scaled to the dimensionless relative thickness t by the formula $t = h/H$.

The problem of linear elasticity may be formulated in the following form. Find a displacement field $\underline{U} = \{U_i\}_{i=1}^{n}$ that satisfies the given kinematical constraints and the variational formulation

$$\mathcal{A}(\underline{U}, \underline{V}) = \mathcal{Q}(\underline{V}) \quad \forall \underline{V} \in \mathcal{V}.$$

The bilinear form $\mathcal{A}$ represents the virtual work due to the deformation of the body, the linear form $\mathcal{Q}$ is the external load potential, and $\mathcal{V}$ is the energy space associated to the problem.

Many of the results in the thesis are given with respect to the energy norm $|||\cdot|||$, defined as $|||\cdot||| = \{\mathcal{A}(\cdot,\cdot)\}^{1/2}$. By standard linear elasticity theory we have for any $\underline{U} \in \mathcal{V}$

$$c\,||\underline{U}||_1 \leq |||\underline{U}||| \leq C\,||\underline{U}||_1,$$

where c, C are positive constants and $||\cdot||_1$ denotes the standard H^1-norm over Ω. However, unlike in more standard (thick body) elliptic problems, where we would have $c \sim C \sim 1$, we have typically $C \sim 1$ and $c = c(t) \sim t$, so the parametric dependence on the energy norm is severely non-uniform when t is small.

2.1 Dimension Reduction and Asymptotics

In [I] we study different shell models for the cylindrical shell Ω_c in some benchmark cases. The models studied are (1) the *K-model*, the most commonly used classical model, often named after Koiter, (2) the *R-model*, a variant of the classical model similar to the Reissner-Mindlin model for plate bending, (3) the quadratic model, (4) the cubic model and (5) the quartic model. Here the last three models are based on a polynomial Ansatz of a given degree in the "thin" direction within the original $3D$ energy formulation. In [II] we call these *n-models* (n=degree, here $n = 2, 3$ or 4).

In [I], Chapter 6, which is the part of the paper the author is mainly responsible for, the behavior of the K- and R-models is studied analytically as truncated symbolic expansions in terms of the thickness parameter t. This is done by solving the equations for the eigenvalues and eigenvectors by the symbolic calculus program MATHEMATICA. The solutions were found to consist of a smooth part and a boundary layer. In case of the K-model, the boundary layer decays exponentially in a length scale $\sqrt{t}$. In case of the R-model, also a shorter t-scale is present in the solution. Based on the computations, also the gap between the R- and K-models is given as a truncated expansion in terms of the parameter t.

All of the five models above are studied also purely numerically with a high-order finite element method. In addition to the analysis of the displacement and stress fields, we also study how the energy of the solution is distributed among the *membrane* and *bending* energies. In case of clamped boundary, we end up with a membrane dominated deformation, whereas free boundary leads to a bending dominated deformation field. In case of the partly clamped simple sliding support, an intermediate state is found to occur, where neither of the membrane nor bending parts dominates asymptotically. In this case, unlike in the others, the energy is concentrated asymptotically in the boundary layer.

From the numerical solutions the gaps between various model pairs in the range $0.001 \leq t \leq 0.1$ is estimated. The measure is chosen to be the relative energy norm

$$d(A,B) = |||\underline{U}^A - \underline{U}^B|||/|||\underline{U}^K|||,$$

where $\underline{U}^X$ is the displacement field corresponding to model X. The gap between models A and B was found to behave roughly as $\sim ct^\alpha$, where the coefficient c depends on (A,B) but the exponent α is more or less the same for all model pairs in a given problem.

In [II] we analyze the asymptotics of the elastic strip and derive estimates for the dimension reduction error of the so called *n-models*, which are based on n:th degree polynomial expansion of the displacement field in the z-coordinate and on the straightforward use of the energy principle.

In case of elastic strip, it is possible to split the load and the boundary conditions by simple symmetry considerations in such a way that the membrane and bending states are analyzed separately. The asymptotics for the two states are very different from each other, which is also reflected in the results obtained for the gaps between the various models. In addition to analyzing the membrane and bending parts separately, we also split the analysis for technical reasons into the following two steps.

1. We first change the boundary conditions of the original problem so that they correspond to the asymptotic behavior of the displacement field caused by the external load f. For this altered problem an asymptotic expansion of the solution is computed (again with MATHEMATICA). The expansion is given in terms of the thickness parameter t, the load f and some material parameters. The asymptotic expansion gives direct information about the behavior of the solution for small t, but we use it here mainly as a tool to conclude that the error (in the problem with modified boundary conditions) between the $2D$- and the n-models measured in the relative energy norm behaves as [II, Theorem 3.1]

$$C(n,f) \cdot \begin{cases} \min\{1, t^{n-1}\} & \text{(Bending case)}, \\ t^n & \text{(Membrane case)}. \end{cases}$$

2. In Step 2 we consider the problem that is left, namely the problem where the external load is zero and the boundary conditions are obtained by superposition of the original ones and the changed ones given in Step 1. Here we show that the result depends essentially on the type of the boundary conditions (displacement type, stress type, mixed type). The results are given separately for the membrane and bending cases and for each combination of the boundary conditions [II, Theorem 4.2].

2.2 A Posteriori Error Estimation and Adaptivity

In [III] we propose an $h-p-n$ adaptive FE-scheme and test its performance with the cylindrical shell problem $\mathcal{P}_c$. In the scheme, adaptivity relates to three parameters, h referring to the refinement of the mesh, p to the order of the FE-space, and n to the degree of the dimension reduction model. The main idea of the algorithm is to adaptively capture and resolve the various length scales that may occur in shells, as shown in [I].

Three kinds of indicators are used for guiding the adaptive process. These are called T (Take), D (Drop) and S (Split). Take indicates the expected best degrees of freedom that should be added to the FE space to improve the accuracy, whereas Drop shows those degrees of freedom which may be dropped out without losing in accuracy too much. Split indicates whether it pays off to split a subdomain and lower the order of the local FE-space in such a way that the total number of d.o.f:s remains approximately the same. All of the indicators are based on a simple derivation of geometric nature. Let us denote the current FE-space by $\mathcal{U}^{FE}$ and the corresponding solution by $\underline{U}^{FE}$. We consider at the same time the possibility to drop L^d degrees of freedom from $\mathcal{U}^{FE}$ and to add L^t new d.o.f:s into the space. Let us denote this new FE space by $\tilde{\mathcal{U}}^{FE}$ and the corresponding solution by $\tilde{\underline{U}}^{FE}$. In III we show that the indicators D and T may be defined in such a way that they can be computed locally with the work of inverting an $L^t \times L^t$ matrix and so that

$$|||\underline{U}^{3D} - \tilde{\underline{U}}^{FE}||| \leq |||\underline{U}^{3D} - \underline{U}^{FE}|||^2 + D^2 - T^2. \tag{2.1}$$

The Split indicator is defined as $S = D^2 - T^2$, with the d.o.f.:s to be dropped out from the old space and taken into the new space chosen so that they correspond to splitting the subdomain and lowering it's degree in the desired way. Based on (2.1), the indicators may be interpreted as reliable though not necessarily sharp bounds for the increase or decrease in accuracy if the old FE system is replaced by the new one. The sharpness of the bounds is discussed in the later paper [IV] in the context of a posteriori error estimation. Utilizing the three indicators, an adaptive scheme for finding and resolving the different length scales in the cylindrical shell problem is proposed. In the numerical examples the performance of the algorithm is tested both when applied as a full $h-p-n$ -procedure and as a $h-p$ procedure with the model order n limited to the values $n = 1, 2, 3$.

In [IV], a posteriori error estimation based on energy and complementary energy principles is analyzed. These two well-known principles may be formulated in an abstract Hilbert space setting as follows. Let us be given two Hilbert spaces, the "displacement" space $\mathcal{U}$ and the "stress" space $\mathbf{\Sigma}$ with inner products $(\cdot,\cdot)_U$ and $(\cdot,\cdot)_\Sigma$, where

$$(u_1, u_2)_U = (Su_1, Su_2)_\Sigma$$

and $S : \mathcal{U} \to \mathbf{\Sigma}$ is a linear injection. Let there also be given a bounded linear mapping $L : \mathcal{U} \to \mathbf{R}$, and let $u \in \mathcal{U}$ be such that

$$(u, v)_U = L\ v \ \ \forall \ \ v \in \mathcal{U}.$$

Let $\mathcal{U}^1$ be a subspace of $\mathcal{U}$. Our aim is to derive a posteriori error estimates for $||u - u^1||_U$, where $u^1 \in \mathcal{U}^1$ satisfies

$$(u^1, v)_U = L\ v \ \ \forall \ \ v \in \mathcal{U}^1.$$

Thus u^1 is the orthogonal projection of u onto $\mathcal{U}^1$. Let $\mathcal{U}^0 \subset \mathcal{U}^1$ (possibly $\mathcal{U}^0 = \mathcal{U}^1$) be another subspace of $\mathcal{U}$, let $\mathcal{U}^2$ be a 'residual' subspace such that

$$\mathcal{U} = \mathcal{U}^0 \oplus \mathcal{U}^2,$$

and let $u^2 \in \mathcal{U}^2$ be such that

$$(u^2, v)_U = L\ v - (u^1, v)_U \ \ \forall \ \ v \in \mathcal{U}^2.$$

Then u^2 is the projection of $u - u^1$ onto $\mathcal{U}^2$. Let us further define the angle between the spaces $\mathcal{U}^0$ and $\mathcal{U}^2$ as

$$c = \sup_{v^0 \in \mathcal{U}^0, v^2 \in \mathcal{U}^2} \frac{(v^0, v^2)_U}{||v^0||_U\ ||v^2||_U} \quad \text{and} \quad K = \frac{1}{1 - c^2}.$$

and the space of statically admissible stresses as

$$\mathbf{\Sigma}_{SA} = \{\sigma \in \mathbf{\Sigma} \mid (\sigma, Sv)_\Sigma = Lv \ \ \forall v \in \mathcal{U}\}.$$

After these preliminaries from [IV], we have by the energy principle [IV, Theorem 2.1] that

$$||u^2||_U^2 \leq ||u - u^1||_U^2 \leq K||u^2||_U^2$$

and by the complementary energy principle [IV, Corollary 2.1] that

$$||u - u^1||_U^2 \leq ||\sigma||_\Sigma^2 - ||u^1||_U^2$$

for any $\sigma \in \mathbf{\Sigma}_{SA}$.

In case of elasticity and finite element analysis, $\mathcal{U}^1$ represents the FE-space and $\mathcal{U}$ the total space with respect to which the error estimate is to be derived. Since in real applications we have to limit to finite computations, the reference space $\mathcal{U}$ will in practice be some bigger finite dimensional space than $\mathcal{U}^1$. Spaces $\mathcal{U}^0$ and $\mathcal{U}^2$ then represent a splitting of $\mathcal{U}$ to global and local degrees of freedom in a suitable way. In [IV] we discuss some possibilities in choosing the spaces $\mathcal{U}^0$ and $\mathcal{U}^2$. We also discuss the utilization of the complementary energy principle in the elasticity context and give a general procedure for the construction of the statically admissible stress field needed in the principle.

The main emphasis in the analysis in [IV] is then given on the study of efficiency of the energy principle applied to thin body elasticity, in particular to the problem $\mathcal{P}_s$ of elastic strip. In other words, we study how the constant K representing the gap between the lower and upper error estimates behaves with respect to the thickness parameter t. As a negative result we first show that if $\mathcal{U}^0$ is taken to be the space of piecewise linear functions in the x-direction, and $\mathcal{U}^2$ the space completing $\mathcal{U}^0$ to the full $2D$-model, the constant K will not be finite even for constant values of t [IV, Theorem 4.1]. Next we restrict $\mathcal{U}$ to the simplest possible 'thin' elastic problem, the 1-dimensional Timoshenko beam problem with clamped boundary, and obtain [IV, Theorem 4.2] $K = \mathcal{O}(1 + (h/t)^2)$, where h refers to the length of a subinterval. Going then up in the model hierarchy, we restrict the axially piecewise linear space $\mathcal{U}^0$ as $\mathcal{U}^0 \subset \mathcal{U}^{2D,2}$. Letting $\mathcal{U}$ be still the full 2D-space $\mathcal{U} = \mathcal{U}^{2D}$, we obtain [IV, Theorem 4.3]

$$K = \begin{cases} \mathcal{O}(1 + \frac{h}{t}) & \text{in the membrane case,} \\ \mathcal{O}(1 + \frac{h^2}{t^2}) & \text{in the bending case.} \end{cases}$$

The proof of this theorem utilizes the complementary energy principle. In the practical case where $\mathcal{U} \subset \mathcal{U}^{2D,2}$ and $\mathcal{U}$ is finite dimensional, we further show that in the membrane case K is then independent of t and h [IV, Theorem 4.4]. In the bending case this holds only if the axial order of $\mathcal{U}^0$ is raised properly [IV, Theorem 4.5].

Shell Deformation States and the Finite Element Method: A Benchmark Study of Cylindrical Shells

J. Pitkäranta, Y. Leino, O. Ovaskainen and J. Piila

Helsinki University of Technology, Institute of Mathematics,
P.O. Box 1000, 02015 HUT, Finland

Abstract. We demonstrate some of the basic mathematical characteristics of shell deformation states and shell models from the point of view of finite element approximation. As benchmark cases, we analyze in detail three simple cylindrical shell problems. These problems are seemingly similar but turn out to be quite different. We (1) compute the exact displacement and strain fields in the model problems both numerically and symbolically using two variants of classical shell models, (2) for comparison, compute numerically the displacements and strains corresponding to certain higher-order dimension reduction models derived from the energy principle, (3) demonstrate the dissimilarity of the three benchmark problems as to their asymptotic behaviour in the limit of zero thickness and (4) show, both theoretically and experimentally, how this diversity is reflected in the accuracy of standard finite element approximations of both low and high order.

Subject classification. (AMS) 73C02, 73K15

1 Introduction

In this work we analyze the deformation and stress fields of certain cylindrical shells loaded by a smoothly varying, self-balancing, axially non-symmetric pressure distribution. We use various shell models for a linearly elastic, isotropic material, and we apply both numerical methods (FEM) and symbolic calculus (MATHEMATICA) in computing the deformation and stress fields essentially exactly. We also test the performance of some straightforward low-order finite element methods in the benchmark cases studied.

The primary purpose of the paper is to contribute to better understanding of the mathematical characteristics of shell deformations from the finite element designer's point of view. The secondary purpose is to give exact reference results that can be used in further benchmark evaluations of finite element algorithms. For recent, closely related mathematical and numerical analyses of shells, the reader is referred to [15], [16], [17], [18], [19], [20], [22], [7].

The present contribution proceeds from the basic assertion that for reliable numerical modelling of shells, better theoretical understanding of shell deformation states and shell models is needed than is currently available. Indeed, we want to demonstrate that in the numerical analysis of shells, there arise fundamental questions of shell theory whereto the classical theory of shells - developed largely before the computer - gives only very insufficient answers. Such computing-related issues of linear shell theory may be condensed essentially to the following three.

Q1: *Shell asymptotics.* Assuming any shell model in a given problem, find the asymptotic behaviour of the deformation field as the thickness of the shell tends to zero with the problem otherwise fixed. Which deformation types dominate asymptotically?

Q2: *Scale resolution and layers.* With the thickness of the shell considered as variable and the problem otherwise fixed, find the asymptotic behaviour of the layers in a thin shell that arise from boundaries and from local irregularities of the load. Which are the relevant characteristic length scales of the layers, and how strong are the corresponding layer components as compared with the smooth part of the displacement/stress fields?

Q3: *Accuracy of shell models.* In a given dimension reduction model, estimate how accurately the scale resolution of the displacement and stress fields as given by the model corresponds to the actual 3D behaviour. How do various variants of the classical lowest-order shell models differ, and in what sense can higher-order models be better?

We discuss the above questions and their numerical connection in more detail in Chapter 2 below. This extended introduction hopefully serves the reader also by making both the motivation and the message of the paper more clear. In the remaining part of the work we consider benchmark problems only. Although these are fairly simple problems, they are general enough so that we can demonstrate many characteristic features of shell problems and shell models.

The plan of the paper is as follows. After giving the overall perspective in Chapter 2, we proceed to introduce the benchmark problems in Chapter 3. In Chapter 4, a brief introduction to the dimension reduction models for shells is given in the benchmark context. In Chapter 5 we introduce the main asymptotic categories of shell problems, as defined in [20], and classify the benchmark problems in this way. Chapter 6 is devoted to the exact deformation and stress fields of the benchmark shells as given by various dimension reduction models. The results of numerical and symbolic computations given here are based on [14]. More complete symbolic expansions are given in the Appendix. Finally in Chapter 7 we test the performance of some standard finite element methods in the benchmark problems. In particular, we study here the connection of numerics to asymptotics as defined in Chapter 5. The results of this chapter are based mainly on [6]. A more complete survey on both low- and high-order methods will be given in a forthcoming paper [8].

2 Questions of Shell Theory That Arise from Finite Element Modelling

Q1: Shell asymptotics

Shells are in marked contrast to plates in their asymptotic behaviour. While, for example, the asymptotic bending behaviour of plates is uniquely described by the well-understood and well-behaving Kirchhoff model, shell asymptotics varies diversely from case to case, often leads to very irregular solutions, and in fact in many cases is not well understood currently. As demonstrated recently in model cases, the asymptotic character of the shell deformation depends strongly on such details of the problem as the geometry of the shell (elliptic / parabolic / hyperbolic), on the kinematical constraints, and even on the type of loading, see [15], [16], [17], [18], [19], [20]. Roughly speaking, the asymptotic states may be classified as either *membrane states*, *inextensional states* (or bending states) and *intermediate states*, depending on which type of deformation - if any - dominates asymptotically in the total deformation energy, see [20] and Chapter 5 below. These main categories, however, contain further subcategories that may depend strongly on the further details of the problem. For example, the asymptotic membrane theory appears very case-dependent, see the references cited.

From the finite element point of view, the understanding of shell asymptotics is important because of the intimate connection of asymptotics and numerics. The finite element models are typically based on more or less straightforward minimization of the total energy of the shell. When the shell is thin as compared with the mesh spacing used, the finite element model then tries to adapt to the asymptotic behaviour of the solution. In case of failure, numerical *locking* (or overstiffness) or some other unexpected and undesired numerical phenomena are observed.

So far the understanding of numerical failure modes such as locking is very limited in shells, a fact related to the lack of understanding shell asymptotics in general. What can be extrapolated from [22], [6], [7], [8] and from the results of the present work (see Chapter 7) is about the following: 1) The most troublesome cases are those leading to inextensional asymptotics. The numerical "conflict" in such cases was in fact observed early by Morley [10], [11]. 2) In other cases it is often possible to predict the overall deformation pattern with reasonable accuracy even with fairly simple and straightforward finite element methods. 3) In searching for more details of the solution, such as local stress maxima, unexpected numerical error amplification may occur in all asymptotic categories.

For a somewhat more precise formulation of the above three statements, see the comments on **Q2** below. Here we note finally that the asserted interplay of asymptotics and numerics is quite well known in the problem of plate bending, where so called *shear locking* is known to occur in the Reissner-Mindlin model. Indeed, all recent finite element formulations that are made free of this locking are based on various "tricks" derived from the asymptotics of the problem, i.e., from the Kirchhoff model, c.f. [1], [2], [21]. From this lesson it appears clear that if "simple and efficient" finite elements for shell problems are to be found, they should likewise be based on the asymptotics of these problems. Unfortunately, shell asymptotics is case-dependent and very different from that of plates, so one cannot expect to find effective shell elements by any simple extrapolation from plate elements.

Q2: Scale resolution and layers

Consider the rather typical case where the shell is loaded by a piecewise smooth distribution of surface traction and, say, some homogeneous kinematical constraints are imposed at the boundary. Then the deformation field of the shell may in general be split into a piecewise (more or less) smooth component plus various layers that decay exponentially, in some characteristic length scale, from certain lines or points. The layer lines include the boundary line, the lines or points where the load is irregular, discontinuous geometry, and in case of parabolic and hyperbolic shells, certain further characteristic lines [17], [19].

In a typical shell problem, the smallest characteristic length that is possible in layers is proportional to the thickness of the shell, and the largest scale (characterizing the smooth component) may usually be taken to be the diameter or some other characteristic dimension of the shell. These two scales, say d and L, are in fact the ones that typically characterize a plate problem. In shells, however, further intermediate scales arise from curvature effects. In particular, the presence of the scale $\sqrt{dL}$, or $\sqrt{t}L$, where $t = d/L$, is known from many analytical studies [3], [9], [24]. We demonstrate this scale also here (see Chapter 6). Not as well known are the longer scales $\sqrt[4]{t}L$ and $\sqrt[3]{t}L$ that may appear in parabolic and hyperbolic shells [17], [19].

We conclude that as compared with plates, the boundary layers of shells are slowly (sometimes extremely slowly) decaying. We should add that the components of the layers that correspond to the mentioned intermediate scales are typically quite strong in their amplitude at practical values of the thickness (see Chapter 6). Accordingly, the smooth component alone (or asymptotic theory) typically gives a rather poor approximation for the deformation of a shell. Again this is somewhat in contrast to plate bending problems where the asymptotic Kirchhoff model is often reasonably accurate. In shell problems, the asymptotic model is usually a meaningful approximation model only if special hypotheses are made on the boundary conditions and on the load so as to supress the layers. The *classical membrane theory* found in most shell books may be seen as such an asymptotic formulation.

In the finite element analysis of shells, the problem of scale resolution is converted into the problem of numerical scale resolution. The finite element method may then be understood as a projection method which is trying to separate the different length scales that appear in the solution. Obviously, this can only be succesful if sufficiently fine meshes are used in regions where the layers have significant amplitudes. Roughly speaking this means that if the smooth component of the solution is captured with mesh spacing h_L, then a local refinement with mesh spacing $h_l \sim (l/L)h_L$ is needed to capture, with the same relative accuracy, a boundary layer component with characteristic length scale l. If locking occurs, however, the situation gets more complicated. In that case substantial *overrefinement* may be needed to achieve the desired accuracy, see Chapters 7, 8 below.

We finally return to the three statements on locking made above (see **Q1**). We can now make these statements somewhat more precise by relating them to scale resolution: 1) In case of inextensional asymptotics, locking occurs already in approximating the dominant, smooth component of the solution. Hence one can immediately "see" the numerical failure. The phenomenon also gets worse as the thickness of the shell tends to zero. 2) In membrane states, locking *does not appear* in the largest length scale (smooth component). In this case the overall accuracy of FEM generally improves asymptotically as the thickness t tends to zero. However, at practical values of t, poor resolution of layers can cause large errors. 3) Weaker or more hidden forms of locking appear as a rule a) in the intermediate deformation states and b) in resolving the intermediate length scales of layers in all asymptotic categories. In case of intermediate asymptotics there may be a considerable numerical coupling in between different length scales, so that, e.g. the poor resolution of layers is reflected as large global errors.

The above statements are largely conjectures based on preliminary analysis of simple model cases, such as the ones studied in this paper (see also [22]). We make these comments here only to point the path that one inevitably has to follow in searching for reliable - possibly adaptive - finite element procedures for shells. One has to accept that this path is rather stony. In order to understand the various numerical failures that can occur, not only the understanding of shell asymptotics is necessary. One should also gain more information on the layer behaviour, i.e., on the full scale resolution of shell deformations.

Q3: Accuracy of shell models

One of the main achievements of classical shell theory is that it gives reasonable dimension reduction models for shells, i.e. models where the original 3D elastic model (taken here as exact) is replaced by an approximate 2D model. Since the 3D model is usually untractable for analytical methods even in simple cases, the current understanding of shell deformations is largely based on further analysis of dimension reduction models. Also finite element computations are usually based on models given by the classical theory.

In the finite element analysis of shells, error bounds for dimension reduction models are needed primarily for balancing the overall approximation error that consists of a modelling error and a numerical approximation error within the model. One would basically need to know how accurately a given model is able to predict the true scale resolution of the 3D displacement field. Compared with such demands, very little theory exists up to now. The modelling error estimates known so far are of global nature, guaranteeing basically only the asymptotic validity of classical shell models, see [15], [16] and the further references therein.

Besides increasing the importance of modelling error analysis, finite elements are leading to somewhat new ways of thinking in the actual derivation of dimension reduction models as well. We note that in the classical theory of plates and shells, dimension reduction models were derived essentially by asymptotic analysis of the differential equations of 3D elasticity. This approach is rather natural if one thinks of further solving the resulting simplified equations by separation of variables, Fourier expansions, etc. In the finite element context, however, a different approach seems more natural: Since the numerical model is anyway based on the energy principle, then why not dimension reduction as well? Indeed, the most commonly used classical shell models may be derived also in this way. They arise as simplifications of the so called *quadratic model* where one assumes a quadratic polynomial expansion of the 3D displacement field in directions normal to the midsurface of the shell, see [15] and Chapter 4 below.

The quadratic shell model itself is closely related to the direct 3D finite element approach where the shell is discretized with one layer of quadratic 3D elements. The same analogy obviously holds as well in the higher order cubic, quartic, etc. models based on polynomial expansions of higher degree. In the design of an optimal (adaptive) numerical model for a shell in such a *hierarchic-model* framework, the basic question then is: How should the order of the model vary in different regions of the shell in an optimal scheme? This question again calls for local error analysis of dimension reduction models.

In the present work we study five different shell models. These are (1) the (most commonly used) classical model, often named after Koiter and given here the name *K-model*, (2) a variant of the classical model similar to the Reissner-

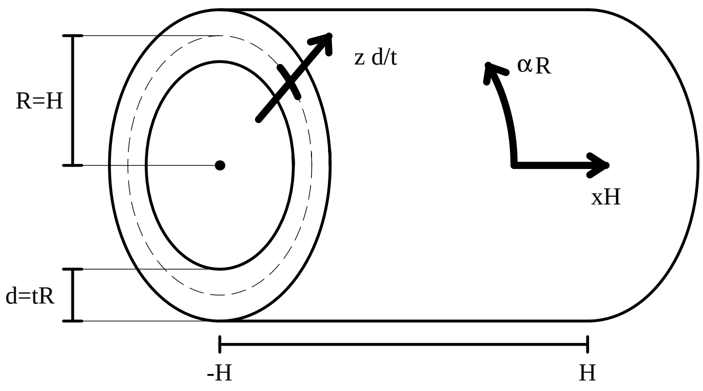

Figure 1: The bechmark shell and the load profile.

Mindlin model for plate bending, here referred to as the *R-model* (sometimes: reduced 3D model), (3) the quadratic model, (4) the cubic model and (5) the quartic model. By comparing the displacement and stress fields given by these models we hope to gain here some insight on the accuracy of the models in representing the actual 3D behaviour, without trying to compute the latter directly.

3 The Benchmark Problems

In all benchmark cases to be studied, we consider a cylindrical shell of half-length H equal to the radius R (as measured to the middle surface) and with varying thickness d (Fig. 1). The shell is assumed to consist of homogeneous isotropic material with Young's modulus E and Poisson's ratio ν. Further, we assume in all cases the shell to be loaded by a normal pressure distribution that acts on the outer surface of the shell, is axially constant and varies angularly as

$$p = P_0 \cos k\alpha \,, \tag{3.1}$$

where k is an integer.

In the computations that follow (Chapters 6 and 7) we choose in fact $\nu = 1/3$ (for the ease of symbolic computations) and $k = 2$ in (3.1), so the load will be unique up to normalization, and self-balancing. Choosing $R = H$ as the length unit, the only parameter that essentially remains to be varied is the dimensionless thickness $t = d/H$.

In order to specify the benchmark problems uniquely, it remains to set the boundary conditions at the ends of the cylinder. It is only at this point where the benchmark problems actually differ. We consider three cases where in each case, the same set of homogeneous kinematical constraints is imposed at both ends of the cylinder.

Case 1. Clamped (built-in) ends: All displacements vanish.

Case 2. Free ends: No kinematical constraints.

Case 3. Simple sliding support at the ends: The radial average of the normal deflection vanishes; no further constraints.

In Case 2 we have to exclude the case $k = 1$ where the load (3.1) is not self-balancing. In the remaining part of the work, we approach the above three problems both analytically and numerically. We are interested especially in the behaviour of thin shells, corresponding to relatively small values of the dimensionless thickness t. In the numerical computations that follow, t will range from 0.1 down to 0.0001. We also study the asymptotics, i.e., the limit behaviour as $t \to 0$. As this analysis will reveal, the three benchmark problems are not as similar as they might superficially look.

4 The Shell Models

In what follows, we use dimensionless variables choosing $R = H$ for the length unit. The dimensionless cylindrical coordinates, x (axial), α (angular), z (radial), are chosen in such a way that the shell occupies in these coordinates the region

$$\Omega = \{(x, \alpha, z) \,|\, -1 < x < 1,\, 0 \le \alpha < 2\pi,\, -t/2 < z < t/2\}.$$

The exact deformation of the shell under the load (3.1) is assumed to obey the laws of 3D linear elasticity. We denote by $\underline{U} = (U_1, U_2, U_3)$ the dimensionless displacement field, obtained by scaling the actual field by R. Due to the special shape of the load (3.1), the displacement field is of the form

$$\underline{U}(x, \alpha, z) = (U(x, z)\cos k\alpha,\ V(x, z)\sin k\alpha,\ W(x, z)\cos k\alpha), \tag{4.1}$$

(dropping the arbitrary rigid body modes in Case 2), so we have in fact a problem in 2D only. The energy of the shell may then be expressed as

$$\begin{aligned}\mathcal{F}(U, V, W) \ &= \ F_0 \left\{ \frac{1}{2} \int_{-1}^{1} \int_{-t/2}^{t/2} \left[\frac{\nu(1-\nu)}{1-2\nu} (\mathrm{tr}\underline{\underline{\epsilon}})^2 + (1-\nu) \sum_{i,j=1}^{3} \epsilon_{ij}^2 \right] \cdot (1+z)\, dx\, dz \right. \\ &\qquad \left. - Q_0 \int_{-1}^{1} W(x, \frac{t}{2}) \cdot \left(1 + \frac{t}{2}\right) dx \right\},\end{aligned}$$

where $F_0 = l\pi ER^3/(1-\nu^2)$ is a scaling factor, with $l = 2$ for $k = 0$ and otherwise $l = 1$, $Q_0 = P_0/E$ is the dimensionless load amplitude, and the strain amplitudes ϵ_{ij} are given by

$$\begin{aligned} \epsilon_{11} &= \frac{\partial U}{\partial x} & \epsilon_{22} &= \frac{1}{r}(kV + W) \\ \epsilon_{12} &= \frac{1}{2}\left(-\frac{k}{r}U + \frac{\partial V}{\partial x}\right) & \epsilon_{23} &= \frac{1}{2}\left(\frac{\partial V}{\partial z} - \frac{1}{r}(V + kW)\right) \\ \epsilon_{13} &= \frac{1}{2}\left(\frac{\partial U}{\partial z} + \frac{\partial W}{\partial x}\right) & \epsilon_{33} &= \frac{\partial W}{\partial z} \end{aligned}$$

where $r = 1 + z$. Below we measure the energy in units of F_0, so we may take $F_0 = 1$.

We now proceed to carry out a further dimension reduction from 2D to 1D following the energy method of [15]. The idea here is simply to assume a polynomial expansion of the displacement amplitudes U, V, W with respect to z and use this as an Ansatz in the energy principle. The simplest expression that leads to the classical shell models is of the form

$$\begin{aligned} U(x,z) &= u(x) - z\theta(x), \\ V(x,z) &= v(x) - z\phi(x), \\ W(x,z) &= w(x) + z\psi_1(x) + \frac{1}{2}z^2\psi_2(x). \end{aligned} \tag{4.2}$$

Here u, v, w play the role of the displacements of the middle surface, θ, ϕ are rotations, and ψ_1, ψ_2 are auxiliary functions that are needed in the process but will be eliminated at the end.

In what follows, we need the *membrane strains* β_{ij} as defined by

$$\beta_{11} = u', \quad \beta_{12} = \frac{1}{2}(-ku + v'), \quad \beta_{22} = kv + w, \tag{4.3a}$$

the changes of curvature κ_{ij}, or *bending strains*, as defined by

$$\kappa_{11} = \theta', \quad \kappa_{12} = \frac{1}{2}(-k\theta + \phi' - v'), \quad \kappa_{22} = k\phi, \tag{4.3b}$$

and the *transverse shear strains*

$$\rho_1 = -\theta + w', \quad \rho_2 = -\phi - kw - v. \tag{4.3c}$$

The curvature components (4.3b) are not completely compatible with the kinematics assumption (4.2). However, the fact that any linear combination of membrane strains can be added to the bending strains, without loosing the accuracy significally, according to Houghton and Johns [4], is utilized. Then, assuming expansion (4.2), the energy of the shell may be rewritten as

$$\begin{aligned}\mathcal{F}(u,v,w,\theta,\phi,\psi_1,\psi_2) &= \mathcal{F}_R(u,v,w,\theta,\phi)\\ &\quad+\frac{(1-\nu)^2}{1-2\nu}\int_{-1}^{1}\left\{\frac{t}{2}\left[\psi_1+\frac{\nu}{1-\nu}(\beta_{11}+\beta_{22})\right]^2\right.\\ &\quad\left.+\frac{t^3}{24}\left[\psi_2+\frac{\nu}{1-\nu}(\kappa_{11}+\kappa_{22})\right]^2\right\}dx+\text{remainder},\end{aligned}$$

where

$$\begin{aligned}\mathcal{F}_R(u,v,w,\theta,\phi) &= \frac{t}{2}\int_{-1}^{1}\left[\nu(\beta_{11}+\beta_{22})^2+(1-\nu)\sum_{i,j=1}^{2}\beta_{ij}^2\right]dx\\ &\quad+\frac{t^3}{24}\int_{-1}^{1}\left[\nu(\kappa_{11}+\kappa_{22})^2+(1-\nu)\sum_{i,j=1}^{2}\kappa_{ij}^2\right]dx\\ &\quad+\frac{1-\nu}{4}t\int_{-1}^{1}(\rho_1^2+\rho_2^2)\,dx-Q_0\int_{-1}^{1}w\,dx\end{aligned}\tag{4.4}$$

Here we have so far only (1) expanded $1/r$ into a power series in z, (2) integrated over z, and (3) rearranged the terms. It can be verified (see [15] for more details) that the remainder in the above splitting is small as compared with the other terms, so it can be neglected (Simplification # 1). Furthermore, disregarding boundary effects, the remaining part of the energy may be minimized with respect to ψ_1 and ψ_2 by setting (Simplification # 2)

$$\psi_1=-\frac{\nu}{1-\nu}(\beta_{11}+\beta_{22}),\quad \psi_2=-\frac{\nu}{1-\nu}(\kappa_{11}+\kappa_{22}).\tag{4.5}$$

What is then left of the energy is the expression $\mathcal{F}_R$ only. We give the resulting shell model the name *R-model.*

We note that the first three terms of $\mathcal{F}_R$ in (4.4) correspond to the portions of deformation energy that arise from membrane, bending, and transverse shear deformations, respectively. One can further simplify the model by eliminating the rotations from the so called Kirchhoff-Love constraints

$$\rho_1=\rho_2=0.\tag{4.6}$$

In the resulting model, the deformation energy then consists of the membrane and bending parts only, and the changes of curvature have the new expressions

$$\kappa_{11}=w'',\quad \kappa_{12}=-kw'-v',\quad \kappa_{22}=-k^2w-kv.\tag{4.3b'}$$

This model is referred to as the *K-model.*

In the theoretical analysis of shells, the K-model (named, e.g. after Koiter [5], Novozhilov [13], etc.) or some close variant to it, is used most often. Instead, the R-model (sometimes named after Naghdi [12]) gives a more natural basis for finite element algorithms, since the energy in this model does not contain second derivatives of the displacement field. The two models are obviously analogous to the Kirchhoff (K) and Reissner-Mindlin (R) models of plate bending. Historically, many formulations have been given for the simplest dimension reduction model for shells. Both the K-model and the R-model studied here are representatives of such a family of models, which could be named vaguely as "The classical shell model". Many variants of the classical model have been given a name, like Flügge's, Vlasov's, Donnell's, etc., but the differences in between these appear to be rather insignificant, c.f. [4] and also the discussion in Chapter 6 below.

In the finite element context, the R-model is often referred to with terms like "Reduced 3D model". A common way of modifying this model is to multiply the transverse shear energy in (4.4) by a "shear correction factor", the value of which is somewhat up to taste. Indeed, the K-model corresponds to choosing this factor to be infinite. Here we will not enter into further modifications of this type, i.e., the R-model is understood in the unique sense as described.

The energy approach assumed above obviously involves various further possibilities of deriving shell models. For example, one could simply assume the Ansatz (4.2) in the energy principle and drop the further simplifications made above. Another approach, more parallel with 3D finite element analysis, is to complete (4.2) into a full quadratic expansion for all displacement components. The resulting model (with no further simplifications) is named *quadratic model*. This might still be considered a variant of "The classical shell model". Instead, the *cubic model*, the *quartic model*, etc., based on higher-order polynomial expansions of each displacement component in (4.2), are "models of higher order" formally. The distinction, however, is based on either asymptotic expansions or approximation theory that relies on rather unrealistic regularity assumptions on the exact 3D displacement field. In more realistic situations where layers are typically strong, the gap between models of different formal order need not be large. We study these questions in the benchmark context in Chapter 6 below.

As a final remark, we note that the displacement fields given by the K- and R-models can be interpreted in a natural way as 3D fields by using the Ansatz (4.2) together with (4.5). The resulting field does not necessarily satisfy the kinematical constraints of the problem - a discrepancy that arises from the simplifications made in deriving the models. Instead, the quadratic, cubic, etc. models are in this sense kinematically consistent with the original problem.

5 Asymptotics

In this chapter we introduce some asymptotic classification rules for shell problems and then apply these rules to the problems of Chapter 3. By asymptotics we mean the limit behaviour of the displacement field as $t \to 0$. For a fixed load, no limit obviously exists, so asymptotics means rather the limit shape of the displacement field. This can be obtained by appropriate (case-dependent) re-scaling during the limit process.

In general, it is expected that any reasonable shell model shares the asymptotics of the actual 3D model (for some rigorous proofs, see [15],[16]), so in classifying shell asymptotics we may as well choose the simplest model at hand, the K-model. To further simplify (and also generalise) the notation, let us express the energy of the shell according to the K-model as

$$\mathcal{F}_K(\underline{u}) = t\, a(\underline{u}, \underline{u}) + t^3\, b(\underline{u}, \underline{u}) - q(\underline{u}), \tag{5.1}$$

where $\underline{u} = (u, v, w)$ denotes the displacement (amplitude) field, a and b are bilinear forms (independent of t) corresponding to membrane and bending deformations, respectively, and $q(\underline{u})$ stands for the external load potential, which takes in the benchmark cases the form

$$q(\underline{u}) = Q_0 \int_{-1}^{1} w\, dx. \tag{5.2}$$

The set of kinematically admissible displacement fields in minimizing (5.1) is denoted by $\mathcal{U}$. In the benchmark cases this is defined as

$$\begin{aligned} \mathcal{U} \;=\; & \{\underline{u} = (u, v, w) \mid u, v \in H^1(-1,1),\ w \in H^2(-1,1); \\ & \underline{u} \text{ satisfies the kinematical constraints at } x = \pm 1\}, \end{aligned}$$

where $H^l(-1,1)$ contains all continuous scalar functions on $[-1,1]$ having square integrable (weak) derivatives of orders $\leq l$. The kinematical constraints in the three cases are

Case 1: $u(\pm 1) = v(\pm 1) = w(\pm 1) = w'(\pm 1) = 0$.

Case 2: No constraints.

Case 3: $w(\pm 1) = 0$.

We will finally need the set of *inextensional* displacements defined by

$$\mathcal{U}_0 = \{\underline{u} \in \mathcal{U} \mid a(\underline{u}, \underline{u}) = 0\}. \tag{5.3}$$

Since $a(\underline{u}, \underline{u}) = 0$ is equivalent to having $\beta_{11}(\underline{u}) = \beta_{12}(\underline{u}) = \beta_{22}(\underline{u}) = 0$, $\mathcal{U}_0$ consists of (kinematically admissible) displacements corresponding to pure bending. This is a rather small set in general. In the benchmark cases, as easily checked from (4.3a), one has

Case 1: $\mathcal{U}_0 = \{0\}$.

Case 2: $\mathcal{U}_0 = \mathcal{U}_0^k =$
$$\begin{cases} \{0\}, \text{ if } k = 0, 1 \\ \{(u, v, w) = (A, kAx + B, -k^2Ax - kB), \ A, B \in \mathbf{R}\}, \text{ if } k \geq 2. \end{cases}$$

Case 3: $\mathcal{U}_0 = \{0\}$.

Here we have eliminated the rigid body motions of the form $(A, B, 0)$ if $k = 0$ and $(A, Ax + B, -Ax - B)$ if $k = 1$ in Case 2. We conclude that inextensional deformations are possible only in Case 2 if $k \geq 2$.

We should comment at this point on the dependence of $\mathcal{U}_0$ on parameter k, set in (3.1) (Case 2). This dependence arises because we have treated the assumed form (4.1) of the displacement field essentially as an a priori *kinematical constraint* of the problem. Dropping this constraint would mean that we take all k-modes of the form (4.1) to be kinematically admissible even if k in (3.1) is fixed. This would not change the solution, but it would change the space $\mathcal{U}_0$ in Case 2 so that all k-modes with amplitudes $(u^k, v^k, w^k) \in \mathcal{U}_0^k$, $k \geq 2$, would be possible. Both of these standpoints are physically (and computationally) possible, so we allow both interpretations in the sequel.

We now come to the classification of shell asymptotics corresponding to the limit $t \to 0$. We give first the general idea of the classification, whereafter a more precise definition follows in Table 1 below.

Recall from (5.1) that the total deformation energy $\mathcal{E}(\underline{u})$ in the K-model consists of 1) the membrane energy $\mathcal{E}_m(\underline{u}) = t\, a(\underline{u}, \underline{u})$, and 2) the bending energy $\mathcal{E}_b(\underline{u}) = t^3\, b(\underline{u}, \underline{u})$. The asymptotic classification is based roughly on checking, which part of the deformation energy dominates asymptotically as $t \to 0$. To this end, denote by $\underline{u}^t$ the exact displacement field in a given problem, where only t can vary. Obviously there are basically three possibilities: either membrane energy, bending energy, or neither dominates asymptotically.

Assume first that for small t, bending energy is negligible, i.e.,

$$\mathcal{E}_b(\underline{u}^t)/\mathcal{E}(\underline{u}^t) \to 0 \quad \text{as } t \to 0. \tag{5.4}$$

Then the problem (or the deformation field) is called *membrane-dominated*, and the corresponding asymptotic deformation state is referred to as the *membrane state*. The asymptotic displacement field is obtained formally by dropping the bending energy, i.e., by minimizing (over some appropriate energy space) the reduced energy

$$\mathcal{F}_m(\underline{u}) = \frac{1}{2} t\, a(\underline{u}, \underline{u}) - q(\underline{u}). \tag{5.5}$$

Assume next that instead of (5.4),

$$\mathcal{E}_m(\underline{u}^t)/\mathcal{E}(\underline{u}^t) \to 0 \text{ as } t \to 0, \tag{5.6}$$

i.e., membrane energy is negligible for small t. Then the problem is called *bending-dominated*, and the asymptotic deformation state is referred to as the *inextensional state*. The asymptotic displacement field is obtained this time by minimizing the reduced energy

$$\mathcal{F}_b(\underline{u}) = \frac{1}{2}\, t^3 b(\underline{u}, \underline{u}) - q(\underline{u}) \tag{5.7}$$

over the space $\mathcal{U}_0$ of inextensional displacements, as defined by (5.3). We note from (5.5) and (5.7) that for a fixed load the asymptotic displacement field scales in the membrane state like $\underline{u}^t \sim t^{-1}$, whereas in the inextensional state it scales like $\underline{u}^t \sim t^{-3}$. Hence, bending-dominated shells are relatively "sensitive".

Finally we have to cover the "remainder" where neither (5.4) nor (5.6) is true. Indeed, there exist such states as well, and we call them *intermediate states*. The asymptotics of intermediate states appears rather subtle - see below for an example.

We now turn our attention to the more practical problem of identifying the asymptotic category of a given shell problem directly from its settings. Following [20] we set a few basic hypotheses that can be checked once the geometry of the shell, the load, and the boundary conditions are known. In this way we end up redefining the asymptotic categories based on these hypotheses only. The limit properties like (5.4) or (5.6) are then understood rather as consequences.

The classification is based on checking through the three hypotheses below (either True or False) and then applying Table 1. For simplicity, we assume here that the kinematical constraints at the boundary (if any) are homogeneous. With this limitation the classification applies to a general shell problem.

(H1) Inextensional displacements are kinematically possible: $\mathcal{U}_0 \neq \{0\}$.

(H2) The external loads are able to excite inextensional displacements: $q(\underline{u}) \neq 0$ for some $\underline{u} \in \mathcal{U}_0$.

(H3) The shell geometry, the external loads, and the boundary conditions combine into the fulfillment of the "membrane hypothesis": $|q(\underline{u})| \leq C\{a(\underline{u}, \underline{u})\}^{1/2}$ for all kinematically admissible displacements $\underline{u}$, where C is a constraint independent of $\underline{u}$.

Note that the hypotheses H1 and H2 are not independent: H2 can pass only if H1 passes. As to the seemingly abstract hypothesis H3, we note that this is

State	H1	H2	H3
Membrane state (hard type)	False		True
Membrane state (soft type)	True	False	True
Inextensional state	True	True	
Intermediate state, type a)	False		False
Intermediate state, type b)	True	False	False

Table 1: Classification of shell asymptotics based on hypotheses H1, H2, and H3

nothing but an explicit, weak formulation of (often implicit and stronger) assumptions behind the classical membrane theory of shells.

Based on the above hypotheses, we can find the asymptotic category of a given shell problem from Table 1. Here we have further subdivided the membrane states into "hard" and "soft" subcategories, indicating the way the inextensional deformations are prevented: In the "hard" case, inextensional modes are prohibited kinematically, while in the "soft" case they do not arise, albeit being possible, because of the special type of the load. Obviously, the soft membrane state is unstable with respect to load perturbations, whereas the hard state is stable.

The rigorous justification of Table 1 is given in [20], cf. also [15], [16]. We note here only that one can indeed prove the limit properties (5.4) or (5.6) from the above basic hypotheses, as indicated by Table 1. Instead, finding the actual limit behaviour (and possible further subcategories) of intermediate states, as defined in Table 1, remains largely an open problem. Based on the example studied here (Case 3) it appears characteristic to these states that the deformation energy is concentrated asymptotically in layers, i.e., the layers are very strong.

We close this chapter by classifying asymptotically the three benchmark problems of Chapter 3. In checking the most technical hypothesis H3 we rewrite the load potential (5.2), applying (4.3a) and integrating by parts, as

$$
\begin{aligned}
q(\underline{u}) &= Q_0 \int_{-1}^{1} [\beta_{22} + 2k(x+1)\beta_{12} - \frac{1}{2}k^2(x+1)^2\beta_{11}]\, dx \\
&\quad -2kQ_0[-ku(1) + v(1)]
\end{aligned}
\tag{5.8}
$$

From this form it is easily seen that H3 holds if and only if the second term on the right hand side vanishes, that is, if either a) $k = 0$, or b) $u(1) = v(1) = 0$ for all kinematically admissible displacements. We already checked above the hypothesis H1 in all three cases, and based on (5.8) it is easy to check H2 as well. In this way we come to the following conclusions:

Case 1: Membrane state (hard type).

Case 2 ($k \neq 1$): $\begin{cases} \text{Membrane state (hard or soft), if } k = 0, \\ \text{Inextensional state, if } k \geq 2. \end{cases}$

Case 3: Intermediate state, type a).

Whether Case 2, $k = 0$ should be characterized as a hard or soft membrane state depends on our interpretation of constraint (4.1) (or its corresponding form in the K-model). If (4.1) is taken as a kinematical constraint, then $\mathcal{U}_0 = \{0\}$ and we have thus a hard membrane state. On the other hand, if (4.1) is not assumed a priori, then H1 passes (see above), H2 fails and H3 passes (since $k = 0$ in (5.8)), so we have a soft membrane state in this interpretation. Another way of expressing the same is: If the load is axisymmetric then Case 2 is asymptotically a membrane state which is 1) *stable* with respect to axisymmetric perturbations of the load but 2) *unstable* with respect to non-axisymmetric load perturbations.

6 The Exact Deformation Fields

In this and the subsequent chapter we freeze parameters k and ν as

(6.1) $$k = 2, \ \nu = 1/3,$$

whereas t is left as an active parameter. In the present chapter we analyze the behaviour of the exact displacement and strain fields in the three benchmark problems, as given by the five shell models introduced in Chapter 4: the K-model, the R-model, and the quadratic, cubic and quartic models. The displacement and strain fields are computed numerically and, in case of K- and R-models, also analytically as truncated symbolic expansions in terms of parameter t.

In the numerical computations, 1D finite elements of odd degree $2k+1$ were used, with C^k-conforming shape functions, and with k ranging from 1 to 4. The computations were performed with quadruple precision with t ranging from 0.1 down to 10^{-6}. In order to assure the correct capturing of boundary layers, exponential mesh refinements were imposed near the boundary in length scales $\sim t$ and $\sim \sqrt{t}$. The refinement parameters were checked experimentally so as to assure sufficient accuracy in all length scales. In case of K- and R-models, the numerical results were double checked also by analytical means.

We start by comparing visually the deformation pattern in the three benchmark cases. In Fig. 2 the transverse deflection profiles for the three cases are shown at $t = 0.01$. All models produce about identical profiles; shown are those given by the R-model. We observe that the deflection profile resembles qualitatively a quadratic shape in Case 1, is practically constant in Case 2 (note the magnified scale!), and close to constant away from the boundaries in Case 3. As t

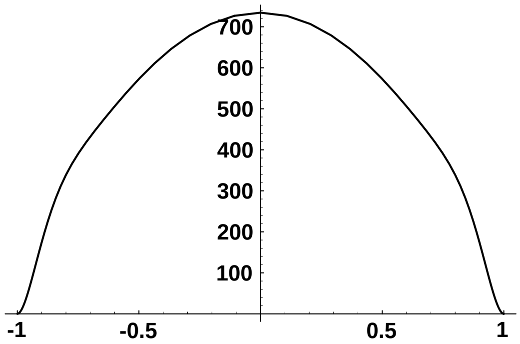

Case 1

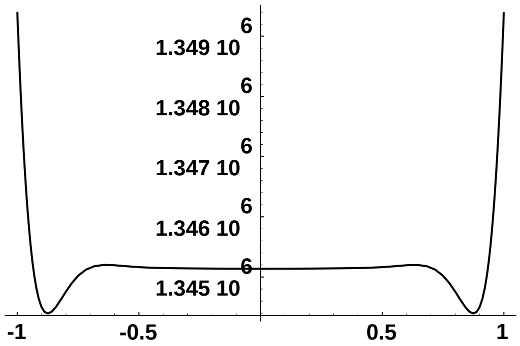

Case 2

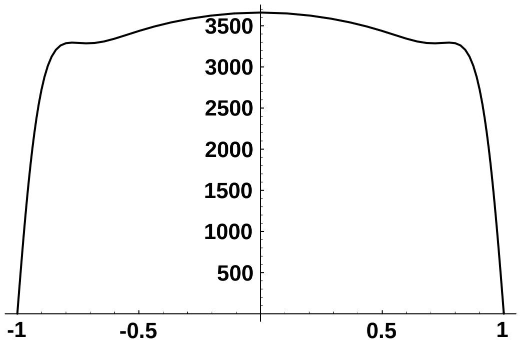

Case 3

Figure 2: Axial profiles of the transverse deflection w amplitudes at $t = 0.01$. Scaling factor P_0R/E.

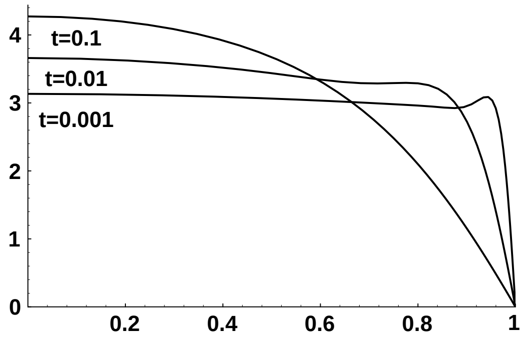

Figure 3: Normalized transverse deflection profile in Case 3 with varying t.

gets smaller, the asymptotics of the profiles become more clear. In fact, symbolic calculus (see below) will confirm the following asymptotic behaviour away from the boundary:

$$\begin{aligned}
\text{Case 1} \quad &: \quad w(x) = \frac{P_0 R}{Et}\left[\left(\frac{15}{2} - \frac{27}{4}x^2 + \frac{3}{4}x^4\right) + O(\sqrt{t})\right] \\
\text{Case 2} \quad &: \quad w(x) = \frac{P_0 R}{Et^3}\left[\frac{4}{3} + O(\sqrt{t})\right] \\
\text{Case 3} \quad &: \quad w(x) = \frac{P_0 R}{Et^{3/2}}\left[2.8752439 + O(\sqrt{t})\right]
\end{aligned}$$

Note that the deflections scale quite differently in all the three cases. Another feature that emphasizes the dissimilarity of the three problems is the relative strength of the boundary layers: In Case 2 the layers are visible only in a sufficiently magnified scale, in Case 1 they are seen as clear distortions in the global profile, and in Case 3 they dominate the whole profile near the boundary.

In Fig. 3 we show the convergence of the normalized profiles as a function of t in Case 3. The convergence is obviously non-uniform (unlike in the other cases), since the asymptotic profile does not obey the kinematical constraints at the ends. We also observe from this figure that the dominant length scale in the boundary layers varies proportionally to $\sqrt{t}$ - a rather typical feature of shell problems in general.

In Fig. 4 the convergence towards asymptotics is shown for Case 2 in a magnified scale. We confirm here the rather slow $O(\sqrt{t})$ convergence towards asymptotics. This again is one of the characteristic features of shell problems - in fact there are cases where convergence is even slower than here [17], [19].

In Fig. 5 we finally show the profile of the angular rotation ϕ in Case 2. As the local zoom with varying t shows, the boundary layer actually contains a length

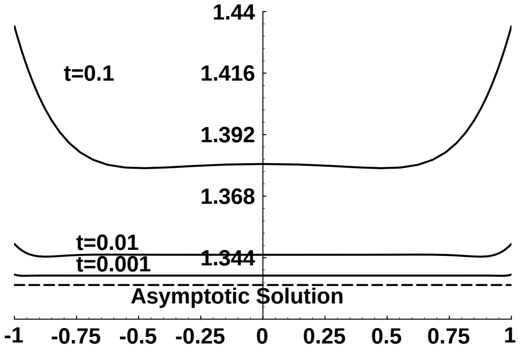

Figure 4: Convergence of the normalized transverse deflection as $t \to 0$. Case 2.

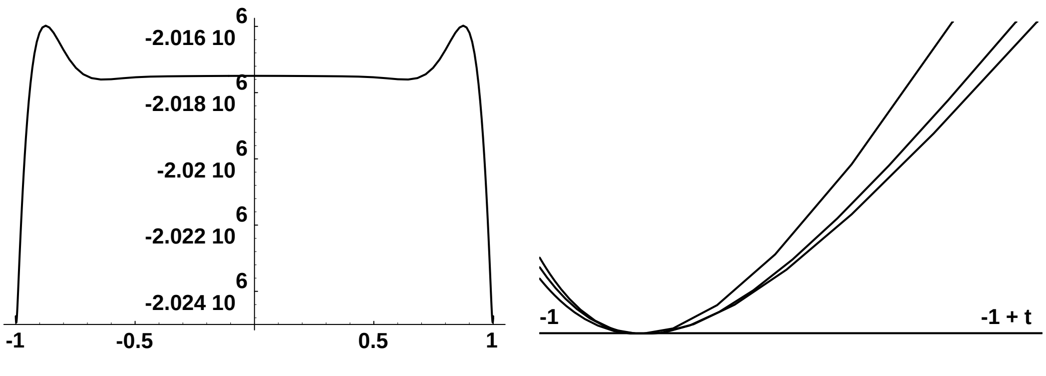

Figure 5: Angular rotation profile in Case 2. Global profile at $t = 0.01$ and zoom at the end with $t = 10^{-2}$, 10^{-4} and 10^{-6}. Scaling factor P_0/E.

Case	t	Bending	Membrane	Shear
1	0.1	23.3980	74.0304	2.5716
	0.01	1.9392	98.0272	0.0336
	0.001	0.3226	99.6767	0.0007
	0	0	100	0
2	0.1	98.2155	0.7417	1.0427
	0.01	99.7695	0.2184	0.0121
	0.001	99.9310	0.0689	0.0002
	0	100	0	0
3	0.1	36.9105	60.8474	2.2421
	0.01	22.5254	77.2724	0.2022
	0.001	23.9248	76.0547	0.0204
	0	25.0000	75.0000	0

Table 2: The percentage shares of membrane, bending and transverse shear energies at various values of t ($t = 0$ means asymptotic).

scale proportional to t as well. Thus, in addition to the global scale $L_1 \sim 1$, we have found the length scales $L_2 \sim \sqrt{t}$ and $L_3 \sim t$ in the boundary layers. It turns out that these three length scales are the relevant scales, not only in the R-model, but in the actual 2D/3D deformation fields as well.

Let us next compare the benchmark problems in the energy perspective, still using the R-model. Fig. 6 shows the distributions of total strain energy and its less dominant (bending or membrane) part. The total percentage shares of bending, membrane and shear energies are given in Table 2 for various values of t, $t = 0$ meaning asymptotic. We observe that Case 1 is membrane-dominated and Case 2 bending-dominated as expected from the classification of Chapter 5. In the intermediate Case 3, neither bending nor membrane energy overtakes asymptotically. The transverse shear energy is rather small in all cases and vanishes asymptotically.

Let us also compare the visual deformation profiles of Fig. 2 to the energy profiles of Fig. 6. The first observation is that the layers have higher relative amplitudes in the energy profiles in all three cases. This is rather natural since energy involves differentiation that tends to amplify smaller scales. Yet, in Cases 1 and 2 layers still fade off asymptotically even in the energy scale, but Case 3 is different: Here the layers are so strong that in the energy scale, it is in fact the smooth component that fades off asymptotically.

We note that in finite element approximations, shell deformation states are "visualized" more or less in the energy perspective of Fig. 6. Therefore we expect

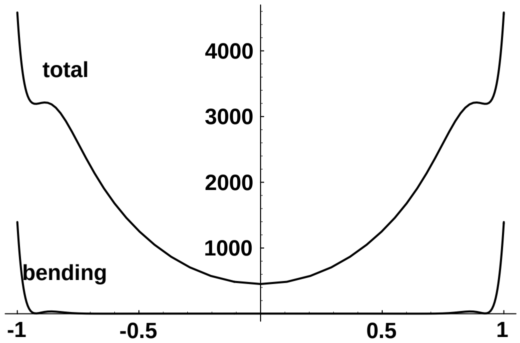

Case 1

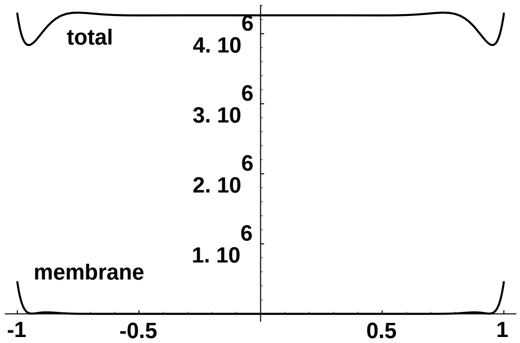

Case 2

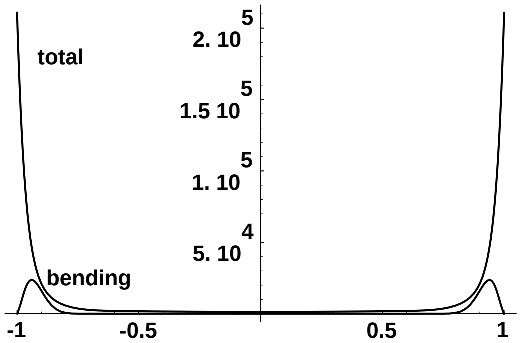

Case 3

Figure 6: Axial density of deformation energy at $t = 0.01$. Scaling factor $\frac{P_0^2 R^2}{E(1-\nu^2)}$.

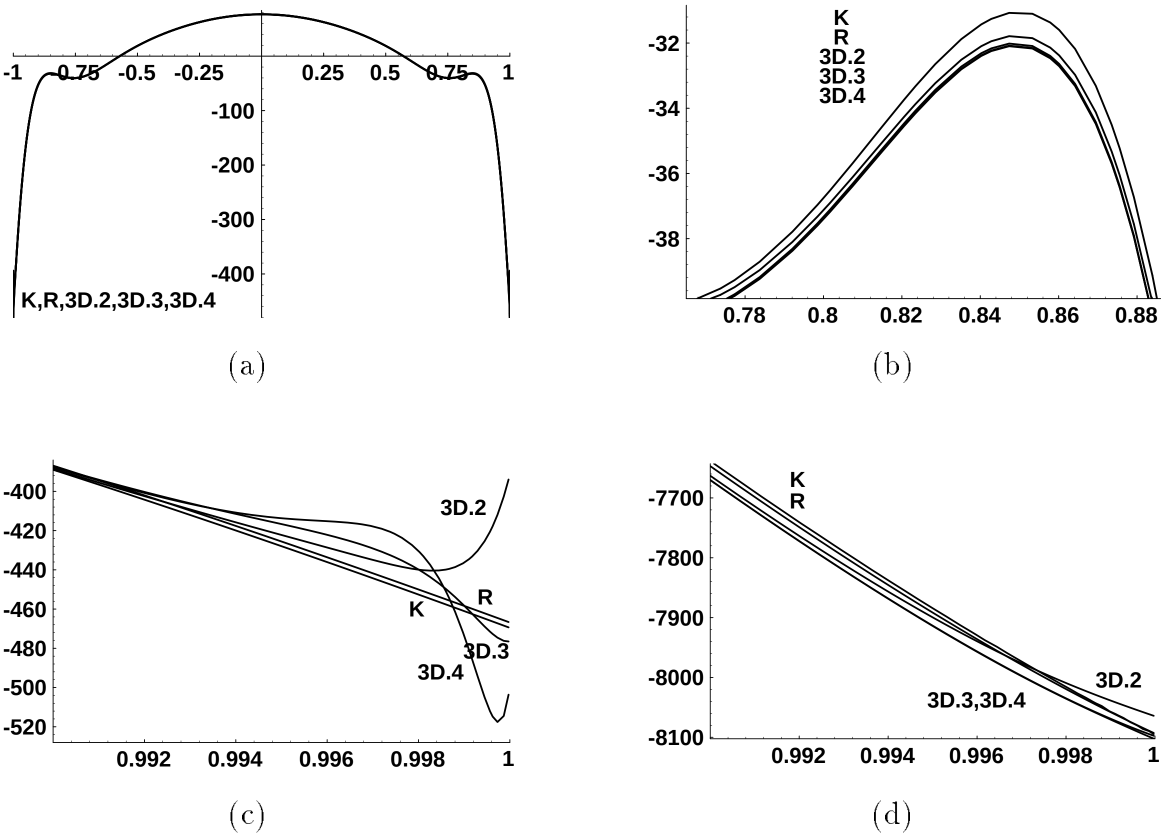

Figure 7: The axial profile of the strain ϵ_{e11} along the outer surface, as given by different models at $t = 0.01$. (a) Global profile, (b) the $\sqrt{t}$-scale and (c) the t-scale in Case 1. (d) The local t-scale in Case 2. Scaling factor P_0/E.

difficulties, e.g. in approximating the visually dominating smooth component of the displacement field in Case 3, since this component has small energy. As will be seen in the next chapter, Case 2 is even worse in this sense, due to the concentration of energy in the (small-looking) bending part. Instead, in Case 1 it is relatively easy to capture the smooth component of the displacement field numerically.

So far we have used the R-model only in our computations. Indeed, the differences in different models are rather small in global profiles, unless t is relatively large, say $t \geq 0.1$. In more local details, though, some characteristic differencies can be seen even at lower values of t. In Fig. 7 the axial profile of the strain (amplitude) ϵ_{e11} is shown, as given by different models along the outer surface of the shell at $t = 0.01$. As seen from Fig. 7 (a), hardly no differences are seen in the global profile (Case 1). A closer look at the $\sqrt{t}$-scale in Fig. 7 (b) already

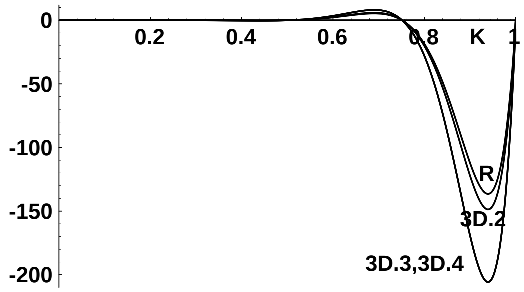

Figure 8: Transverse shear strain in Case 2. Midsurface, $t = 0.01$. Scaling factor P_0/E.

reveals some differences, and even more variation is seen in the very local t-scale at the end in Fig. 7 (c). The latter effect depends strongly on the boundary conditions, as seen from Fig. 7(d) where the same scale is resolved in Case 2.

The results for other strain components are qualitatively similar to those shown in Fig. 7, except for the tranverse shear strains ϵ_{e13} and ϵ_{e23}, where the relative gap between different models is larger. In Fig. 8 this effect is shown for ϵ_{e13} in Case 2. Note that for the K-model, $\epsilon_{e13} = \epsilon_{e23} = 0$ on the midsurface. We find experimentally that at a distance of order $\sim \sqrt{t}$ from the boundary, the gap between different models is proportional to $\sqrt{t}$ for ϵ_{e13} and ϵ_{e23} and to t for other strain components. Thus the convergence of transverse shear strains is, relatively speaking, slowest. We should note, however, that the transverse shear strains are rather small and so have little effect on principal stresses.

The maximal (absolute values of) strains observed in the different models at $t = 0.1$, 0.01 and 0.001 are given in Tables 3 through 5 for the three cases. The location of the maxima is outlined qualitatively in Table 6. Here (L,+), (L,-) or (L,0) indicates that the maximum is observed at a distance of order L from the boundary (or possibly at the boundary if $L = t$), and that the maximum is located respectively, on the outer surface, on the inner surface, or in the interior of the shell.

In Table 7 we show some global measures for the gaps in between different model pairs. The measure is here chosen to be

$$d(A, B) = |||\underline{U}^A - \underline{U}^B|||/|||\underline{U}^K|||,$$

where $\underline{U}^A$ and $\underline{U}^B$ are the 3D displacement fields corresponding to models A and B, and $|||\cdot|||$ stands for for the energy norm, i.e., the square root of strain energy.

t	Model	ϵ_{e11}	ϵ_{e12}	ϵ_{e13}	ϵ_{e22}	ϵ_{e23}	ϵ_{e33}
0.1	K	-5.51	-2.52	-0.22	1.52	-0.07	2.76
	R	-5.22	-2.51	0.72	1.50	0.12	2.62
	3D.2	-4.81	-2.62	3.66	1.58	0.13	2.27
	3D.3	-5.87	-2.62	3.66	1.58	0.17	2.28
0.01	K	-4.69	-2.87	-0.05	1.31	-0.01	2.34
	R	-4.67	-2.87	0.19	1.31	0.01	2.33
	3D.2	-4.40	-2.88	2.75	1.32	0.01	2.16
	3D.3	-4.76	-2.88	2.98	1.32	0.02	2.18
0.001	K	-3.88	-2.95	-0.01	1.46	$-6 \cdot 10^{-4}$	1.94
	R	-3.88	-2.95	0.05	1.46	$1 \cdot 10^{-3}$	1.93
	3D.2	-3.72	-2.95	2.16	1.46	$1 \cdot 10^{-3}$	1.87
	3D.3	-3.88	-2.95	2.42	1.46	$2 \cdot 10^{-3}$	1.86

Table 3: Maximal scaled strains. Case 1. Scaling factor $P_0/(Et)$.

t	Model	ϵ_{e11}	ϵ_{e12}	ϵ_{e13}	ϵ_{e22}	ϵ_{e23}	ϵ_{e33}
0.1	K	-0.82	0.35	-0.03	2.32	0.03	1.06
	R	-0.82	0.28	0.04	2.31	-0.27	1.06
	3D.2	-0.79	0.30	0.05	2.47	-0.29	1.08
	3D.3	-0.83	0.30	0.06	2.48	-0.37	1.15
0.01	K	-0.81	0.11	-0.01	2.41	$2 \cdot 10^{-3}$	1.03
	R	-0.81	0.10	0.01	2.41	-0.07	1.03
	3D.2	-0.81	0.10	0.01	2.43	-0.07	1.03
	3D.3	-0.81	0.10	0.02	2.43	-0.09	1.04
0.001	K	-0.80	0.04	$-4 \cdot 10^{-3}$	2.41	$2 \cdot 10^{-4}$	1.02
	R	-0.80	0.04	$5 \cdot 10^{-3}$	2.41	-0.02	1.02
	3D.2	-0.80	0.04	$5 \cdot 10^{-3}$	2.41	-0.02	1.03
	3D.3	-0.80	0.04	$6 \cdot 10^{-3}$	2.41	-0.02	1.03

Table 4: Maximal scaled strains. Case 2. Scaling factor $P_0/(Et^2)$.

t	Model	ϵ_{e11}	ϵ_{e12}	ϵ_{e13}	ϵ_{e22}	ϵ_{e23}	ϵ_{e33}
0.1	K	1.33	-1.41	-0.18	-1.90	0.03	0.82
	R	1.37	-1.42	0.44	-2.13	0.69	0.85
	3D.2	1.39	-1.48	0.46	-2.22	0.68	0.92
	3D.3	1.41	-1.49	0.59	-2.22	0.84	1.21
0.01	K	1.81	-0.53	-0.07	-2.72	$5 \cdot 10^{-3}$	1.14
	R	1.81	-0.53	0.16	-2.74	0.22	1.14
	3D.2	1.82	-0.53	0.16	-2.75	0.21	1.15
	3D.3	1.82	-0.53	0.22	-2.75	0.28	1.15
0.001	K	1.87	-0.17	-0.02	-2.84	$4 \cdot 10^{-4}$	1.19
	R	1.87	-0.17	0.05	-2.84	0.07	1.19
	3D.2	1.87	-0.17	0.05	-2.84	0.07	1.19
	3D.3	1.87	-0.17	0.07	-2.84	0.09	1.19

Table 5: Maximal scaled strains. Case 3. Scaling factor $P_0/(Et^{3/2})$.

Case	ϵ_{e11}	ϵ_{e12}	ϵ_{e13}	ϵ_{e22}	ϵ_{e23}	ϵ_{e33}
1	t,+	$\sqrt{t}$,-	t,+	$\sqrt{t}$,+	t,0	t,+
2	t,+	t,-	$\sqrt{t}$,0	t,+	t,0	$\sqrt{t}$,-
3	$\sqrt{t}$,+	$\sqrt{t}$,-	t,0	t,-	t,0	$\sqrt{t}$,-

Table 6: Location of maximal strains

Case	3D.4 - 3D.3	3D.3 - 3D.2	3D.2 - R	R - K
1	$0.174\,t^{0.66}$	$0.513\,t^{0.78}$	$0.708\,t^{0.75}$	$1.585\,t^{0.85}$
2	$0.072\,t^{1.56}$	$0.407\,t^{0.98}$	$0.562\,t^{0.99}$	$0.794\,t^{0.96}$
3	$0.078\,t^{0.76}$	$0.295\,t^{0.55}$	$0.295\,t^{0.64}$	$0.776\,t^{0.55}$

Table 7: The gap in between different model pairs in the relative energy norm. Approximate behaviour in the range $0.001 \leq t \leq 0.1$.

The variations shown are curve fits to values at $t = 0.1$, 0.01 and 0.001. We observe that the gap between models A and B behaves roughly as $\sim ct^{\alpha}$ where the coefficient c depends on (A,B) but the exponent α is more or less the same for all model pairs in a given problem. Thus we expect that all models we are discussing converge towards the 3D-model nearly with the same asymptotic rate as $t \to 0$. This obviously is due to the boundary layers and is somewhat to be expected from Figs. 7 and 8 as well. Of course, raising the model order at a given t still improves the accuracy quantitatively, as also indicated by Table 7.

In Appendix A we give the 15-decimal benchmark values of the total deformation energy in the three model problems at $t = 0.1/0.01/0.001$ and for the different shell models considered. The (scaled) asymptotic energies are also given there.

In Appendix B through E we finally present the results of symbolic computation in case of K- and R-models. Here we treat t as a parameter and present truncated asymptotic expansions of the displacement and strain fields. We separate here the length scales so that the precise behaviour of displacements and strains can be seen (at small values of t), both in the interior of the shell and at the boundary.

The expansions of Appendix B through E were computed using MATHEMATICA. The first step is to solve the characteristic equation associated to the homogeneous Euler equations in the K- and R-models. The Euler equations constitute a system of ODE's of total order 8 in the K-model and of order 10 in the R-model. The characteristic equations are the following ($k = 2$, $\nu = 1/3$):

K-model:

$$\begin{aligned}&\lambda^8\,(72\,t^4 + 216\,t^2) - \lambda^6\,(288\,t^4 + 3456\,t^2)\\ &+\lambda^4\,(256\,t^4 + 14784\,t^2 + 2304) - 31104\,\lambda^2\,t^2 + 31104\,t^2 = 0\end{aligned}$$

R-model:

$$\begin{aligned}&27\,\lambda^{10}\,t^4 - \lambda^8\,(24t^6 + 720\,t^4 + 324\,t^2)\\ &+ \lambda^6\,(192\,t^6 + 4776\,t^4 + 6336\,t^2)\\ &- \lambda^4\,(224\,t^6 + 13104\,t^4 + 26784\,t^2 + 3456)\\ &+ \lambda^2\,(19440\,t^4 + 46656\,t^2)\; - \;15552\,t^4 - 46656\,t^2 = 0.\end{aligned}$$

The roots are as follows:

K-model:

$$\lambda_1 \;=\; 1.35540301\,(1+i)\,\sqrt{t} + 1.24501716\,(1-i)\,t^{\frac{3}{2}}$$

$$
\begin{aligned}
& -2.74610296\,(1-i)\,t^{\frac{5}{2}} + \mathrm{O}(t^{\frac{7}{2}}) \\
\lambda_2 &= -\lambda_1 \\
\lambda_3 &= \bar{\lambda}_1 \\
\lambda_4 &= -\bar{\lambda}_1 \\
\lambda_5 &= 1.27788621\,(1+i)\,t^{-\frac{1}{2}} + 1.56508458\,(1-i)\,\sqrt{t} \\
& \quad +0.98503729\,(1+i)\,t^{\frac{3}{2}} - 2.91823062\,(1-i)\,t^{\frac{5}{2}} + \mathrm{O}(t^{\frac{7}{2}}) \\
\lambda_6 &= -\lambda_5 \\
\lambda_7 &= \bar{\lambda}_5 \\
\lambda_8 &= -\bar{\lambda}_5
\end{aligned}
$$

R-model:

$$
\begin{aligned}
\lambda_1 &= 1.35540301\,(1+i)\,\sqrt{t} + 1.24501716\,(1-i)\,t^{\frac{3}{2}} \\
& \quad -3.08495372\,(1-i)\,t^{\frac{5}{2}} + \mathrm{O}(t^{\frac{7}{2}}) \\
\lambda_2 &= -\lambda_1 \\
\lambda_3 &= \bar{\lambda}_1 \\
\lambda_4 &= -\bar{\lambda}_1 \\
\lambda_5 &= 1.27788621\,(1+i)\,t^{-\frac{1}{2}} + 1.82593201\,(1-i)\,\sqrt{t} \\
& \quad +0.95841466\,(1+i)\,t^{\frac{3}{2}} - 3.08126027\,(1-i)\,t^{\frac{5}{2}} + \mathrm{O}(t^{\frac{7}{2}}) \\
\lambda_6 &= -\lambda_5 \\
\lambda_7 &= \bar{\lambda}_5 \\
\lambda_8 &= -\bar{\lambda}_5 \\
\lambda_9 &= 3.46410162\,t^{-1} + 1.15470054\,t + 0.51320024\,t^3 + \mathrm{O}(t^5) \\
\lambda_{10} &= -\lambda_9
\end{aligned}
$$

We observe from these expansions that eigenvalues λ_1 through λ_4 actually contribute to the smooth part of the solution, λ_5 through λ_8 represent the dominant $\sqrt{t}$-scale of the boundary layer in both models, and finally λ_9 and λ_{10} represent the shorter t-scale of the layer that is only captured by the R-model or by higher-order models.

Once the roots of the characteristic equation are known, the solution may be expanded as

$$
\begin{aligned}
\text{K-model} &: \quad (u,v,w) = (u,v,w)^0 + \sum_{i=1}^{8} a_i \underline{c}^i e^{\lambda_i x} \\
\text{R-model} &: \quad (u,v,w,\theta,\phi) = (u,v,w,\theta,\phi)^0 + \sum_{i=1}^{10} a_i \underline{c}^i e^{\lambda_i x}
\end{aligned}
$$

where

$$
\begin{aligned}
(u,v,w)^0 &= \frac{P_0 R}{Et^3}(0,-\frac{2}{3}-\frac{2t^2}{9},\frac{4}{3}+\frac{t^2}{9}) \\
(u,v,w,\theta,\phi)^0 &= \frac{P_0 R}{Et^3}(0,-\frac{2}{3}-\frac{8t^2}{9},\frac{4}{3}+\frac{13t^2}{9},0,-2)
\end{aligned}
$$

are special solutions to the full Euler equations, and $\underline{c}^i$:s are the eigenvectors associated to the characteristic values λ_i. Finally the (expansions of the) coefficients a_i are obtained by imposing the essential and natural boundary conditions at $x=\pm 1$ in each of the three cases. Note that only this last step of the symbolic computation is actually different in the three cases, so the dissimilarity of the benchmark problems is not so prominent in the symbolic "perspective".

In Appendix B we present truncated expansions of the displacement field in the three cases according to the K-model. Here the smooth component of $(u^s,v^s,w^s,\theta^s,\phi^s)$ (where $\theta^s=-dw^s/dx$ and $\phi^s=2w^s+v^s$ according to (4.6) and (4.3c)) is expanded first. Then follow the boundary layers in the form

$$
\begin{aligned}
A_\pm(x) &= e^{a(t)(x-1)}\{C(t)\cos[\,b(t)(x-1)\,]+S(t)\sin[\,b(t)(x-1)\,]\}+ \\
& \quad e^{-a(t)(x+1)}\{\pm C(t)\cos[\,b(t)(x+1)\,]\mp S(t)\sin[\,b(t)(x+1)\,]\}.
\end{aligned}
$$

Here

$$
\begin{aligned}
a(t) &= 1.27788621\,t^{-\frac{1}{2}}+1.56508458\,\sqrt{t} \\
&\quad +0.98503729\,t^{\frac{3}{2}}-2.91823062\,t^{\frac{5}{2}}+\mathrm{O}(t^{\frac{7}{2}}) \\
b(t) &= 1.27788621\,t^{-\frac{1}{2}}-1.56508458\,\sqrt{t} \\
&\quad +0.98503729\,t^{\frac{3}{2}}+2.91823062\,t^{\frac{5}{2}}+\mathrm{O}(t^{\frac{7}{2}})
\end{aligned}
$$

and the truncated expansions of $C(t)$ and $S(t)$ are given. The upper signs (A_+) are relevant for the components v,w and ϕ that are even in x, whereas lower signs (A_-) should be used for u and θ.

In Appendix C the gap of R- and K-models is given for the displacement fields. Here $a(t)$ and $b(t)$ contain only the leading terms (common to both models) in the expansions:

$$a_0(t)=b_0(t)=1.27788621t^{-1/2}.$$

The additional t-scale boundary layers are given in the form

$$B_\pm(x)=K(t)[e^{c(t)(x-1)}\pm e^{-c(t)(x+1)}],$$

where the signs are again chosen on the basis of parity,

$$c(t)=3.46410162\,t^{-1}+1.15470054\,t+0.51320024\,t^3+\mathrm{O}(t^5),$$

and the truncated expansions of $K(t)$ are given.

In Appendix D we give the leading terms in the expansions of the strains in the K-model. For the boundary layers we now present a different type of expansion for clarity: The leading terms of $C(t,x)$ and $S(t,x)$ are given in the expansion

$$A(x) = e^{-a_0(t)x}\left\{C(t,x)\cos\left[b_0(t)x\right] + S(t,x)\sin\left[b_0(t)x\right]\right\},$$

where x now measures the distance to the right end of the cylinder. In Appendix E we finally present the gap between R- and K-models for strains, including the transverse shear strains ρ_1 and ρ_2 that vanish in the K-model. The short t-scale of the boundary layer is here given the representation

$$B(x) = K(t,x)e^{-c_0(t)x},$$

where x again measures the distance to the right end, and

$$c_0(t) = 3.46410162t^{-1}.$$

7 2D Finite Element Analysis

In this final chapter, we solve the benchmark problems approximately by finite element discretization in the coordinates (x,α). The approximation is based on the R-model where the trigonometric angular variation of the solution is now ignored. The displacement field $\underline{u} = (u,v,w,\theta,\phi)$ then depends on the two variables x,α, and the energy expression (4.1) of the R-model is replaced by

$$\begin{aligned} \text{(7.1)} \qquad \mathcal{F}_R(\underline{u}) &= \frac{t}{2}\int_\omega \left[\nu(\beta_{11}+\beta_{22})^2 + (1-\nu)\sum_{i,j=1}^{2}\beta_{ij}^2\right] dxd\alpha \\ &+ \frac{t^3}{24}\int_\omega \left[\nu(\kappa_{11}+\kappa_{22})^2 + (1-\nu)\sum_{i,j=1}^{2}\kappa_{ij}^2\right] dxd\alpha \\ &+ \frac{1-\nu}{4}t\int_\omega (\rho_1^2+\rho_2^2)\,dxd\alpha - \int_\omega wP_0\cos k\alpha\,dxd\alpha, \end{aligned}$$

where

$$\text{(7.2a)} \qquad \beta_{11} = \frac{\partial u}{\partial x},\ \ \beta_{12} = \frac{1}{2}\left(\frac{\partial u}{\partial \alpha} + \frac{\partial v}{\partial x}\right),\ \ \beta_{22} = \frac{\partial v}{\partial \alpha} + w,$$

$$\text{(7.2b)} \qquad \kappa_{11} = \frac{\partial \theta}{\partial x},\ \ \kappa_{12} = \frac{1}{2}\left(\frac{\partial \theta}{\partial \alpha} + \frac{\partial \phi}{\partial x} - \frac{\partial v}{\partial x}\right),\ \ \kappa_{22} = \frac{\partial \phi}{\partial \alpha},$$

$$\text{(7.2c)} \qquad \rho_1 = -\theta + \frac{\partial w}{\partial x},\ \ \rho_2 = -\phi + \frac{\partial w}{\partial \alpha} - v.$$

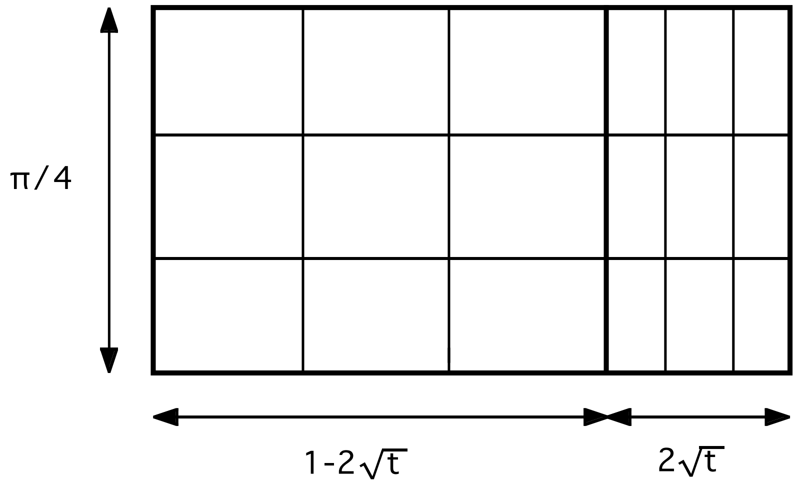

Figure 9: The refined grid used in the numerical computations ($N = 3$).

We will choose $k = 2$, $\nu = 1/3$ as in the previous chapter. The computational domain is chosen to be

$$\omega = \{(x, \alpha) \mid 0 < x < 1,\ 0 < \alpha < \pi/4\},$$

with symmetry boundary conditions imposed at $x = 0$, $\alpha = 0$ and antisymmetry condition at $\alpha = \pi/4$.

The finite element models will be based on rectangular subdivisions of ω. We assume the standard energy formulation where the five components of the displacement field are approximated by Lagrange elements of equal degree p ($p \geq 1$). Elements of reduced type are used when $p \geq 2$. In order to separate boundary layer effects from other sources of error, we compute with two kinds of meshes. Either we use a uniform $N \times N$ grid with varying N, or we use a piecewise uniform $(2N) \times N$ grid where half of the axial mesh intervals are concentrated on the zone $1 - 2\sqrt{t} < x < 1$ where the layers have a significant amplitude (Fig. 9). In the computations, N will range from 2 to 32 and p from 1 to 8. We have used a "p-version" code where both N and p are at the user's disposal [6].

In what follows, we first consider the simplest case where the elements are bilinear ($p = 1$). In Chapter 7.1 we carry out an asymptotic error analysis, showing how the asymptotics and the boundary-layer behaviour of the exact solution is reflected in the numerical approximation error. In Chapter 7.2 we present numerical results obtained with both bilinear and higher-order elements.

7.1 Error Analysis of the Bilinear Scheme

The error analysis will be based on the *energy norm* defined by

$$|||\underline{u}||| = \{\mathcal{A}(\underline{u}, \underline{u})\}^{1/2},$$

where $\mathcal{E}(\underline{u}) = \frac{1}{2}\mathcal{A}(\underline{u}, \underline{u})$ denotes the total deformation energy of the R-model, i.e., the quadratic part of (7.1). Denote the exact solution (for given t) by $\underline{u}$ and its finite element approximation by $\underline{u}_h = (u_h, v_h, w_h, \theta_h, \phi_h)$, where $h = 1/N$ is the (axial) mesh spacing. Since we use the standard energy formulation, $\underline{u}_h$ is the energy projection of $\underline{u}$, i.e., the best approximation of $\underline{u}$ in the energy norm. Our aim is to estimate the relative error

$$e(h,t) = \frac{|||\underline{u} - \underline{u}_h|||}{|||\underline{u}|||}.$$

Recall from the previous section that $\underline{u}$ may be split uniquely as $\underline{u} = \underline{u}^s + \underline{u}^b$, where $\underline{u}^s$ is the smooth part and $\underline{u}^b$ is the boundary layer part (see Appendices B, C). Denote by A_s and A_b the relative amplitudies of these components in the energy norm:

$$A_s = \frac{|||\underline{u}^s|||}{|||\underline{u}|||}, \quad A_b = \frac{|||\underline{u}^b|||}{|||\underline{u}|||}.$$

Then we may estimate $e(h,t)$ (by the triangle inequality) as

$$e(h,t) \leq A_s \frac{|||\underline{u}^s - \underline{u}_h^s|||}{|||\underline{u}^s|||} + A_b \frac{|||\underline{u}^b - \underline{u}_h^b|||}{|||\underline{u}^b|||} \doteq e_s(h,t) + e_b(h,t) \tag{7.3}$$

Here $\underline{u}_h^s$ and $\underline{u}_h^b$ are the finite element approximations of $\underline{u}^s$, resp. $\underline{u}^b$. These are again defined by the energy projection principle. However, since $\underline{u}^s$ and $\underline{u}^b$ need not satisfy the kinematical constraints of the original problem at $x = \pm 1$, we have to impose here the corresponding inhomogeneous constraints. Thus in Case 1, $\underline{u}_h^{s/b}$ is assumed to interpolate $\underline{u}^{s/b}$ at $x = 1$, in Case 3, the interpolation condition is imposed on $w_h^{s/b}$ only, and in Case 2 there is no constraint.

We estimate now the two components of the error in (7.3), in each of the three cases. First we note that as $t \to 0$, the amplitudes A_s, A_b behave qualitatively as (see Appendix D)

$$A_s \sim 1, \quad A_b \sim t^{1/4} \quad \text{(Cases 1,2)} \tag{7.4a}$$

$$A_s \sim t^{1/4}, \quad A_b \sim 1 \quad \text{(Case 3)} \tag{7.4b}$$

Hence by (7.3), it remains to estimate the relative approximation error for each component separately in the three benchmark cases. To this end, we need some basic approximation theory in Sobolev norms. Below, C or c denotes a positive constant which is independent of both t and of the mesh parameters.

Let $\underline{u} = (u, v, w, \theta, \phi)$ be a vector field defined on ω, sufficiently smooth, and restricted at the boundary by the symmetry/antisymmetry conditions

(7.5a) $$u = \theta = 0 \quad \text{at} \quad x = 0,$$

(7.5b) $$v = \phi = 0 \quad \text{at} \quad \alpha = 0,$$

(7.5c) $$u = w = \theta = 0 \quad \text{at} \quad \alpha = \pi/4.$$

For such fields, we define for $k = 1, 2, \ldots$ the seminorms

$$|\underline{u}|_{k,\omega} = \left\{ |u|^2_{H^k(\omega)} + |v|^2_{H^k(\omega)} + |w|^2_{H^k(\omega)} + |\theta|^2_{H^k(\omega)} + |\phi|^2_{H^k(\omega)} \right\}^{1/2},$$

where $|\cdot|_{H^k(\omega)}$ is the standard Sobolev seminorm

$$|\phi|_{H^k(\omega)} = \left\{ \int_\omega \sum_{i,j \geq 0, i+j=k} \left(\frac{\partial^k \phi}{\partial x^i \partial \alpha^j} \right)^2 dx d\alpha \right\}^{1/2},$$

and the norm is defined as

$$||\underline{u}||_{k,\omega} = \left\{ \sum_{l=0}^{k} |\underline{u}|^2_{l,\omega} \right\}^{1/2}.$$

In this notation, the *energy space* (where the minimum of (7.1) is sought) is the set of vector fields $\underline{u}$ such that $||\underline{u}||_{1,\omega}$ is finite and such that (7.5 a,b,c) hold. At $x = 1$, further kinematical constraints are imposed in the minimization process in Cases 1, 3.

We denote the energy space again by $\mathcal{U}$ and let $\mathcal{U}_0$ denote the subspace of inextensional fields satisfying $\beta_{ij}(\underline{u}) = \rho_i(\underline{u}) = 0$, $i, j = 1, 2$. From the quadratic part of (7.1) representing the energy norm we conclude that

(7.6a) $$|||\underline{u}||| \leq Ct^{1/2} ||\underline{u}||_{1,\omega}, \quad \underline{u} \in \mathcal{U},$$

(7.6b) $$|||\underline{u}||| \leq Ct^{3/2} ||\underline{u}||_{1,\omega}, \quad \underline{u} \in \mathcal{U}_0,$$

where C is independent of t. More generally, we call any displacement field $\underline{u}$ (possibly varying with t) *bending-dominated* if inequality (7.6b) holds as t varies and *membrane-dominated* if

(7.6c) $$|||\underline{u}||| \geq ct^{1/2} ||\underline{u}||_{1,\omega}.$$

We note finally that by the Korn inequality

(7.6d) $$|||\underline{u}||| \geq ct^{3/2} ||\underline{u}||_{1,\omega}, \quad \underline{u} \in \mathcal{U}.$$

This is because of the scaling of the energy norm, and because of the symmetry conditions (7.5) which rule out rigid body motions.

The notation required in the error estimates is now set. By the energy projection principle, $\underline{u}_h^{s/b}$ is the best approximation of $\underline{u}^{s/b}$ in the energy norm, within the interpolation constraint at $x = 1$ set in Cases 1 and 3. Hence the error is bounded by the interpolation error, and so we have by (7.6a) and by standard approximation theory

$$|||\underline{u}^{s/b} - \underline{u}_h^{s/b}||| \leq C t^{1/2} h |\underline{u}^{s/b}|_{2,\omega}.$$

Hence

$$\frac{|||\underline{u}^{s/b} - \underline{u}_h^{s/b}|||}{|||\underline{u}^{s/b}|||} \leq ChK(\underline{u}^{s/b}, t), \tag{7.7}$$

where

$$K(\underline{u}, t) = \frac{t^{1/2}|\underline{u}|_{2,\omega}}{|||\underline{u}|||}. \tag{7.8}$$

Thus we have reduced the error estimation problem to that of estimating $K(\underline{u}^s, t)$ and $K(\underline{u}^b, t)$, as defined by (7.8), in the benchmark cases.

Consider first $K(\underline{u}^s, t)$. Since $\underline{u}^s$ is smooth, we have $|\underline{u}^s|_{2,\omega}/||\underline{u}^s||_1 \leq C$ in all the cases, so by (7.6) and (7.8), $K(\underline{u}^s, t) \sim C$ if $\underline{u}^s$ corresponds to a membrane-dominated deformation with $|||\underline{u}^s||| \sim t^{1/2}||\underline{u}^s||_1$, or $K(\underline{u}^s, t) \sim Ct^{-1}$ if $\underline{u}^s$ correspons to a bending-dominated deformation with $|||\underline{u}^s||| \sim t^{3/2}||\underline{u}^s||_1$. Now, from Appendix D we see that $\underline{u}^s$ is membrane-dominated in Cases 1 and 3 and bending-dominated in Case 2. Hence we conclude from (7.7) that

$$\frac{|||\underline{u}^s - \underline{u}_h^s|||}{|||\underline{u}^s|||} \leq \begin{cases} Ch & \text{(Cases 1, 3)}, \\ \min\{1, Ct^{-1}h\} & \text{(Case 2)}. \end{cases} \tag{7.9}$$

In Case 2, we have taken into account as well that the error of the projection scheme cannot exceed 100%, when the kinematical constraints are homogeneous. The estimate for Case 2 predicts in fact that at $t = 0$, the asymptotic finite element solution will be zero for every h, a phenomenon called (extreme) *locking*. We will see that the estimate is quite realistic in this sense. Note that the *locking factor* $1/t$ in estimate (7.9) for Case 2 arises because of the unfavorable scaling of the energy norm with respect to the Sobolev norm $||\cdot||_{1,\omega}$ in this case. In the standard finite element method, locking in Case 2 can be avoided only if there are enough inextensional displacement fields in the finite element space so as to approximate $\underline{u}^s$. In the piecewise bilinear case, unfortunately, the only such fields are globally bilinear, see [22].

Consider next $K(\underline{u}^b, t)$. From Appendices D, E we conclude that the dominant contribution to $K(\underline{u}^b, t)$ comes from the layer with scale $\sim \sqrt{t}$, and that $K(\underline{u}^b, t) \sim Ct^{-1}$ in all the three cases. Thus

$$\frac{|||\underline{u}^b - \underline{u}_h^b|||}{|||\underline{u}^b|||} \leq Ct^{-1}h \text{ (Cases 1, 2, 3).} \tag{7.10}$$

Note that since the dominant length scale of the layer is $L \sim \sqrt{t}$, the relative interpolation error in the norm $||\cdot||_{1,\omega}$ is of order $\mathrm{O}(h/\sqrt{t})$. As compared with such an optimal bound, estimate (7.10) contains an additional locking factor $1/\sqrt{t}$. Again, this factor arises because of the unfavorable scaling of $|||\underline{u}^b|||$ as compared with $||\underline{u}^b||_1$.

If an axial mesh refinement is imposed at the boundary layer zone that is sufficiently wide, estimate (7.10) is improvable. Assume that the axial mesh spacing is h_0 ($< h$) in the zone $1 - |\log h|\sqrt{t} < x < 1$, while the angular mesh spacing remains the same as globally. Then it can be shown that (7.10) is improvable as

$$\frac{|||\underline{u}^b - \underline{u}_h^b|||}{|||\underline{u}^b|||} \leq C(h + t^{-1}h_0). \tag{7.11}$$

Here the first term arises both from the approximation error outside the refinement zone and from the angular approximation error.

Let us finally combine (7.3), (7.4), (7.9) and (7.11) (assuming mesh refinement as above) to an estimate of the global approximation error. We have

$$\frac{|||\underline{u} - \underline{u}_h|||}{|||\underline{u}|||} \leq \begin{cases} C_1 h + C_2 t^{-3/4} h_0 & \text{(Case 1)} \\ \min\{1, C_1 t^{-1} h\} + C_2 t^{-3/4} h_0 & \text{(Case 2)} \\ C_1 h t^{1/4} + C_2 t^{-1} h_0 & \text{(Case 3)} \end{cases} \tag{7.12}$$

7.2 Numerical Results

In Fig. 10 (a) we show the transverse deflection profiles for the three benchmark problems at $t = 0.01$, as computed with bilinear elements with N $(= 1/h) = 4$, 8, 16 and 32. Comparing the profiles obtained with uniform and refined meshes, Fig. 10 (b), we can roughly estimate the relative contribution due to the smooth and boundary-layer parts of the solution to the overall approximation error.

In Case 1, the simple bilinear scheme performs fairly well even on uniform meshes. Still better accuracy is achieved on refined grids, especially near the boundary. This indicates that the boundary layer component of the error is large. In fact, estimate (7.12) predicts that the boundary layer approximation error is significant in all the numerical models considered. Note that we have

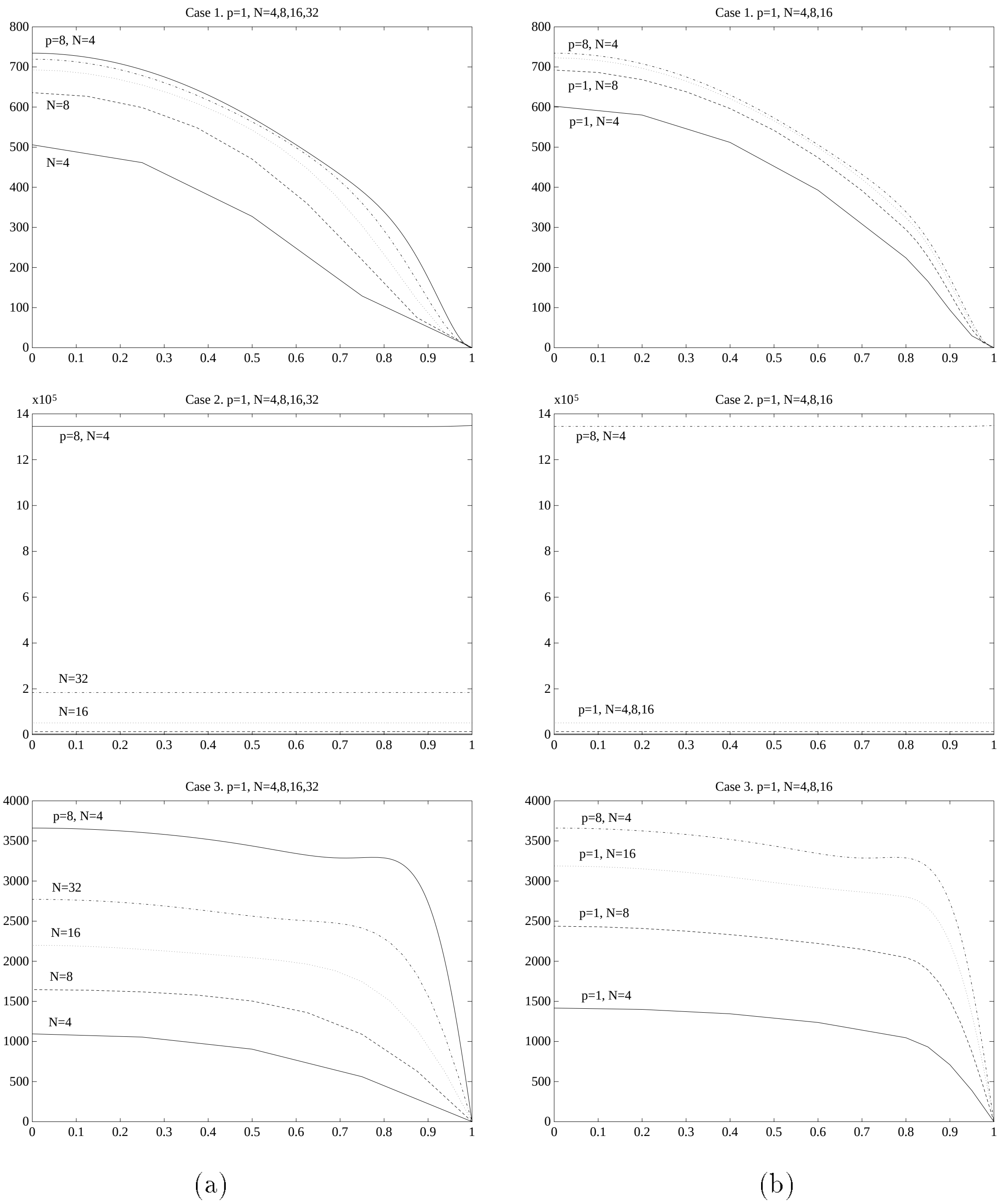

Figure 10: Convergence of the transverse deflection profiles at $t = 0.01$ using bilinear elements with (a) uniform and (b) refined grids. Scaling factor P_0R/E.

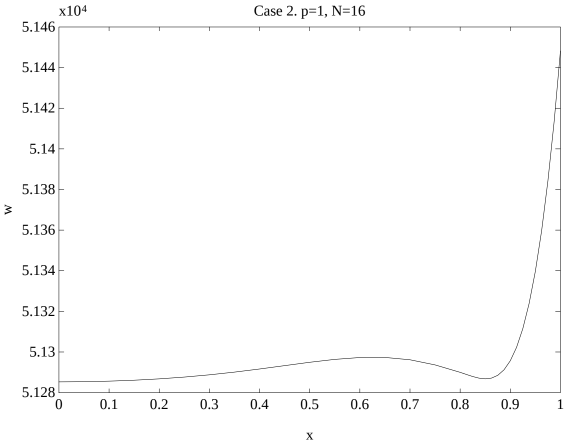

Figure 11: Zoom of the transverse deflection profile in Case 2 at $t = 0.01$ using bilinear elements and a refined grid ($N = 16$). Scaling factor P_0R/E.

$t^{-3/4}h_0 \sim 0.5$ on our finest refined grid.

In Case 2, the bilinear scheme fails completely. Even with the finest mesh, the error is about 90%. This is obvious due to the dominating smooth component as predicted by (7.12). Indeed, as the magnified scale in Fig. 11 reveals, the layer behaviour with the finest refined grid is qualitatively correct, but the global error remains about as large as for the uniform grid.

In Case 3 we finally see the error behaviour "of the third kind". This is qualitatively similar to Case 1, but now the error remains fairly large, and the mesh refinement does not seem to help as much as in Case 1. Partly this is expected since the boundary layer error now grows faster as $t \to 0$, according to estimate (7.12). However, the convergence of the transverse deflection remains slow even at $x = 0$, and this cannot be a boundary layer effect. To explain this phenomenon, we first have to look at the expansion of the smooth component $\underline{u}^s$ in more detail.

We have seen that the leading term in the expansion of $\underline{u}^s$ is a membrane-dominated deformation in the energy scale. However, as shown by Appendices B.3.1 and D.3, the contribution of this leading term to w^s at $x = 0$ is of relative order $O(\sqrt{t})$ only. Instead, the leading part of $w^s(0)$ is due to

$$\underline{u}^0 = (0, v^0, w^0, 0, \phi^0) = \frac{cP_0R}{Et^{3/2}}(0, -\frac{1}{2}\sin 2\alpha, \cos 2\alpha, 0, -2\sin 2\alpha),\ c = 2.8752439$$

which is purely inextensional and therefore has small energy. Note that it is this component that determines the asymptotic profile of the transverse deflection as $t \to 0$.

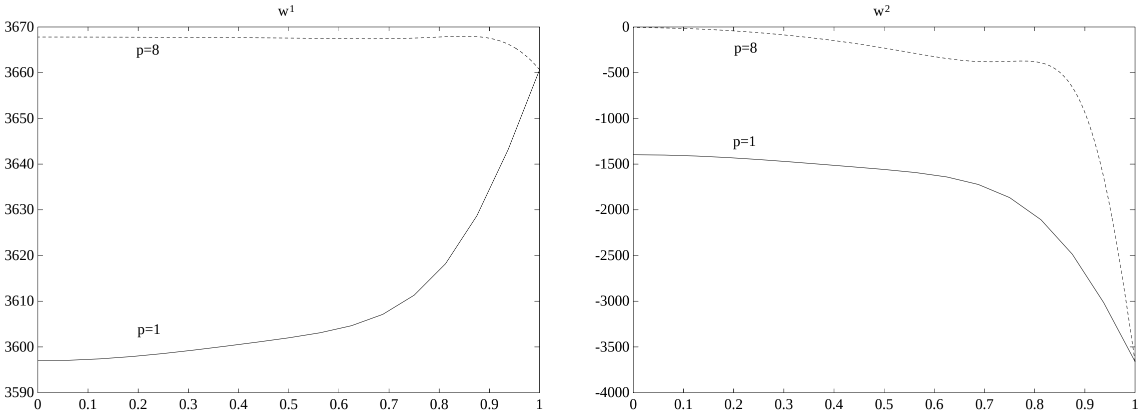

Figure 12: The maximum transverse deflections w^1 and w^2 and their bilinear approximations with $N = 10$ (refined grid) in Case 3. Scaling factor P_0R/E.

We may now understand the error behaviour by splitting the exact solution (at $t = 0.01$) as $\underline{u} = \underline{u}^1 + \underline{u}^2$, where $\underline{u}^1$ is the displacement field that results from zero load together with the constraint $w^1 = w^0$ at $x = 1$. In this splitting, both $\underline{u}^1$ and $\underline{u}^2$ have a boundary layer, but the layer of $\underline{u}^1$ is relatively weak. In Fig. 12 we show the transverse deflections w^1 and w^2 and their bilinear finite element approximations w_h^1 and w_h^2, as obtained with the refined 20×10 grid ($N = 10$). As is seen, the overall error of the transverse deflection is mainly due to the component $\underline{u}^2$. The slow convergence here may be understood as an effect caused by the kinematical constraint at $x = 1$ together with numerical overstiffness (locking). In fact, there is severe locking in approximating $\underline{u}^1$ as well, as seen from the total deformation energy associated to $\underline{u}_h^1$. This is too large by a factor over 10. Also, the deformation state corresponding to $\underline{u}_h^1$ is membrane-dominated, as opposed to its exact counterpart which is nearly inextensional. Why such major discrepancies are not reflected more clearly in the convergence of the transverse deflection w_h^1 is apparently because of the incidentally favorable coupling of the kinematical constraint at $x = 1$ with numerical locking in this case.

In Figs. 13 and 14 we finally show how higher-order elements perform in the three benchmark problems. We have here computed with p ranging from 1 to 8 and with N simultaneously decreasing so that $N(p) = 16/p$. The total number of degrees of freedom is then roughly the same in each numerical model. The refined grid is used throughout these computations, and the parameters k, ν and t are set as before.

In Fig. 13 we show the transverse deflection profiles in the three cases. In contrast to the bilinear scheme where only N was varied, we now observe fast convergence as p goes up. In fact, in Cases 1 and 3 we obtain practically the exact deformation profile already at $p = 2$, and in Case 2 this is achieved at $p = 4$. Convergence in the energy scale is likewise fast, as seen from the energy distributions shown in Fig. 14.

In summary of the numerical experiments, we conclude that the three benchmark problems are indeed seen as three quite different problems by low-order finite element schemes. The accuracy varies between fairly good (Case 1), fair (Case 3) and extremely poor (Case 2). As we have seen, this reflects the fundamentally different asymptotics of these problems at $t = 0$. On the other hand, we also conclude from the experiments that finite element approximations of higher order ($p \geq 4$ in our model cases) perform well in all the three cases. From this comparison we may draw the more general conjecture that raising the order of the elements is a more effective way of improving the accuracy of finite element approximations to shell problems than refining the grid at a fixed, low order. This conclusion is supported as well by theoretical error analysis. For example, the theoretical approximation error of the smooth component in Case 2 behaves as [22]

$$\frac{|||\underline{u}^s - \underline{u}_h^s|||}{|||\underline{u}^s|||} \sim \min\left\{h^{p-2}, \frac{h^p}{t}\right\},$$

so $p = 3$ is a threshold value at which the convergence becomes uniform with respect to t. (For a more general axially varying load, the threshold value for uniform convergence is $p = 4$ [22].)

8 Finite Elements and Shells: The Final Conjecture

We close the paper with a conjecture on the general error behaviour of finite element approximations to shell problems. Hence assume now that we have a general shell of thickness d and a standard finite element scheme, based on the R-model of the shell, where each component of the displacement field is approximated by (triangular or quadrilateral) elements of degree p. Suppose further that we want to resolve a component $\underline{u}^L$ of the displacement field which is (piecewise) smooth in a characteristic length scale L. Then our conjecture is the following: The relative approximation error of $\underline{u}^L$ in the energy norm behaves as

$$\frac{|||\underline{u}^L - \underline{u}_h^L|||}{|||\underline{u}^L|||} \sim \begin{cases} (h/L)^p & \text{in the “best” cases,} \\ (L/d)(h/L)^p & \text{in the “worst” cases.} \end{cases} \tag{8.1}$$

As an example of the “best” and the “worst” error behaviour, we may mention the approximation of the smooth component of the displacement field in Case 1 and Case 2 above, respectively. As to these model problems, it can further be

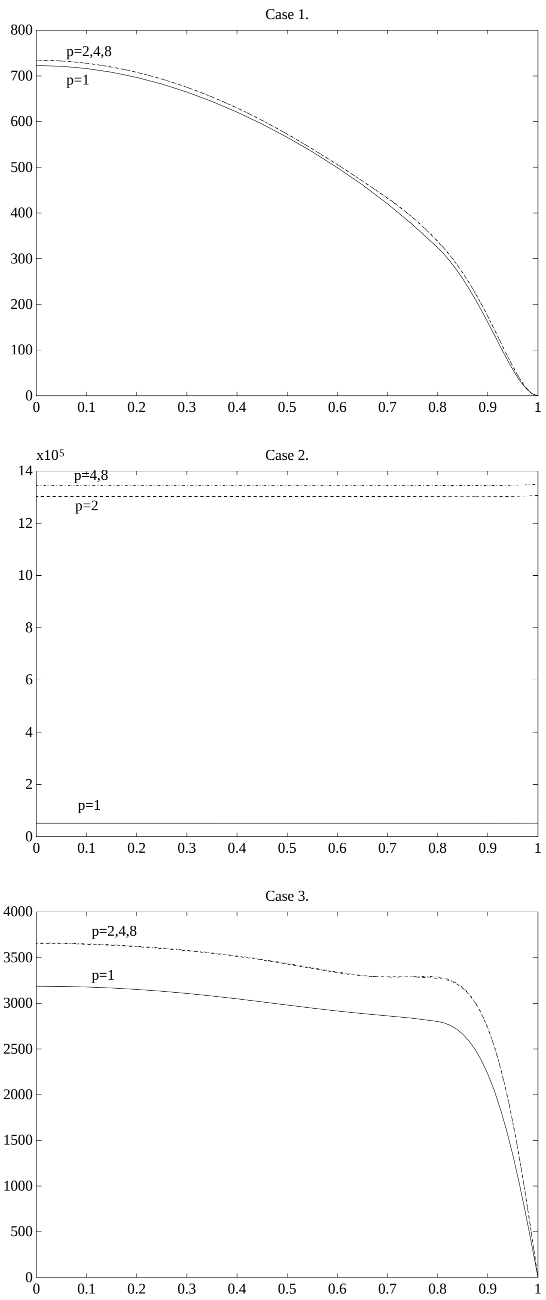

Figure 13: Convergence of the axial transverse deflection profiles at $t = 0.01$ with respect to p. ($N(p) = 16/p$). Scaling factor P_0R/E.

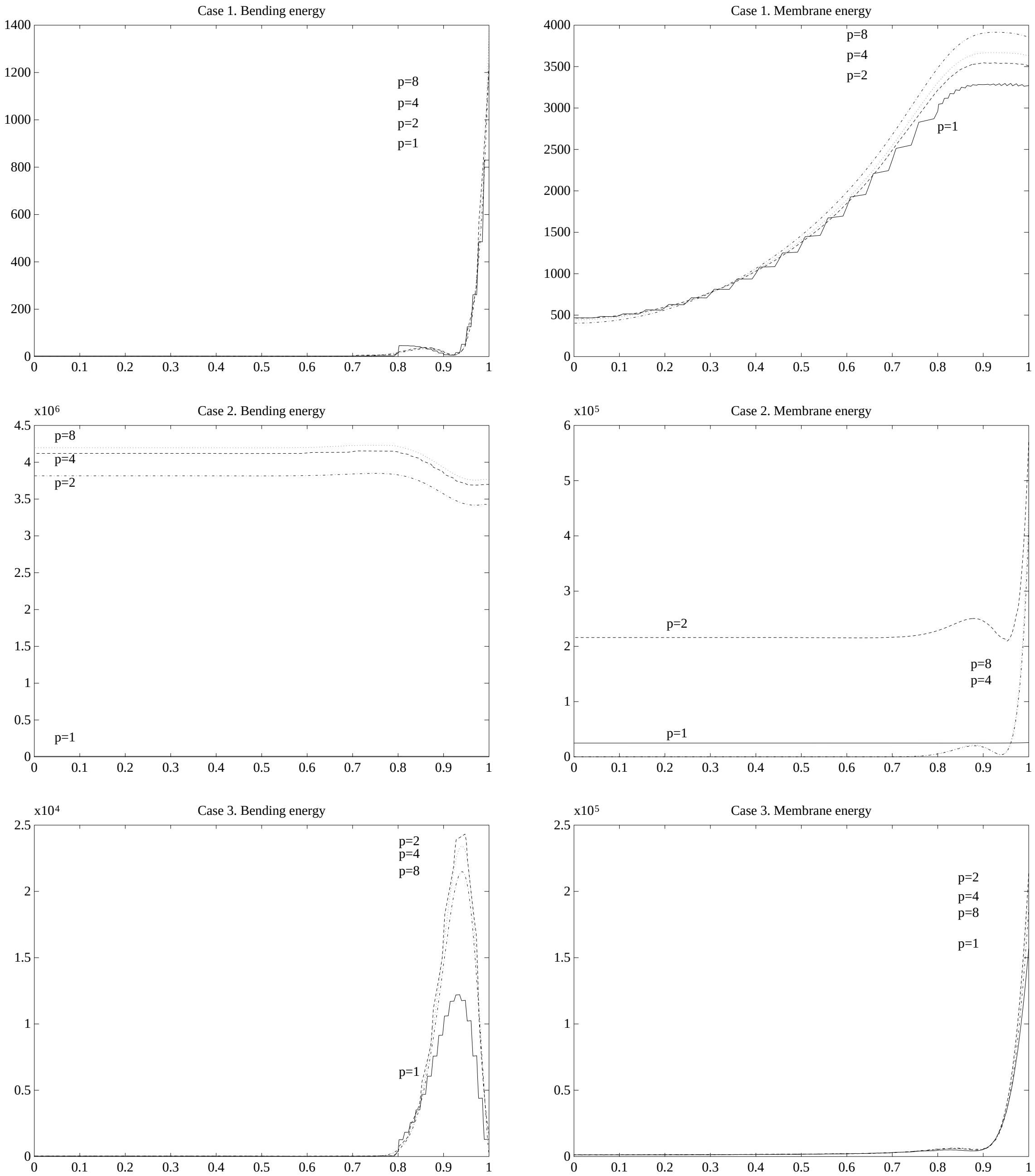

Figure 14: Convergence of the energy density at $t = 0.01$ with respect to p. ($N(p) = 16/p$). Scaling factor $\frac{P_0^2 R^2}{E(1-\nu^2)}$.

shown that the resolution of the $\sqrt{t}$-scale boundary layers follows the worst-case error behaviour in (8.1), i.e., the error behaves as $t^{-1/2}(h/\sqrt{t})^p$.

The estimate (8.1) clearly suggests the use of higher-order elements in case of the worst error behaviour if the locking factor L/d is large. Indeed, the estimates indicate that to achieve given accuracy with $p = 1$, one requires in the "worst" cases a mesh *overrefinement* by factor L/d as compared with the "best" cases. At higher values of p, it suffices to impose overrefinement by factor $(L/d)^{1/p}$ only. By this very simple reasoning, we may conclude that high-order elements are preferable in the standard finite element approximation of shell problems.

We should finally emphasize that our conjectures are limited to *standard* finite element approximations. Obviously there is another path to be explored as well. This is the path of "underintegration", "mixed interpolation" or other numerical ways to modify the energy so as to make the low-order methods work better. Such techniques may be understood as somewhat a compromise between finite element and finite difference thinking. In the plate bending problem, methodology of that kind is in fact now dominating. Even in shell problems, various proposals for "simple and efficient" shell elements have been made, and presumably various technical "secrets" are hidden in commercial computer codes. Yet, the overall state of the art of finite element modelling of shells is a confusion. The message we want to leave is that this is not an unnatural state. It simply reflects the actual plurality involved in the mathematical concept "shell problem".

A Benchmark Values of the Total Deformation Energy

A.1 Case 1

Scaling factor $\dfrac{12P_0^2R^3}{E(1-\nu^2)t}$.

t	Model	Energy
0.1	3D.4	1.997095836008921
	3D.3	1.995659357661373
	3D.2	1.987716337870460
	R	1.828629366566552
	K	1.778293158259208
0.01	3D.4	2.712475376686962
	3D.3	2.712412217501980
	3D.2	2.712229353625928
	R	2.688287959059254
	K	2.687377447673403
0.001	3D.4	2.799119958015472
	3D.3	2.799116802208452
	3D.2	2.799110536380933
	R	2.796612585420251
	K	2.796592819291059
Asymptotic		2.827433388230813

A.2 Case 2

Scaling factor $\dfrac{12P_0^2R^3}{E(1-\nu^2)t^3}$.

t	Model	Energy
0.1	3D.4	0.797735329293354
	3D.3	0.797729869837748
	3D.2	0.795873435421535
	R	0.725874419060530
	K	0.717945967744515
0.01	3D.4	0.711366966830005
	3D.3	0.711366965414426
	3D.2	0.711348511198255
	R	0.704331198817278
	K	0.704242080729323
0.001	3D.4	0.700756984446991
	3D.3	0.700756984443942
	3D.2	0.700756763952115
	R	0.700057056738260
	K	0.700055893395436
Asymptotic		0.698131700797732

A.3 Case 3

Scaling factor $\dfrac{12P_0^2R^3}{E(1-\nu^2)t^{3/2}}$

t	Model	Energy
0.1	3D.4	1.814760587639248
	3D.3	1.814579387322102
	3D.2	1.807510399433229
	R	1.662063771883397
	K	1.611992719420558
0.01	3D.4	1.724413743629826
	3D.3	1.724408013716278
	3D.2	1.723875412211085
	R	1.708129049442806
	K	1.704217314802134
0.001	3D.4	1.576333693216199
	3D.3	1.576333527124537
	3D.2	1.576287317312046
	R	1.574825187982601
	K	1.574489891909070
Asymptotic		1.500360287048183

B The Displacements According to the K-model

B.1 Case 1

Scaling factors $\dfrac{12P_0R}{Et}$ for u, v, w and $\dfrac{12P_0}{Et}$ for θ, ϕ.

B.1.1 Smooth Component

$$\begin{aligned} u^s &= (0.0625\,x - 0.0625\,x^3) - 0.03260593\,x\,\sqrt{t} - 0.09213937\,x\,t \\ &\quad +0.05854513\,x\,t^{\frac{3}{2}} + (-0.62189781\,x + 0.68098958\,x^3 - 0.04921875\,x^5 \\ &\quad +0.00100446\,x^7)\,t^2 + (-0.00658607\,x - 0.06113612\,x^3 \\ &\quad +0.00366817\,x^5)\,t^{\frac{5}{2}} + \mathrm{O}(t^3) \end{aligned}$$

$$\begin{aligned} v^s &= (-0.28125 + 0.3125\,x^2 - 0.03125\,x^4) + (0.03260593 - 0.03260593\,x^2)\,\sqrt{t} \\ &\quad +(0.27074800 - 0.09213937\,x^2)\,t + (0.93536636 + 0.05854513\,x^2)\,t^{\frac{3}{2}} \\ &\quad +(2.95498485 - 3.81460614\,x^2 + 0.69986979\,x^4 - 0.02578125\,x^6 \\ &\quad +0.00025112\,x^8)\,t^2 + (-2.26168797 + 0.27056433\,x^2 - 0.05502250\,x^4 \end{aligned}$$

$$+0.00122272\,x^6)\,t^{\frac{5}{2}} + \mathrm{O}(t^3)$$

$$\begin{aligned}
w^s \;=\;& (0.625 - 0.5625\,x^2 + 0.0625\,x^4) + (-0.05434321 + 0.06521186\,x^2)\,\sqrt{t} \\
& +(-0.51078287 + 0.18427874\,x^2)\,t + (-1.89024777 - 0.11709027\,x^2)\,t^{\frac{3}{2}} \\
& +(-7.04989265 + 7.88572271\,x^2 - 1.38020833\,x^4 + 0.04921875\,x^6 \\
& -0.00050223\,x^8)\,t^2 + (4.64512637 - 0.54520440\,x^2 + 0.10393140\,x^4 \\
& -0.00244544\,x^6)\,t^{\frac{5}{2}} + \mathrm{O}(t^3)
\end{aligned}$$

$$\begin{aligned}
\theta^s \;=\;& (-1.125\,x + 0.25\,x^3) + 0.13042372\,x\,\sqrt{t} + 0.36855748\,x\,t \\
& -0.23418054\,x\,t^{\frac{3}{2}} + (15.77144541\,x - 5.52083333\,x^3 + 0.2953125\,x^5 \\
& -0.00401786\,x^7)\,t^2 + (-1.09040879\,x + 0.41572559\,x^3 \\
& -0.01467267\,x^5)\,t^{\frac{5}{2}} + \mathrm{O}(t^3)
\end{aligned}$$

$$\begin{aligned}
\phi^s \;=\;& (-0.96875 + 0.8125\,x^2 - 0.09375\,x^4) + (0.07608050 - 0.09781779\,x^2)\,\sqrt{t} \\
& +(0.75081775 - 0.27641811\,x^2)\,t + (2.84512917 + 0.17563540\,x^2)\,t^{\frac{3}{2}} \\
& +(11.14480046 - 11.95683927\,x^2 + 2.06054687\,x^4 - 0.07265625\,x^6 \\
& +0.00075335\,x^8)\,t^2 + (-7.02856476 + 0.81984447\,x^2 - 0.15284029\,x^4 \\
& +0.00366817\,x^6)\,t^{\frac{5}{2}} + \mathrm{O}(t^3)
\end{aligned}$$

B.1.2 The $\sqrt{t}$-scale Boundary Layers

$$\begin{aligned}
u:\;\; C(t) =\;& 0.03260593\,\sqrt{t} + 0.09213937\,t - 0.05854513\,t^{\frac{3}{2}} \\
& -0.01087749\,t^2 + 0.06405402\,t^{\frac{5}{2}} + \mathrm{O}(t^3) \\
S(t) =\;& -0.08930431\,t + 0.13311315\,t^{\frac{3}{2}} + 0.37615741\,t^2 \\
& -0.23900951\,t^{\frac{5}{2}} + \mathrm{O}(t^3)
\end{aligned}$$

$$\begin{aligned}
v:\;\; C(t) =\;& -0.17860863\,t - 0.99391150\,t^{\frac{3}{2}} + 0.18528164\,t^2 \\
& +2.04492342\,t^{\frac{5}{2}} + \mathrm{O}(t^3) \\
S(t) =\;& -0.17860863\,t - 0.01552987\,t^{\frac{3}{2}} + 0.45611497\,t^2 \\
& +2.81025703\,t^{\frac{5}{2}} + \mathrm{O}(t^3)
\end{aligned}$$

$$\begin{aligned}
w:\;\; C(t) =\;& -0.125 - 0.01086864\,\sqrt{t} + 0.32650413\,t \\
& +2.00733804\,t^{\frac{3}{2}} + 0.49566176\,t^2 - 4.20140792\,t^{\frac{5}{2}} + \mathrm{O}(t^3) \\
S(t) =\;& 0.125 + 0.69559315\,\sqrt{t} - 0.12237999\,t \\
& -1.43051440\,t^{\frac{3}{2}} - 0.86217411\,t^2 - 8.78638051\,t^{\frac{5}{2}} + \mathrm{O}(t^3)
\end{aligned}$$

$$
\begin{aligned}
\theta: \quad C(t) = {} & 0.875 - 0.13042372\sqrt{t} - 0.36855748\,t + 0.23418054\,t^{\frac{3}{2}} \\
& -10.54190672\,t^2 + 0.68935587\,t^{\frac{5}{2}} + \mathrm{O}(t^3) \\
S(t) = {} & 0.31947155\,t^{-\frac{1}{2}} + 0.90277778 - 0.57362282\sqrt{t} - 3.32153245\,t \\
& -1.16942886\,t^{\frac{3}{2}} - 4.26040426\,t^2 + 5.59607973\,t^{\frac{5}{2}} + \mathrm{O}(t^3)
\end{aligned}
$$

$$
\begin{aligned}
\phi: \quad C(t) = {} & 0.25 + 0.02173729\sqrt{t} - 0.47439963\,t \\
& -3.02076458\,t^{\frac{3}{2}} - 1.17660516\,t^2 + 6.35789242\,t^{\frac{5}{2}} + \mathrm{O}(t^3) \\
S(t) = {} & -0.25 - 1.39118629\sqrt{t} + 0.42336860\,t \\
& +2.87655867\,t^{\frac{3}{2}} + 1.26823325\,t^2 + 14.76250400\,t^{\frac{5}{2}} + \mathrm{O}(t^3)
\end{aligned}
$$

B.2 Case 2

Scaling factors $\dfrac{12P_0R}{Et^3}$ for u, v, w and $\dfrac{12P_0}{Et^3}$ for θ, ϕ.

B.2.1 Smooth Component

$$
u^s = -0.03125\,x\,t^2 + (-0.01630296\,x + 0.00543432\,x^3)\,t^{\frac{5}{2}} + \mathrm{O}(t^3)
$$

$$
\begin{aligned}
v^s = {} & -0.05555556 - 0.00483051\sqrt{t} - 0.00042001\,t \\
& +0.00193553\,t^{\frac{3}{2}} + (-0.00776209 - 0.03125\,x^2)\,t^2 \\
& +(0.04609529 - 0.03804025\,x^2 + 0.00271716\,x^4)\,t^{\frac{5}{2}} + \mathrm{O}(t^3)
\end{aligned}
$$

$$
\begin{aligned}
w^s = {} & 0.11111111 + 0.00966102\sqrt{t} + 0.00084002\,t \\
& -0.00387105\,t^{\frac{3}{2}} + (-0.00183693 + 0.0625\,x^2)\,t^2 \\
& +(-0.09641728 + 0.07064618\,x^2 - 0.00543432\,x^4)\,t^{\frac{5}{2}} + \mathrm{O}(t^3)
\end{aligned}
$$

$$
\theta^s = 0.125\,x\,t^2 + (0.14129236\,x - 0.02173729\,x^3)\,t^{\frac{5}{2}} + \mathrm{O}(t^3)
$$

$$
\begin{aligned}
\phi^s = {} & -0.16666667 - 0.01449152\sqrt{t} - 0.00126003\,t \\
& +0.00580658\,t^{\frac{3}{2}} + (0.01143595 - 0.09375\,x^2)\,t^2 \\
& +(0.14673927 - 0.10325211\,x^2 + 0.00815148\,x^4)\,t^{\frac{5}{2}} + \mathrm{O}(t^3)
\end{aligned}
$$

B.2.2 The $\sqrt{t}$-scale Boundary Layers

$$
u: \quad C(t) = 0.02898305\,t^{\frac{5}{2}} + 0.00252005\,t^3 - 0.01161316\,t^{\frac{7}{2}} + \mathrm{O}(t^4)
$$

$$
\begin{aligned}
S(t) = &\ -0.00887421\,t^{\frac{3}{2}} - 0.00077160\,t^2 + 0.00355579\,t^{\frac{5}{2}} + \mathrm{O}(t^3)
\end{aligned}
$$

$$
\begin{aligned}
v: \ C(t) = &\ -0.04861111\,t^2 - 0.00422669\,t^{\frac{5}{2}} + 0.09602445\,t^3 + \mathrm{O}(t^{\frac{7}{2}}) \\
S(t) = &\ 0.04861111\,t^2 + 0.00422669\,t^{\frac{5}{2}} + 0.05706866\,t^3 + \mathrm{O}(t^{\frac{7}{2}})
\end{aligned}
$$

$$
\begin{aligned}
w: \ C(t) = &\ 0.03402069\,t + 0.00295807\,t^{\frac{3}{2}} + 0.04192387\,t^2 \\
&+0.00243762\,t^{\frac{5}{2}} + \mathrm{O}(t^3) \\
S(t) = &\ 0.03402069\,t + 0.00295807\,t^{\frac{3}{2}} - 0.06918724\,t^2 \\
&-0.00722340\,t^{\frac{5}{2}} + \mathrm{O}(t^3)
\end{aligned}
$$

$$
\begin{aligned}
\theta: \ C(t) = &\ 0.08694914\,\sqrt{t} + 0.00756015\,t - 0.03483949\,t^{\frac{3}{2}} \\
&-0.00611568\,t^2 - 0.11854375\,t^{\frac{5}{2}} + \mathrm{O}(t^3) \\
S(t) = &\ -0.03549684\,t^{\frac{3}{2}} - 0.00308642\,t^2 + 0.01422316\,t^{\frac{5}{2}} + \mathrm{O}(t^3)
\end{aligned}
$$

$$
\begin{aligned}
\phi: \ C(t) = &\ -0.06804138\,t - 0.00591614\,t^{\frac{3}{2}} - 0.03523663\,t^2 \\
&-0.00064854\,t^{\frac{5}{2}} + \mathrm{O}(t^3) \\
S(t) = &\ -0.06804138\,t - 0.00591614\,t^{\frac{3}{2}} + 0.08976337\,t^2 \\
&+0.01022010\,t^{\frac{5}{2}} + \mathrm{O}(t^3)
\end{aligned}
$$

B.3 Case 3

Scaling factors $\dfrac{12P_0R}{Et}$ for u, v, w and $\dfrac{12P_0}{Et}$ for θ, ϕ.

B.3.1 Smooth Component

$$
\begin{aligned}
u^s \ = &\ (0.15625\,x - 0.0625\,x^3) + (-0.85358805\,x + 0.13477706\,x^3)\,t^{\frac{3}{2}} \\
&+(-2.21276042\,x + 0.80403646\,x^3 - 0.05976563\,x^5 + 0.00100446\,x^7)\,t^2 \\
&+(0.87118966\,x - 0.13755626\,x^3)\,t^{\frac{5}{2}} + \mathrm{O}(t^3)
\end{aligned}
$$

$$
\begin{aligned}
v^s \ = &\ -0.11980183\,t^{-\frac{1}{2}} + (-0.328125 + 0.40625\,x^2 - 0.03125\,x^4) + 0.12227223\,\sqrt{t} \\
&+0.37794861\,t + (3.20819323 - 1.39269630\,x^2 + 0.06738853\,x^4)\,t^{\frac{3}{2}} \\
&+(4.44607050 - 5.99140625\,x^2 + 0.83170573\,x^4 - 0.02929688\,x^6 \\
&+0.00025112\,x^8)\,t^2 + (-5.00309956 + 1.42141471\,x^2 \\
&-0.06877813\,x^4)\,t^{\frac{5}{2}} + \mathrm{O}(t^3)
\end{aligned}
$$

$$
\begin{aligned}
w^s \;=\;& 0.23960366\,t^{-\frac{1}{2}} + (0.6875 - 0.75\,x^2 + 0.0625\,x^4) - 0.24454447\,\sqrt{t} \\
& -0.75589723\,t + (-6.37146077 + 2.65061553\,x^2 - 0.13477706\,x^4)\,t^{\frac{3}{2}} \\
& +(-9.75177641 + 12.30377604\,x^2 - 1.62630208\,x^4 + 0.05625\,x^6 \\
& -0.00050223\,x^8)\,t^2 + (9.96034703 - 2.70527315\,x^2 \\
& +0.13755626\,x^4)\,t^{\frac{5}{2}} + \mathrm{O}(t^3)
\end{aligned}
$$

$$
\begin{aligned}
\theta^s \;=\;& (-1.5\,x + 0.25\,x^3) + (5.30123107\,x - 0.53910824\,x^3)\,t^{\frac{3}{2}} \\
& +(24.60755208\,x - 6.50520833\,x^3 + 0.3375\,x^5 - 0.00401786\,x^7)\,t^2 \\
& +(-5.41054630\,x + 0.55022505\,x^3)\,t^{\frac{5}{2}} + \mathrm{O}(t^3)
\end{aligned}
$$

$$
\begin{aligned}
\phi^s \;=\;& -0.35940550\,t^{-\frac{1}{2}} + (-1.046875 + 1.09375\,x^2 - 0.09375\,x^4) + 0.36681670\,\sqrt{t} \\
& +1.13384584\,t + (9.53472831 - 3.90853477\,x^2 + 0.20216559\,x^4)\,t^{\frac{3}{2}} \\
& +(15.05748233 - 18.61614583\,x^2 + 2.42089844\,x^4 - 0.08320313\,x^6 \\
& +0.00075335\,x^8)\,t^2 + (-14.91759450 + 3.98913160\,x^2 \\
& -0.20633439\,x^4)\,t^{\frac{5}{2}} + \mathrm{O}(t^3)
\end{aligned}
$$

B.3.2 The $\sqrt{t}$-scale Boundary Layers

$$
\begin{aligned}
u: \; C(t) =\;& 0.03125 - 0.11163039\,t - 0.06738853\,t^{\frac{3}{2}} \\
& +0.04401042\,t^2 + 0.53239368\,t^{\frac{5}{2}} + \mathrm{O}(t^3) \\
S(t) =\;& 0.03125 + 0.04784160\,t - 0.12978532\,t^{\frac{3}{2}} \\
& -0.11875\,t^2 + 0.02929439\,t^{\frac{5}{2}} + \mathrm{O}(t^3)
\end{aligned}
$$

$$
\begin{aligned}
v: \; C(t) =\;& -0.78370365\,t^{\frac{3}{2}} - 0.34179688\,t^2 + 0.79986419\,t^{\frac{5}{2}} + \mathrm{O}(t^3) \\
S(t) =\;& -0.34236225\,\sqrt{t} + 0.34942201\,t^{\frac{3}{2}} + 1.08007812\,t^2 \\
& +5.77817815\,t^{\frac{5}{2}} + \mathrm{O}(t^3)
\end{aligned}
$$

$$
\begin{aligned}
w: \; C(t) =\;& -0.23960366\,t^{-\frac{1}{2}} + 0.24454447\,\sqrt{t} + 0.75589723\,t \\
& +3.85562229\,t^{\frac{3}{2}} - 0.98144531\,t^2 - 7.39263014\,t^{\frac{5}{2}} + \mathrm{O}(t^3) \\
S(t) =\;& 0.56245227\,\sqrt{t} + 0.23920798\,t - 0.57405045\,t^{\frac{3}{2}} \\
& -1.77441406\,t^2 - 11.01326380\,t^{\frac{5}{2}} + \mathrm{O}(t^3)
\end{aligned}
$$

$$
\begin{aligned}
\theta: \; C(t) =\;& -0.30618622\,t^{-1} + 0.65625 + 1.27163122\,\sqrt{t} + 3.45990426\,t \\
& -2.71301232\,t^{\frac{3}{2}} - 15.09368490\,t^2 - 27.65420900\,t^{\frac{5}{2}} + \mathrm{O}(t^3) \\
S(t) =\;& 0.30618622\,t^{-1} + 0.03125 - 0.66027006\,\sqrt{t} - 4.16158101\,t
\end{aligned}
$$

$$+0.54409999\,t^{\frac{3}{2}} + 1.52154948\,t^2 + 25.32313983\,t^{\frac{5}{2}} + \mathrm{O}(t^3)$$

$$\begin{aligned}\phi:\quad C(t) = {}& 0.47920733\,t^{-\frac{1}{2}} - 0.48908893\,\sqrt{t} - 1.51179445\,t \\ & -6.92754094\,t^{\frac{3}{2}} + 2.3046875\,t^2 + 13.98539610\,t^{\frac{5}{2}} + \mathrm{O}(t^3) \\ S(t) = {}& -0.78254229\,\sqrt{t} - 0.47841597\,t + 0.79867888\,t^{\frac{3}{2}} \\ & +2.46875\,t^2 + 16.24834945\,t^{\frac{5}{2}} + \mathrm{O}(t^3)\end{aligned}$$

C The Gap of R- and K-models for the Displacements

C.1 Case 1

Scaling factors $\dfrac{12P_0R}{Et}$ for u, v, w and $\dfrac{12P_0}{Et}$ for θ, ϕ.

C.1.1 Smooth Component

$$\begin{aligned}u^s &= 0.01996697\,x\,t^{\frac{3}{2}} + \mathrm{O}(t^2)\\ v^s &= (-0.01996697 + 0.01996697\,x^2)\,t^{\frac{3}{2}} + \mathrm{O}(t^2)\\ w^s &= (0.03327829 - 0.03993394\,x^2)\,t^{\frac{3}{2}} + \mathrm{O}(t^2)\\ \theta^s &= -0.07986789\,x\,t^{\frac{3}{2}} + \mathrm{O}(t^2)\\ \phi^s &= (-0.04658960 + 0.05990092\,x^2)\,t^{\frac{3}{2}} + \mathrm{O}(t^2)\end{aligned}$$

C.1.2 The $\sqrt{t}$-scale Boundary Layers

$$\begin{aligned}u:\quad C(t,x) = {}& -0.00850517\,x\,t - 0.01996697t^{\frac{3}{2}} + \mathrm{O}(t^2)\\ S(t,x) = {}& -0.00850517\,x\,t + 0.01331131\,t^{\frac{3}{2}} + \mathrm{O}(t^2)\end{aligned}$$

$$\begin{aligned}v:\quad C(t,x) = {}& 0.14583333\,t^2 + \mathrm{O}(t^{\frac{5}{2}})\\ S(t,x) = {}& 0.09317920\,x\,t^{\frac{3}{2}} + 0.07291667\,t^2 + \mathrm{O}(t^{\frac{5}{2}})\end{aligned}$$

$$\begin{aligned}w:\quad C(t,x) = {}& 0.06521186\,x\,\sqrt{t} + \mathrm{O}(t^{\frac{3}{2}})\\ S(t,x) = {}& -0.15309311\,t + \mathrm{O}(t^{\frac{3}{2}})\end{aligned}$$

$$\begin{aligned}\theta:\quad C(t,x) = {}& 0.08333333\,x + \mathrm{O}(t)\\ S(t,x) = {}& -0.08333333\,x - 0.19563557\,\sqrt{t} + \mathrm{O}(t)\end{aligned}$$

$$\begin{aligned} \phi: \quad C(t,x) &= -0.13042372\, x\sqrt{t} - 0.20412415\, t + \mathrm{O}(t^{\frac{3}{2}}) \\ S(t,x) &= 0.10206207\, t + \mathrm{O}(t^{\frac{3}{2}}) \end{aligned}$$

C.1.3 The t-scale Boundary Layers

$$\begin{aligned} u: \quad K(t) &= -0.01309457\, t^4 - 0.07286795\, t^{\frac{9}{2}} + 0.07117881\, t^5 + \mathrm{O}(t^{\frac{11}{2}}) \\ v: \quad K(t) &= 0.03402069\, t^3 + 0.18931648\, t^{\frac{7}{2}} - 0.18492798\, t^4 + \mathrm{O}(t^{\frac{9}{2}}) \\ w: \quad K(t) &= 0.01827037\, t^5 + 0.10166996\, t^{\frac{11}{2}} - 0.09931318\, t^6 + \mathrm{O}(t^{\frac{13}{2}}) \\ \theta: \quad K(t) &= -0.11785113\, t^2 - 0.65581151\, t^{\frac{5}{2}} + 0.64060933\, t^3 + \mathrm{O}(t^{\frac{7}{2}}) \\ \phi: \quad K(t) &= 0.20412415\, t + 1.13589885\, t^{\frac{3}{2}} - 1.10956790\, t^2 \\ & \quad -3.04368965\, t^{\frac{5}{2}} + \mathrm{O}(t^3) \end{aligned}$$

C.2 Case 2

Scaling factors $\dfrac{12P_0R}{Et^3}$ for u, v, w and $\dfrac{12P_0}{Et^3}$ for θ, ϕ.

C.2.1 Smooth Component

$$\begin{aligned} u^s &= (-0.04097791\, x + 0.00110928\, x^3)\, t^{\frac{7}{2}} + \mathrm{O}(t^4) \\ v^s &= -0.00098602\, t^{\frac{3}{2}} + \mathrm{O}(t^2) \\ w^s &= 0.00197205\, t^{\frac{3}{2}} + \mathrm{O}(t^2) \\ \theta^s &= \mathrm{O}(t^3) \\ \phi^s &= -0.00295807\, t^{\frac{3}{2}} + \mathrm{O}(t^2) \end{aligned}$$

C.2.2 The $\sqrt{t}$-scale Boundary Layers

$$\begin{aligned} u: \quad C(t,x) &= -0.00231481\, x\, t^2 + \mathrm{O}(t^3) \\ S(t,x) &= 0.00231481\, x\, t^2 - 0.00181144\, t^{\frac{5}{2}} + \mathrm{O}(t^3) \end{aligned}$$

$$\begin{aligned} v: \quad C(t,x) &= 0.02536017\, x\, t^{\frac{5}{2}} + \mathrm{O}(t^{\frac{7}{2}}) \\ S(t,x) &= 0.01984540\, t^3 + \mathrm{O}(t^{\frac{7}{2}}) \end{aligned}$$

$$\begin{aligned} w: \quad C(t,x) &= 0.04159203\, t^{\frac{5}{2}} + \mathrm{O}(t^3) \\ S(t,x) &= -0.01774842\, x\, t^{\frac{3}{2}} + 0.01388889\, t^2 + \mathrm{O}(t^{\frac{5}{2}}) \end{aligned}$$

$$
\begin{aligned}
\theta: \quad C(t,x) &= -0.02268046\, x\, t + 0.01774842\, t^{\frac{3}{2}} + \mathrm{O}(t^2) \\
S(t,x) &= -0.02268046\, x\, t - 0.03549684\, t^{\frac{3}{2}} + \mathrm{O}(t^2)
\end{aligned}
$$

$$
\begin{aligned}
\phi: \quad C(t,x) &= -0.05555556\, t^2 + \mathrm{O}(t^{\frac{5}{2}}) \\
S(t,x) &= 0.03549684\, x\, t^{\frac{3}{2}} + 0.02777778\, t^2 + \mathrm{O}(t^{\frac{5}{2}})
\end{aligned}
$$

C.2.3 The t-scale Boundary Layers

$$
\begin{aligned}
u: \quad K(t) &= -0.00644068\, t^{\frac{9}{2}} - 0.00056001\, t^5 + 0.00126601\, t^{\frac{11}{2}} + \mathrm{O}(t^6) \\
v: \quad K(t) &= 0.01673337\, t^{\frac{7}{2}} + 0.00145495\, t^4 - 0.00328918\, t^{\frac{9}{2}} + \mathrm{O}(t^5) \\
w: \quad K(t) &= 0.00898644\, t^{\frac{11}{2}} + 0.00078136\, t^6 - 0.00176641\, t^{\frac{13}{2}} + \mathrm{O}(t^7) \\
\theta: \quad K(t) &= -0.05796610\, t^{\frac{5}{2}} - 0.00504010\, t^3 + 0.01139405\, t^{\frac{7}{2}} + \mathrm{O}(t^4) \\
\phi: \quad K(t) &= 0.10040022\, t^{\frac{3}{2}} + 0.00872971\, t^2 - 0.01973507\, t^{\frac{5}{2}} + \mathrm{O}(t^3)
\end{aligned}
$$

C.3 Case 3

Scaling factors $\dfrac{12P_0R}{Et}$ for u, v, w and $\dfrac{12P_0}{Et}$ for θ, ϕ.

C.3.1 Smooth Component

$$
\begin{aligned}
u^s &= 0.13258252\, x\, t^2 + \mathrm{O}(t^{\frac{5}{2}}) \\
v^s &= -0.02445445\, \sqrt{t} + \mathrm{O}(t) \\
w^s &= 0.04890889\, \sqrt{t} + \mathrm{O}(t) \\
\theta^s &= (0.93841991\, x - 0.1875\, x^3)\, t^2 + \mathrm{O}(t^{\frac{5}{2}}) \\
\phi^s &= -0.07336334\, \sqrt{t} + \mathrm{O}(t)
\end{aligned}
$$

C.3.2 The $\sqrt{t}$-scale Boundary Layers

$$
\begin{aligned}
u: \quad C(t,x) &= -0.02764181\, x^2\, t + 0.06655657\, x\, t^{\frac{3}{2}} + \mathrm{O}(t^{\frac{5}{2}}) \\
S(t,x) &= -0.01630296\, x\, \sqrt{t} + 0.01275776\, t + \mathrm{O}(t^{\frac{3}{2}})
\end{aligned}
$$

$$
\begin{aligned}
v: \quad C(t,x) &= -0.08930431\, x\, t + \mathrm{O}(t^2) \\
S(t,x) &= 0.08930431\, x\, t - 0.06988440\, t^{\frac{3}{2}} + \mathrm{O}(t^2)
\end{aligned}
$$

$$
\begin{aligned}
w: \quad C(t,x) &= 0.0625\, x - 0.04890889\, \sqrt{t} + \mathrm{O}(t) \\
S(t,x) &= 0.0625\, x - 0.09781779\, \sqrt{t} + \mathrm{O}(t)
\end{aligned}
$$

$$\begin{aligned}\theta: \quad C(t,x) &= \; 0.15973578\, x\, t^{-\frac{1}{2}} + \mathrm{O}(\sqrt{t}) \\ S(t,x) &= \; 0.125 + \mathrm{O}(t)\end{aligned}$$

$$\begin{aligned}\phi: \quad C(t,x) &= \; -0.125\, x + 0.09781779\, \sqrt{t} + \mathrm{O}(t) \\ S(t,x) &= \; -0.125\, x - 0.19563557\, \sqrt{t} + \mathrm{O}(t)\end{aligned}$$

C.3.3 The t-scale Boundary Layers

$$\begin{aligned}u: \quad K(t) &= \; 0.02268046\, t^3 + 0.03472222\, t^4 - 0.06686943\, t^{\frac{9}{2}} + \mathrm{O}(t^5) \\ v: \quad K(t) &= \; -0.05892557\, t^2 - 0.09021098\, t^3 + 0.17373186\, t^{\frac{7}{2}} + \mathrm{O}(t^4) \\ w: \quad K(t) &= \; -0.03164521\, t^4 - 0.04844664\, t^5 + 0.09330045\, t^{\frac{11}{2}} + \mathrm{O}(t^6) \\ \theta: \quad K(t) &= \; 0.20412415\, t + 0.3125\, t^2 - 0.60182483\, t^{\frac{5}{2}} + \mathrm{O}(t^3) \\ \phi: \quad K(t) &= \; -0.35355339 - 0.54126588\, t + 1.04239119\, t^{\frac{3}{2}} \\ & \quad +4.23944889\, t^2 + 1.45368834\, t^{\frac{5}{2}} + \mathrm{O}(t^3)\end{aligned}$$

D The Strains According to the K-model

D.1 Case 1

Scaling factors $\dfrac{12P_0}{Et}$ for the β_{ij} and $\dfrac{12P_0}{ERt}$ for the κ_{ij}.

$$\begin{aligned}\beta_{11}^s &= (0.0625 - 0.1875\, x^2) + \mathrm{O}(\sqrt{t}) \\ C(t,x) &= 0.04166667 + \mathrm{O}(\sqrt{t}) \\ S(t,x) &= -0.04166667 + \mathrm{O}(\sqrt{t})\end{aligned}$$

$$\begin{aligned}\beta_{12}^s &= 0.25\, x + \mathrm{O}(t^2) \\ C(t,x) &= -0.26084743\, \sqrt{t} + \mathrm{O}(t) \\ S(t,x) &= 0.71443451\, t + \mathrm{O}(t^{\frac{3}{2}})\end{aligned}$$

$$\begin{aligned}\beta_{22}^s &= (0.0625 + 0.0625\, x^2) + \mathrm{O}(\sqrt{t}) \\ C(t,x) &= -0.125 + \mathrm{O}(\sqrt{t}) \\ S(t,x) &= 0.125 + \mathrm{O}(\sqrt{t})\end{aligned}$$

$$\begin{aligned}\kappa_{11}^s &= (-1.125 + 0.75\, x^2) + \mathrm{O}(\sqrt{t}) \\ C(t,x) &= 0.40824829\, t^{-1} + \mathrm{O}(t^{-\frac{1}{2}})\end{aligned}$$

$$
\begin{aligned}
S(t,x) &= 0.40824829\,t^{-1} + \mathrm{O}(t^{-\frac{1}{2}})
\end{aligned}
$$

$$
\begin{aligned}
\kappa^s_{12} &= (1.625\,x - 0.375\,x^3) + \mathrm{O}(\sqrt{t}) \\
C(t,x) &= -1.75 + \mathrm{O}(\sqrt{t}) \\
S(t,x) &= -0.63894310\,t^{-\frac{1}{2}} + \mathrm{O}(1)
\end{aligned}
$$

$$
\begin{aligned}
\kappa^s_{22} &= (-1.9375 + 1.625\,x^2 - 0.1875\,x^4) + \mathrm{O}(\sqrt{t}) \\
C(t,x) &= 0.5 + \mathrm{O}(\sqrt{t}) \\
S(t,x) &= -0.5 + \mathrm{O}(\sqrt{t})
\end{aligned}
$$

D.2 Case 2

Scaling factors $\dfrac{12P_0}{Et^3}$ for the β_{ij} and $\dfrac{12P_0}{ERt^3}$ for the κ_{ij}.

$$
\begin{aligned}
\beta^s_{11} &= -0.03125\,t^2 + \mathrm{O}(t^{\frac{5}{2}}) \\
C(t,x) &= -0.01134023\,t + \mathrm{O}(t^{\frac{3}{2}}) \\
S(t,x) &= -0.01134023\,t + \mathrm{O}(t^{\frac{3}{2}})
\end{aligned}
$$

$$
\begin{aligned}
\beta^s_{12} &= -0.02173729\,x\,t^{\frac{5}{2}} + \mathrm{O}(t^3) \\
C(t,x) &= 0.11111111\,x\,t^2 - 0.00724576\,t^{\frac{5}{2}} + \mathrm{O}(t^3) \\
S(t,x) &= 0.07099368\,t^{\frac{3}{2}} + \mathrm{O}(t^2)
\end{aligned}
$$

$$
\begin{aligned}
\beta^s_{22} &= -0.01736111\,t^2 + \mathrm{O}(t^{\frac{5}{2}}) \\
C(t,x) &= 0.03402069\,t + \mathrm{O}(t^{\frac{3}{2}}) \\
S(t,x) &= 0.03402069\,t + \mathrm{O}(t^{\frac{3}{2}})
\end{aligned}
$$

$$
\begin{aligned}
\kappa^s_{11} &= 0.125\,t^2 + \mathrm{O}(t^{\frac{5}{2}}) \\
C(t,x) &= 0.11111111 + \mathrm{O}(\sqrt{t}) \\
S(t,x) &= -0.11111111 + \mathrm{O}(\sqrt{t})
\end{aligned}
$$

$$
\begin{aligned}
\kappa^s_{12} &= -0.1875\,x\,t^2 + \mathrm{O}(t^{\frac{5}{2}}) \\
C(t,x) &= -0.17389829\,\sqrt{t} + \mathrm{O}(t) \\
S(t,x) &= 0.27216553\,x\,t - 0.05324526\,t^{\frac{3}{2}} + \mathrm{O}(t^2)
\end{aligned}
$$

$$
\begin{aligned}
\kappa^s_{22} &= -0.33333333 + \mathrm{O}(\sqrt{t}) \\
C(t,x) &= -0.13608276\,t + \mathrm{O}(t^{\frac{3}{2}})
\end{aligned}
$$

$$S(t,x) = -0.13608276\,t + \mathrm{O}(t^{\frac{3}{2}})$$

D.3 Case 3

Scaling factors $\frac{12P_0}{Et}$ for the β_{ij} and $\frac{12P_0}{ERt}$ for the κ_{ij}.

$$\begin{aligned}
\beta^s_{11} &= (0.15625 - 0.1875\,x^2) + \mathrm{O}(t^{\frac{3}{2}}) \\
C(t,x) &= 0.07986789\,t^{-\frac{1}{2}} + \mathrm{O}(\sqrt{t}) \\
S(t,x) &= -0.125\,x + 0.30160484\,\sqrt{t} + \mathrm{O}(t)
\end{aligned}$$

$$\begin{aligned}
\beta^s_{12} &= 0.25\,x + \mathrm{O}(t^{\frac{3}{2}}) \\
C(t,x) &= -0.25 + \mathrm{O}(t) \\
S(t,x) &= -0.25 + \mathrm{O}(t)
\end{aligned}$$

$$\begin{aligned}
\beta^s_{22} &= (0.03125 + 0.0625\,x^2) + \mathrm{O}(t^{\frac{3}{2}}) \\
C(t,x) &= -0.23960366\,t^{-\frac{1}{2}} + \mathrm{O}(\sqrt{t}) \\
S(t,x) &= 0.375\,x - 0.12227223\,\sqrt{t} + \mathrm{O}(t)
\end{aligned}$$

$$\begin{aligned}
\kappa^s_{11} &= (-1.5 + 0.75\,x^2) + \mathrm{O}(t^{\frac{3}{2}}) \\
C(t,x) &= 1.22474487\,x\,t^{-1} - 0.07986789\,t^{-\frac{1}{2}} + \mathrm{O}(1) \\
S(t,x) &= 0.78254229\,t^{-\frac{3}{2}} + \mathrm{O}(t^{-\frac{1}{2}})
\end{aligned}$$

$$\begin{aligned}
\kappa^s_{12} &= (2.1875\,x - 0.375\,x^3) + \mathrm{O}(t^{\frac{3}{2}}) \\
C(t,x) &= 0.61237244\,t^{-1} + \mathrm{O}(1) \\
S(t,x) &= -0.61237243\,t^{-1} + \mathrm{O}(1)
\end{aligned}$$

$$\begin{aligned}
\kappa^s_{22} &= -0.71881099\,t^{-\frac{1}{2}} + \mathrm{O}(1) \\
C(t,x) &= 0.95841466\,t^{-\frac{1}{2}} + \mathrm{O}(\sqrt{t}) \\
S(t,x) &= -1.5\,x - 1.56508458\,\sqrt{t} + \mathrm{O}(t)
\end{aligned}$$

E The Gap of R- and K-models for the Strains

E.1 Case 1

Scaling factors $\frac{12P_0}{Et}$ for the β_{ij}, ρ_{ij} and $\frac{12P_0}{ERt}$ for the κ_{ij}.

$$\beta^s_{11} = 0.01996697\,t^{\frac{3}{2}} + \mathrm{O}(t^2)$$

$$
\begin{aligned}
C(t,x) &= -0.02173729\,x\,\sqrt{t} + \mathrm{O}(t^{\frac{3}{2}}) \\
S(t,x) &= 0.05103104\,t + \mathrm{O}(t^{\frac{3}{2}}) \\
K(t,x) &= -0.04536092\,t^3 + \mathrm{O}(t^{\frac{7}{2}})
\end{aligned}
$$

$$
\begin{aligned}
\beta^s_{12} &= \mathrm{O}(t^3) \\
C(t,x) &= 0.06804138\,x\,t + 0.15973578\,t^{\frac{3}{2}} + \mathrm{O}(t^2) \\
S(t,x) &= 0.06804138\,x\,t - 0.10649052\,t^{\frac{3}{2}} + \mathrm{O}(t^2) \\
K(t,x) &= 0.05892557\,t^2 + \mathrm{O}(t^{\frac{5}{2}})
\end{aligned}
$$

$$
\begin{aligned}
\beta^s_{22} &= -0.00665566\,t^{\frac{3}{2}} + \mathrm{O}(t^2) \\
C(t,x) &= 0.06521186\,x\,\sqrt{t} + \mathrm{O}(t^{\frac{3}{2}}) \\
S(t,x) &= -0.15309311\,t + \mathrm{O}(t^{\frac{3}{2}}) \\
K(t,x) &= 0.06804138\,t^3 + \mathrm{O}(t^{\frac{7}{2}})
\end{aligned}
$$

$$
\begin{aligned}
\kappa^s_{11} &= -0.07986789\,t^{\frac{3}{2}} + \mathrm{O}(t^2) \\
C(t,x) &= -0.33333333 + \mathrm{O}(\sqrt{t}) \\
S(t,x) &= -0.21298104\,x\,t^{-\frac{1}{2}} - 0.16666667 + \mathrm{O}(\sqrt{t}) \\
K(t,x) &= -0.40824829\,t + \mathrm{O}(t^{\frac{3}{2}})
\end{aligned}
$$

$$
\begin{aligned}
\kappa^s_{12} &= 0.11980183\,x\,t^{\frac{3}{2}} + \mathrm{O}(t^2) \\
C(t,x) &= -0.16666667\,x + \mathrm{O}(t) \\
S(t,x) &= 0.16666667\,x + 0.39127115\,\sqrt{t} + \mathrm{O}(t) \\
K(t,x) &= 0.35355339 + \mathrm{O}(\sqrt{t})
\end{aligned}
$$

$$
\begin{aligned}
\kappa^s_{22} &= (-0.09317920 + 0.11980183\,x^2)\,t^{\frac{3}{2}} + \mathrm{O}(t^2) \\
C(t,x) &= -0.26084743\,x\,\sqrt{t} - 0.40824829\,t + \mathrm{O}(t^{\frac{3}{2}}) \\
S(t,x) &= 0.20412415\,t + \mathrm{O}(t^{\frac{3}{2}}) \\
K(t,x) &= 0.40824829\,t + \mathrm{O}(t^{\frac{3}{2}})
\end{aligned}
$$

$$
\begin{aligned}
\rho^s_1 &= (-1.1875\,x + 0.1875\,x^3)\,t^2 + \mathrm{O}(t^{\frac{5}{2}}) \\
C(t,x) &= -0.26084743\,\sqrt{t} + \mathrm{O}(t) \\
S(t,x) &= 0.71443451\,t + \mathrm{O}(t^{\frac{3}{2}}) \\
K(t,x) &= 0.11785113\,t^2 + \mathrm{O}(t^{\frac{5}{2}})
\end{aligned}
$$

$$
\begin{aligned}
\rho_2^s &= (-1.42708333 + 1.125\,x^2 - 0.09375\,x^4)\,t^2 + \mathrm{O}(t^{\frac{5}{2}}) \\
C(t,x) &= 0.20412415\,t + \mathrm{O}(t^{\frac{3}{2}}) \\
S(t,x) &= 0.20412415\,t + \mathrm{O}(t^{\frac{3}{2}}) \\
K(t,x) &= -0.20412415\,t + \mathrm{O}(t^{\frac{3}{2}})
\end{aligned}
$$

E.2 Case 2

Scaling factors $\dfrac{12P_0}{Et^3}$ for the β_{ij}, ρ_{ij} and $\dfrac{12P_0}{ERt^3}$ for the κ_{ij}.

$$
\begin{aligned}
\beta_{11}^s &= (-0.04097791 + 0.00332783\,x^2)\,t^{\frac{7}{2}} + \mathrm{O}(t^4) \\
C(t,x) &= -0.01386401\,t^{\frac{5}{2}} + \mathrm{O}(t^3) \\
S(t,x) &= 0.00591614\,x\,t^{\frac{3}{2}} - 0.00462963\,t^2 + \mathrm{O}(t^{\frac{5}{2}}) \\
K(t,x) &= -0.02231116\,t^{\frac{7}{2}} + \mathrm{O}(t^4)
\end{aligned}
$$

$$
\begin{aligned}
\beta_{12}^s &= \mathrm{O}(t^3) \\
C(t,x) &= 0.01851852\,x\,t^2 + \mathrm{O}(t^3) \\
S(t,x) &= -0.01851852\,x\,t^2 + 0.01449152\,t^{\frac{5}{2}} + \mathrm{O}(t^3) \\
K(t,x) &= 0.02898305\,t^{\frac{5}{2}} + \mathrm{O}(t^3)
\end{aligned}
$$

$$
\begin{aligned}
\beta_{22}^s &= \mathrm{O}(t^3) \\
C(t,x) &= 0.04159203\,t^{\frac{5}{2}} + \mathrm{O}(t^3) \\
S(t,x) &= -0.01774842\,x\,t^{\frac{3}{2}} + 0.01388889\,t^2 + \mathrm{O}(t^{\frac{5}{2}}) \\
K(t,x) &= 0.03346674\,t^{\frac{7}{2}} + \mathrm{O}(t^4)
\end{aligned}
$$

$$
\begin{aligned}
\kappa_{11}^s &= \mathrm{O}(t^3) \\
C(t,x) &= -0.05796610\,x\,\sqrt{t} + \mathrm{O}(t^{\frac{3}{2}}) \\
S(t,x) &= -0.04536092\,t + \mathrm{O}(t^{\frac{3}{2}}) \\
K(t,x) &= -0.20080045\,t^{\frac{3}{2}} + \mathrm{O}(t^2)
\end{aligned}
$$

$$
\begin{aligned}
\kappa_{12}^s &= \mathrm{O}(t^3) \\
C(t,x) &= 0.04536092\,x\,t - 0.03549684\,t^{\frac{3}{2}} + \mathrm{O}(t^2) \\
S(t,x) &= 0.04536092\,x\,t + 0.07099368\,t^{\frac{3}{2}} + \mathrm{O}(t^2) \\
K(t,x) &= 0.17389829\,\sqrt{t} + \mathrm{O}(t)
\end{aligned}
$$

$$
\kappa_{22}^s = -0.00591620\,t^{\frac{3}{2}} + \mathrm{O}(t^2)
$$

$$
\begin{aligned}
C(t,x) &= -0.11111111\, t^2 + \mathrm{O}(t^{\frac{5}{2}}) \\
S(t,x) &= 0.07099368\, x\, t^{\frac{3}{2}} + 0.05555556\, t^2 + \mathrm{O}(t^{\frac{5}{2}}) \\
K(t,x) &= 0.20080045\, t^{\frac{3}{2}} + \mathrm{O}(t^2)
\end{aligned}
$$

$$
\begin{aligned}
\rho_1^s &= \mathrm{O}(t^3) \\
C(t,x) &= 0.12962963\, x\, t^2 - 0.05796610\, t^{\frac{5}{2}} + \mathrm{O}(t^3) \\
S(t,x) &= 0.07099368\, t^{\frac{3}{2}} + \mathrm{O}(t^2) \\
K(t,x) &= 0.05796610\, t^{\frac{5}{2}} + \mathrm{O}(t^3)
\end{aligned}
$$

$$
\begin{aligned}
\rho_2^s &= -0.16666667\, t^2 + \mathrm{O}(t^{\frac{5}{2}}) \\
C(t,x) &= 0.05555556\, t^2 + \mathrm{O}(t^{\frac{5}{2}}) \\
S(t,x) &= -0.05555556\, t^2 + \mathrm{O}(t^{\frac{5}{2}}) \\
K(t,x) &= -0.10040022\, t^{\frac{3}{2}} + \mathrm{O}(t^2)
\end{aligned}
$$

E.3 Case 3

Scaling factors $\dfrac{12P_0}{Et}$ for the β_{ij}, ρ_{ij} and $\dfrac{12P_0}{ERt}$ for the κ_{ij}.

$$
\begin{aligned}
\beta_{11}^s &= 0.13258252\, t^2 + \mathrm{O}(t^{\frac{5}{2}}) \\
C(t,x) &= -0.02083333\, x + 0.01630296\, \sqrt{t} + \mathrm{O}(t) \\
S(t,x) &= -0.02083333\, x + 0.03260593\, \sqrt{t} + \mathrm{O}(t) \\
K(t,x) &= 0.07856742\, t^2 + \mathrm{O}(t^3)
\end{aligned}
$$

$$
\begin{aligned}
\beta_{12}^s &= -0.11004501\, x\, t^{\frac{5}{2}} + \mathrm{O}(t^3) \\
C(t,x) &= 0.22113449\, x^2\, t - 0.11980183\, x\, t^{\frac{3}{2}} + \mathrm{O}(t^{\frac{5}{2}}) \\
S(t,x) &= 0.13042372\, x\, \sqrt{t} - 0.10206207\, t + \mathrm{O}(t^{\frac{3}{2}}) \\
K(t,x) &= -0.10206207\, t + \mathrm{O}(t^2)
\end{aligned}
$$

$$
\begin{aligned}
\beta_{22}^s &= -0.04419417\, t^2 + \mathrm{O}(t^{\frac{5}{2}}) \\
C(t,x) &= 0.0625\, x - 0.04890889\, \sqrt{t} + \mathrm{O}(t) \\
S(t,x) &= 0.0625\, x - 0.09781779\, \sqrt{t} + \mathrm{O}(t) \\
K(t,x) &= -0.11785113\, t^2 + \mathrm{O}(t^3)
\end{aligned}
$$

$$
\begin{aligned}
\kappa_{11}^s &= (0.93841991 - 0.5625\, x^2)\, t^2 + \mathrm{O}(t^{\frac{5}{2}}) \\
C(t,x) &= 0.20412415\, x\, t^{-1} + \mathrm{O}(1)
\end{aligned}
$$

$$
\begin{aligned}
S(t,x) &= -0.20412415\,x\,t^{-1} + 0.15973578t^{-\frac{1}{2}} + \mathrm{O}(1)\\
K(t,x) &= 0.70710678 + \mathrm{O}(t)
\end{aligned}
$$

$$
\begin{aligned}
\kappa^s_{12} &= (-2.07950487\,x + 0.375\,x^3)\,t^2 + \mathrm{O}(t^{\frac{5}{2}})\\
C(t,x) &= -0.31947155\,x\,t^{-\frac{1}{2}} + \mathrm{O}(\sqrt{t})\\
S(t,x) &= -0.25 + \mathrm{O}(t)\\
K(t,x) &= -0.61237244\,t^{-1} + \mathrm{O}(1)
\end{aligned}
$$

$$
\begin{aligned}
\kappa^s_{22} &= -0.14672668\,\sqrt{t} + \mathrm{O}(t)\\
C(t,x) &= -0.25\,x + 0.19563557\,\sqrt{t} + \mathrm{O}(t)\\
S(t,x) &= -0.25\,x - 0.39127115\,\sqrt{t} + \mathrm{O}(t)\\
K(t,x) &= -0.70710678 + \mathrm{O}(t)
\end{aligned}
$$

$$
\begin{aligned}
\rho^s_1 &= (-1.46875\,x + 0.1875\,x^3)\,t^2 + \mathrm{O}(t^3)\\
C(t,x) &= -0.25 + \mathrm{O}(t)\\
S(t,x) &= -0.25 + \mathrm{O}(t)\\
K(t,x) &= -0.20412415\,t + \mathrm{O}(t^2)
\end{aligned}
$$

$$
\begin{aligned}
\rho^s_2 &= -0.35940550\,t^{\frac{3}{2}} + \mathrm{O}(t^2)\\
C(t,x) &= 0.71443451\,x\,t + 0.25291498\,t^{\frac{3}{2}} + \mathrm{O}(t^2)\\
S(t,x) &= 0.39127115\,\sqrt{t} + \mathrm{O}(t)\\
K(t,x) &= 0.35355339 + \mathrm{O}(t)
\end{aligned}
$$

References

[1] K. J. BATHE, F. BREZZI AND M. FORTIN: *Mixed-interpolated elements for Reissner-Mindlin plates*, Int. J. Numer. Methods in Engrg. 28 (1989) 1787-1801.

[2] F. BREZZI, M. FORTIN AND R. STENBERG: *Error analysis of mixed-interpolated elements for Reissner-Mindlin plates*, Math. Models and Methods in Appl. Sci. (M^3AS) 1 (1991) 125-151.

[3] A. L. GOL'DENVEIZER: *Theory of Elastic Thin Shells*, Pergamon, Oxford, 1961.

[4] D. S. HOUGHTON AND D. J. JOHNS: *A comparison of the characteristic equations in the theory of circular cylindrical shells*, The Aeronautical Quarterly, August 1961 228-236.

[5] W. T. KOITER: *On the foundations of the linear theory of thin elastic shells*, Proc. Kon. Nedel. Akad. Wetensch., B73 (1970) 169-195.

[6] Y. LEINO: *Sources of errors in the finite element approximation of shells, Licentiate thesis*, Helsinki University of Technology, 1994 (in Finnish).

[7] Y. LEINO AND J. PITKÄRANTA: *On the membrane locking of h-p finite elements in a cylindrical shell problem*, Int. J. Numer. Methods in Engrg., 37 (1994) 1053-1070.

[8] H. HAKULA, Y. LEINO AND J. PITKÄRANTA: *Scale resolution, locking and high-order finite element modelling of shells*, to appear.

[9] S. LUKASIEWICZ: *Local Loads in Plates and Shells*, Sijthoff & Noordhoff, Warzawa, 1979.

[10] L. S. D. MORLEY: *Analysis of developable shells with special reference to the finite element method and circular cylinders*, Phil. Trans. R. Soc. Lond. A 281 (1976) 113-170.

[11] L. S. D. MORLEY AND A. J. MORRIS: *A conflict between finite elements and shell theory*, Royal Aircraft Establishment Report, 1978.

[12] P. M. NAGHDI: *Handbuch der Physik*, Springer, Berlin, 1972.

[13] V. V. NOVOZHILOV: *Thin Shell Theory*, Walters Noordhoff, Groningen, 1959.

[14] O. OVASKAINEN: *On the deformation states of cylindrical shells under non-axisymmetric loading, Diploma thesis*, Helsinki University of Technology, 1993 (in Finnish).

[15] J. PIILA AND J. PITKÄRANTA: *Energy estimates relating different linear elastic models of a cylindrical shell. (I) The membrane-dominated case*, SIAM J. Math Anal. 24 (1993) 1-22.

[16] J. PIILA AND J. PITKÄRANTA: *Energy estimates relating different linear elastic models of a cylindrical shell. (II) The case of a free boundary*, to appear in SIAM J. Math Anal.

[17] J. PIILA AND J. PITKÄRANTA: *Characterization of the membrane theory of a clamped shell. The parabolic case*, Math. Models and Meth. in Appl. Sci. (M^3AS) 3 (1993) 417-442.

[18] J. PIILA: *Characterization of the membrane theory of a clamped shell. The elliptic case*, Math. Models and Meth. in Appl. Sci. (M^3AS) 4 (1994) 147-177.

[19] J. PIILA: *Characterization of the membrane theory of a clamped shell. The hyperbolic case*, to appear.

[20] J. PIILA: *Energy estimates and asymptotic analysis in the theory of shells, Doctoral thesis*, Helsinki University of Technology, 1993.

[21] J. PITKÄRANTA: *Analysis of some low-order finite element schemes for Mindlin-Reissner and Kirchhoff plates*, Numer. Math. 53 (1988) 237-254.

[22] J. PITKÄRANTA: *The problem of membrane locking in finite element analysis of cylindrical shells*, Numer. Math. 61 (1992) 523-542.

[23] J. PITKÄRANTA AND M. SURI: *Design principles and error analysis of reduced-shear finite elements for plate bending*, to appear.

[24] J. P. VINSON: *Structural Mechanics: The Behavior of Plates and Shells*, Wiley, New York, 1974.

An Energy Method Approach to the Problem of Elastic Strip

O. Ovaskainen and J. Pitkäranta

Helsinki University of Technology, Institute of Mathematics,
P.O. Box 1000, FIN-02015 HUT, Finland

Abstract. We analyze a thin elastic, homogeneous strip under a smooth load and several different types of boundary conditions. The strip is assumed to obey either a plane strain or a plane stress type deformation of linear theory of elasticity. We characterize the 2D solution and consider dimension reduction of arbitrary order n. Both interior and global energy estimates for the reduction error are derived.

Subject classification. (AMS) 73C02, 73C20

1 Introduction

The special class of geometries consisting of beams, arches, plates and shells is of major importance in the theory of elasticity. A characteristic feature of such problems is that one or two dimensions of the body are small with respect to the others, i.e. the body is thin. This property often makes the numerical solution of the problem more difficult than in thick body cases. On a thin body, displacement and stress fields assume asymptotic shapes that are often difficult to capture by straightforward numerical methods such as FEM. On the other hand, one can also take the advantage of the fact the body is thin. One can carry out, by analytical means, a dimension reduction that converts the 3D problem into a simpler lower-dimensional one.

Before the last few decades dimensional reduction was seen mainly as a theoretic tool. The ultimate goal was typically to obtain analytic solutions, e.g. as Fourier expansions, in special cases. The classical plate and shell models served then as simpler models than the original 3D for such purposes. The analytical point of view was in fact present already in the way the reduced models were derived. One looked directly at the equilibrium and constitutive equations to see what kind of asymptotic solutions could be found as the thickness gets small. More recently, the development of computers has changed the point of view from asymptotic analyses to the direction of numerical ones. One is no more so interested in getting analytic solutions for some special cases but in developing methods for effective and accurate solving of larger groups of problems. Modern finite element methods have their natural basis on variational (or energy) principles rather than in the classical systems of partial differential equations.

In this paper we consider the problem of 2D linear elasticity on a strip

$$\omega = \{(x, z) | -1 < x < 1,\ -t/2 < z < t/2\}, \tag{1.1}$$

where t is constant with respect to x and may be small. We assume either the state of plane strain or plane stress, i.e., the problem itself is the result of dimension reduction applied to a plate problem where the plate is either very long (plane strain) or very thin (plane stress) in the direction perpendicular to the (x, z)-plane. The load is assumed to be acting on the surfaces $z = \pm t/2$ and (sufficiently) smooth. The boundary conditions at $x = \pm 1$ may be given alternatively as displacements, stresses or as mixed conditions.

The aim of the paper is to study the behaviour of the true 2D solution from the point of view of the accuracy of dimension reduction models. The dimension reduction models considered here are so called n-*models* based on n:th degree polynomial expansion of the displacement field in the z-coordinate and on the straightforward use of the energy principle. Such models are obviously directly related to numerical modelling by FEM. The analysis of the exact solution is divided into two parts. In the first part we follow the philosophy of standard asymptotic analysis techniques. We first change the boundary conditions at $x = \pm 1$ to more convenient ones, so that we can give an approximate (asymptotic) solution as a polynomial expansion in the z-direction. We then derive an energy estimate for the truncation error. In the second part we consider what is left, i.e., homogeneous (free) boundary conditions at $z = \pm t/2$, and boundary conditions at $x = \pm 1$ obtained by superposition. Here we give the solution as a sum of three known unit (far-field) solutions and an exponentially decaying boundary layer. The coefficients for the unit solutions are given either exactly or with an estimated error. Estimates for the energy of the boundary layer are also derived. These results give, as a by-product, sharp global and interior convergence rates for dimensionally reduced n-models.

For previous work on the problem of elastic strip the reader is referred to [Go], [Pa], [Fa], [Sm], [Be], [GS], [Gz1], [Gz2], [JL], [Tor], [Br], [Gu], [Bo], [Sp], [Gr1], [Gr2], [Gr3], [GG], [GW], [SW], [HP], [H1], [M]. Many of the results obtained in these works may be seen here as special cases. The traditional approach to boundary layers has been to use Papkovich-Faddle eigenfunction expansions. In this work we concern mainly to the connection between numerical modelling and the energy perspective. Thus we characterize the boundary layers using energy arguments and only to the extent relevant for the error analysis of numerical models. We note that in finite element models, one may need local mesh refinements or some other extra efforts near the ends of the strip to make sure that the layers are captured with sufficient accuracy. In the dimension reduction terminology this corresponds to using the actual 2D model in the boundary layer zone and polynomial expansions in the interior of the domain only. We give energy estimates for the error of such improved n-models as well.

2 Preliminaries

We consider an elastic strip of length $2L$ and width d, $d \ll L$, consisting of some homogeneous and isotropic material. Choosing L to be the length unit and placing the origin of the dimensionless coordinates x, z at the center of the strip, the strip then occupies the region ω in (1.1) where $t = d/L$ is a small dimensionless parameter. This is the main parameter in our study.

We assume no body force and the external loads to be given as surface tractions acting on parts of $\partial\omega$. To this end we split $\partial\omega$ as $\partial\omega = \overline{\Gamma}_l \cup \overline{\Gamma}_s$, where $\Gamma_l = \{(x,z)| -1 < x < 1, z = \pm t/2\}$ and $\Gamma_s = \{(x,z)|x = \pm 1, -t/2 < z < t/2\}$.

On Γ_l we assume given surface tractions throughout, i.e.,

$$\begin{aligned} \tau_{13}(x, \pm t/2) &= \overline{\tau}_{l1}^{\pm}(x), \\ \tau_{33}(x, \pm t/2) &= \overline{\tau}_{l3}^{\pm}(x), \quad -1 < x < 1, \end{aligned}$$

where $\underline{\underline{\tau}} = (\tau_{ij})_{i,j=1,3}$ is the (symmetric) stress tensor field of the problem and $\overline{\tau}_{li}^{\pm}$, $i = 1, 3$, are given functions. It is convenient for our study to split here the load into four components in such a way that each component causes either a pure *membrane state* or a pure *bending state*. As is well known, this is possible by simple symmetry considerations. The four states are referred to as **B.1**, **B.2** (bending states) and **M.1**, **M.2** (membrane states). These correspond to the following loading types:

B.1 $\overline{\tau}_{l1}^{\pm} = 0$,
$\overline{\tau}_{l3}^{+} = -\overline{\tau}_{l3}^{-} = t^3 f(x)$.

B.2 $\overline{\tau}_{l1}^{+} = \overline{\tau}_{l1}^{-} = t^2 f(x)$,
$\overline{\tau}_{l3}^{\pm} = 0$.

M.1 $\overline{\tau}_{l1}^{+} = -\overline{\tau}_{l1}^{-} = t f(x)$,
$\overline{\tau}_{l3}^{\pm} = 0$.

M.2 $\overline{\tau}_{l1}^{\pm} = 0$,
$\overline{\tau}_{l3}^{+} = \overline{\tau}_{l3}^{-} = f(x)$.

For the convenience of our analysis, we have here scaled the loads in such a way that when f is fixed and t varies, a non-trivial limit displacement field is obtained as $t \to 0$. As it turns out, the scalings chosen are the right ones for this goal. Below we assume that f is in each case sufficiently many times continuously differentiable on the closed interval $[-1,1]$ and independent of t.

At the ends of the strip, i.e., at $x=-1$ and $x=+1$ we impose either stress or displacement boundary conditions. At a given end, we allow any legal combination of the conditions

$$\begin{aligned} u(\pm1,z) &= \overline{u}^{\pm}(z), \qquad w(\pm1,z) = \overline{w}^{\pm}(z),\\ \tau_{11}(\pm1,z) &= \overline{\tau}_{s1}^{\pm}(z), \qquad \tau_{13}(\pm1,z) = \overline{\tau}_{s3}^{\pm}(z), \quad -t/2<z<t/2, \end{aligned}$$

meaning that we may have either (u,w), (u,τ_{13}), (τ_{11},w) or (τ_{11},τ_{13}) given. We assume here that $\overline{u}^{\pm}$, $\overline{w}^{\pm}\in H^1(\Gamma_s)$ and that $\overline{\tau}_{s1}^{\pm}$, $\overline{\tau}_{s3}^{\pm}\in L_2(\Gamma_s)$.

To set up the variational formulation of the problem we denote the energy space by $\mathcal{V}$. This is defined as the subspace of $\mathcal{W}=[H^1(\omega)]^2$ where the homogeneous versions of the kinematical constraints on (u,w) on Γ_s (if any) are imposed. Then the variational formulation is as follows: Find $\underline{u}^{2D}\in\mathcal{W}$ that satisfies the given kinematical constraints on Γ_s and such that

$$\mathcal{A}(\underline{u}^{2D},\underline{\tilde{u}}) = \mathcal{Q}(\underline{\tilde{u}}) \quad \forall \underline{\tilde{u}}\in\mathcal{V}, \tag{2.1}$$

where $\mathcal{Q}$ is the external load potential

$$\mathcal{Q}(\underline{u}) = \int_{\Gamma_l}\left(\overline{\tau}_{l1}^{\pm}u+\overline{\tau}_{l3}^{\pm}w\right)\cdot n_z\,dx + \int_{\Gamma_s}\left(\overline{\tau}_{s1}^{\pm}u+\overline{\tau}_{s3}^{\pm}w\right)\cdot n_x\,dz,$$

and

$$\mathcal{A}(\underline{u},\underline{\tilde{u}}) = \int_\omega \tau_{11}\tilde{\varepsilon}_{11}+2\tau_{13}\tilde{\varepsilon}_{13}+\tau_{33}\tilde{\varepsilon}_{33}\,dx\,dz,$$

where the stress tensor and the symmetric strain tensor $\underline{\underline{\varepsilon}}=(\varepsilon_{ij})_{i,j=1,3}$ are related to the displacement field as

$$\begin{array}{ll} \varepsilon_{11} = u_{,x} & \tau_{11} = \frac{E}{1+\nu}\left[\gamma(\varepsilon_{11}+\varepsilon_{33})+\varepsilon_{11}\right]\\ \varepsilon_{13} = \frac{1}{2}(u_{,z}+w_{,x}) & \tau_{13} = \frac{E}{1+\nu}\varepsilon_{13}\\ \varepsilon_{33} = w_{,z} & \tau_{33} = \frac{E}{1+\nu}\left[\gamma(\varepsilon_{11}+\varepsilon_{33})+\varepsilon_{33}\right]. \end{array}$$

Here $E>0$ is the Young's modulus and $\nu\in[0,1/2)$ the Poisson's ratio of the (homogeneous and isotropic) material, and

$$\gamma = \begin{cases} \nu/(1-2\nu) & \text{(plane strain)}\\ \nu/(1-\nu) & \text{(plane stress).} \end{cases}$$

Note that due to the assumed dimensionless coordinates, our strain and stress tensors are related to the more ordinary ones through a scaling factor L.

In case that kinematical constraints in $\mathcal{V}$ leave free some rigid body motions $\underline{u}^{RD} = \sum_{i=1}^{3} c_i \underline{u}^{RDi}$, where $\underline{u}^{RD1} = (1,0)$, $\underline{u}^{RD2} = (0,1)$, $\underline{u}^{RD3} = (z,-x)$, we assume that the load satisfies the corresponding equilibrium condition $\mathcal{Q}(\underline{u}^{RD}) = 0$, and we shrink the energy space by imposing the constraint

$$\int_\omega \underline{u}^{RD} \cdot \underline{u}\, dx\, dz = 0, \quad \underline{u} \in \mathcal{V}.$$

The same constraint is then assumed to hold also for the solution $\underline{u}^{2D}$.

We note that for all $\underline{u} \in \mathcal{V}$ the Korn inequality

$$\mathcal{A}(\underline{u}, \underline{u}) \geq ct^2 \left(||u||^2_{H^1(\omega)} + ||v||^2_{H^1(\omega)} \right) \tag{2.2}$$

holds where c is independent of t. This follows from standard results [NH1] by a simple scaling argument. The inequality quarantees that the variational problem (2.1) is uniquely solvable.

We consider dimension reduction models, so called *n-models*, derived from the variational principle (2.1) as follows: For $n \geq 0$ let $\mathcal{W}^n$ and $\mathcal{V}^n$ be subspaces of $\mathcal{W}$, resp. $\mathcal{V}$, defined by

$$\mathcal{W}^n = \left\{ \underline{v} \in \mathcal{W} \,|\, \underline{v} = \sum_{i=0}^{n} \underline{v}_i(x) z^i \right\}, \quad \mathcal{V}^n = \left\{ \underline{v} \in \mathcal{V} \,|\, \underline{v} = \sum_{i=0}^{n} \underline{v}_i(x) z^i \right\}$$

and let $\underline{u}^n \in \mathcal{W}^n$ be an approximation to $\underline{u}^{2D}$ such that $\underline{u}^n$ satisfies the kinematical constraints on Γ_s and

$$\mathcal{A}(\underline{u}^n, \underline{\tilde{u}}) = \mathcal{Q}(\underline{\tilde{u}}) \quad \forall \underline{\tilde{u}} \in \mathcal{V}^n. \tag{2.3}$$

We assume here that the kinematical constraints on Γ_s are polynomials of order at most n. If this is not the case, the remainders of the Taylor expansions of $\overline{u}^{\pm}(z)$ and $\overline{w}^{\pm}(z)$ are simply dropped out and the solution for the 2D problem determined by the remainders is added to the dimension reduction error.

In the next chapters we analyze $\underline{u}^{2D}$ and estimate $\underline{u}^{2D} - \underline{u}^n$ in the energy norm

$$\underline{u} \mapsto |||\underline{u}||| = \sqrt{\mathcal{A}(\underline{u}, \underline{u})}.$$

First we construct by asymptotic analysis a field $\underline{u}_f^n \in \mathcal{W}^n$ which satisfies the equilibrium conditions (Euler equations of (2.1)) approximately, i.e.,

$$
\begin{aligned}
e_1 &= \tau_{11,x} + \tau_{13,z} \approx 0, \\
e_2 &= \tau_{13,x} + \tau_{33,z} \approx 0,
\end{aligned} \tag{2.4}
$$

in ω, and the given stress boundary conditions likewise approximately, i.e.,

$$
\begin{aligned}
b_1^{\pm} = \tau_{13}(x, \pm t/2) - \overline{\tau}_{l1}^{\pm}(x) \approx 0, \\
b_2^{\pm} = \tau_{33}(x, \pm t/2) - \overline{\tau}_{l3}^{\pm}(x) \approx 0,
\end{aligned} \tag{2.5}
$$

on Γ_l, with accuracy growing with n. The field $\underline{u}_f^n$ is uniformly smooth on the whole domain (whenever f is) and is not dependent on the boundary conditions set originally on Γ_s. With n and the field $\underline{u}_f^n$ given, we split $\underline{u}^{2D}$ into two parts as

$$\underline{u}^{2D} = \underline{u}^{as,n} + \underline{u}^{b,n},$$

where $\underline{u}^{as,n}$ is the solution to the 2D elastic problem where the load on Γ_l is the same as in the original problem but the given stresses or displacements on Γ_s are changed so that they correspond to the asymptotic field $\underline{u}_f^n$. Then $\underline{u}^{b,n}$ satisfies (2.1) together with homogeneous (free) boundary conditions on Γ_l, and with the boundary conditions on Γ_s obtained by superposition.

Given the above splitting of the exact displacement field corresponding to a given n, we split the displacement field of the n-model analogously as

$$\underline{u}^n = \underline{u}^{n,as} + \underline{u}^{n,b}$$

where $\underline{u}^{n,as}$ and $\underline{u}^{n,b}$ are obtained from their exact counterparts by the projection principle, i.e.,

$$\mathcal{A}(\underline{u}^{n,as}, \underline{\tilde{u}}) = \mathcal{A}(\underline{u}^{as,n}, \underline{\tilde{u}}), \ \underline{\tilde{u}} \in \mathcal{V}^n, \tag{2.6}$$

$$\mathcal{A}(\underline{u}^{n,b}, \underline{\tilde{u}}) = \mathcal{A}(\underline{u}^{b,n}, \underline{\tilde{u}}), \ \underline{\tilde{u}} \in \mathcal{V}^n, \tag{2.7}$$

with consistent kinematical constraints imposed on Γ_s.

In Chapter 3 below we construct $\underline{u}_f^n$ for arbitrary n, separately in the four cases **B.1**, **B.2**, **M.1**, **M.2**, and obtain an estimate of the form

$$|||\underline{u}^{as,n} - \underline{u}_f^n|||/|||\underline{u}^{as,n}||| \le C(n,f)t^{\alpha_n}.$$

From the projection principle we then conclude that the same estimate holds for $|||\underline{u}^{as,n} - \underline{u}^{n,as}|||/|||\underline{u}^{as,n}|||$ as well.

In Chapter 4 we study the behaviour of $\underline{u}^{b,n}$ and its projection $\underline{u}^{n,b}$. We characterize these solutions as linear combinations of three known far-field solutions plus exponentially decaying boundary layers. Together with the results of Chapter 3 these estimates give both the global and interior convergence rates of the n-model. The details of Chapter 4 turn out to be rather case-dependent.

3 Construction of an Asymptotic Expansion

We are going to construct a displacement field $\underline{u}_f^n \in \mathcal{W}^n$ in such a way that it satisfies (2.4) and (2.5) with accuracy growing with n.

If we substitute an $\underline{u} = \sum_{i=0}^n \underline{u}_i z^i \in \mathcal{W}^n$ into the Euler equations and into the stress boundary conditions on Γ_l, we get formally the following set of equations:

$$(3.1)\quad e_1 = \frac{E}{1+\nu}\left[(1+\gamma)\sum_{i=0}^{n} u_i'' z^i + \frac{1+2\gamma}{2}\sum_{i=0}^{n-1}(i+1)w_{i+1}' z^i + \frac{1}{2}\sum_{i=0}^{n-2}(i+1)(i+2)u_{i+2}z^i\right]$$

$$(3.2)\quad e_2 = \frac{E}{1+\nu}\left[\frac{1}{2}\sum_{i=0}^{n} w_i'' z^i + \frac{1+2\gamma}{2}\sum_{i=0}^{n-1}(i+1)u_{i+1}' z^i + (1+\gamma)\sum_{i=0}^{n-2}(i+1)(i+2)w_{i+2}z^i\right]$$

$$(3.3)\quad \overline{\tau}_{l1}^{\pm} = \frac{E}{2(1+\nu)}\left[\sum_{i=0}^{n}\frac{1}{2^i}w_i'\cdot(\pm t)^i + \sum_{i=0}^{n-1}\frac{i+1}{2^i}u_{i+1}\cdot(\pm t)^i\right]$$

$$(3.4)\quad \overline{\tau}_{l3}^{\pm} = \frac{E}{1+\nu}\left[\gamma\sum_{i=0}^{n}\frac{1}{2^i}u_i'\cdot(\pm t)^i + (1+\gamma)\sum_{i=0}^{n-1}\frac{i+1}{2^i}w_{i+1}\cdot(\pm t)^i\right]$$

The asymptotic field $\underline{u}_f^n$ will be an approximate solution to (3.1) through (3.4) with u_i and w_i of the form

$$(3.5)\qquad u_i = \sum_{j=0,2,\dots}^{n-2} u_i^j t^j, \quad w_i = \sum_{j=0,2,\dots}^{n-2} w_i^j t^j,$$

where further u_i^j and w_i^j will depend on f, but not on t. In the expansions (3.5) we have taken only even powers of t, as it can be shown that all odd powers will be zero. Depending on the case, the expansions will be either purely even or purely odd in z.

Below we present an algorithm for the construction of functions u_i^j and w_i^j in (3.5), thus leading to a double expansion of the asymptotic field $\underline{u}_f^n$. Based on this algorithm, an asymptotic field accurate to any prescribed degree $O(t^n)$ can be constructed by symbolic calculus if f is smooth. The membrane and bending cases will be considered separately since they are quite different. A few leading terms of the asymptotic fields are given in Appendix A for the four cases. At the end of this chapter we give an asymptotic error bound for the n-model (Theorem 3.1). This is based on truncation error estimates for the asymptotic expansion.

The idea of the algorithm is to first solve a set of equations such that the coefficients of the most dominating powers of t in the Eqs. (3.1) through (3.4) will vanish. After the most dominating powers of t are deleted from the equations, we proceed recursively by deleting in each step the most dominating powers of t still present in the equations.

3.1 The Membrane Problem

The construction of the asymptotic expansion is based on the following algorithm.

1. Assume, that u_i^j and w_i^j with $j = 0, 2, \ldots, a-2$ are known from the previous steps of the algorithm. Here a is even and we first set $a = 0$.

2. Force the coefficients of $z^0 t^a$, $z^1 t^a$, t^{1+a} and t^a on the righthand sides of Eqs. (3.1) through (3.4) to vanish with the following choices:

   (a) for a=0 by the choice

   M.1 :

$$\begin{aligned} u_0^0 &= \tfrac{1+\nu}{E(1+2\gamma)}\left[-2(1+\gamma)I_2^x[f]\right] & w_1^0 &= \tfrac{1+\nu}{E(1+2\gamma)}\left[2\gamma I_1^x[f]\right] \\ u_2^0 &= \tfrac{1+\nu}{E(1+2\gamma)}\left[(2+3\gamma)f\right] & w_3^0 &= \tfrac{1+\nu}{E(1+2\gamma)}\left[-\tfrac{1+3\gamma}{3}f'\right] \end{aligned}$$

   M.2 :

$$\begin{aligned} u_0^0 &= \tfrac{1+\nu}{E(1+2\gamma)}\left[-\gamma I_1^x[f]\right] & w_1^0 &= \tfrac{1+\nu}{E(1+2\gamma)}\left[(1+\gamma)f\right] \\ u_2^0 &= \tfrac{1+\nu}{E(1+2\gamma)}\left[-\tfrac{1+\gamma}{2}f'\right] & w_3^0 &= \tfrac{1+\nu}{E(1+2\gamma)}\left[\tfrac{\gamma}{6}f''\right], \end{aligned}$$

(b) for $a \geq 2$ by first defining

$$
\begin{aligned}
B_{1,a} &= \sum_{i=3,5,\ldots}^{a+1} \frac{1}{2^i} \left[\left(w_i^{a+1-i} \right)' + (i+1) u_{i+1}^{a+1-i} \right] \\
B_{2,a} &= \sum_{i=2,4,\ldots}^{a} \frac{1}{2^i} \left[\frac{\gamma}{1+2\gamma} \left(u_i^{a-i} \right)' + \frac{1+\gamma}{1+2\gamma} (i+1) w_{i+1}^{a-i} \right],
\end{aligned}
$$

and then choosing

$$
\begin{aligned}
u_0^a &= \frac{1+\gamma}{1+2\gamma} I_2^x[B_{1,a}] + \gamma I_1^x[B_{2,a}] \\
u_2^a &= -\frac{2+3\gamma}{2(1+3\gamma)} B_{1,a} + \frac{1+\gamma}{2} B'_{2,a} \\
w_1^a &= -\frac{\gamma}{1+2\gamma} I_1^x[B_{1,a}] - (1+\gamma) B_{2,a} \\
w_3^a &= \frac{1+3\gamma}{6(1+2\gamma)} B'_{1,a} - \frac{\gamma}{6} B''_{2,a},
\end{aligned}
$$

where we have used the notation

$$
I_k^x[u] = \int_0^x \int_0^{x_1} \cdots \int_0^{x_{k-1}} u(x_k, z) dx_k \cdots dx_1.
$$

3. Solve u_{i+2}^a and w_{i+2}^a for the remaining values of i by requiring in (3.1) and (3.2) the coefficients of $z^i t^a$ to be zero, i.e., choose

$$
\begin{aligned}
(3.6)\quad u_{i+2}^a &= -\frac{1}{i+2} \left[\frac{2(1+\gamma)}{i+1} \left(u_i^a \right)'' + (1+2\gamma) \left(w_{i+1}^a \right)' \right] \\
(3.7)\quad w_{i+2}^a &= -\frac{1}{2(i+2)(1+\gamma)} \left[\frac{1}{i+1} \left(w_i^a \right)'' + (1+2\gamma) \left(u_{i+1}^a \right)' \right]
\end{aligned}
$$

for $i = 2 \ldots n-2$, where the indices are even for u and odd for w.

4. Raise a by 2. Stop if $a > n-2$, otherwise go back to Step 2.

3.2 The Bending Problem

Finding an asymptotic expansion for the bending problem is a bit more difficult due to the singularity of the underlying set of equations.

1. Assume that u_i^j and w_i^j are known from the previous steps for $j = 0, 2, \ldots, a-4$. Here a is even and we first set $a = 2$.

2. Define first the auxiliary functions $B_{1,a}$ and $B_{2,a}$ as follows:

   (a) if $a \geq 4$, then

$$
\begin{aligned}
B_{1,a} &= \sum_{i=2,4,\ldots}^{a} \frac{1}{2^i}\left[\left(w_i^{a-i}\right)' + (i+1)u_{i+1}^{a-i}\right] \\
B_{2,a} &= \sum_{i=3,5,\ldots}^{a+1} \frac{1}{2^i}\left[\frac{\gamma}{1+2\gamma}\left(u_i^{a+1-i}\right)' + \frac{(1+\gamma)(i+1)}{1+2\gamma} w_{i+1}^{a+1-i}\right].
\end{aligned}
$$

   (b) if $a = 2$, modify the definitions in (a) as follows:

   B.1 : add $-\frac{1+\nu}{E(1+2\gamma)} f$ to $B_{2,a}$

   B.2 : add $-\frac{2(1+\nu)}{E} f$ to $B_{1,a}$

   (c) For $a = 0$ set $B_{1,a} = B_{2,a} = 0$.

We are going to solve u_i^{a-2} and w_i^{a-2} for all i at this step. To this end, we need to take one step to the future and first look at the equations formed by the coefficients of $z^1 t^a$, $z^0 t^a$, t^a and t^{a+1} in Eqs. (3.1) through (3.4). In light of the above definitions, these may now be written as

$$
\begin{aligned}
0 &= (1+\gamma)\left(u_1^a\right)'' + (1+2\gamma)\left(w_2^a\right)' + 3u_3^a, \\
0 &= \frac{1}{2}\left(w_0^a\right)'' + \frac{1+2\gamma}{2}\left(u_1^a\right)' + 2(1+\gamma)w_2^a, \\
0 &= \left(w_0^a\right)' + u_1^a + B_{1,a}, \\
0 &= \frac{\gamma}{2(1+2\gamma)}\left(u_1^a\right)' + \frac{1+\gamma}{1+2\gamma} w_2^a + B_{2,a}.
\end{aligned}
$$

If we try to solve w_0^a, u_1^a, w_2^a and u_3^a from these equations, we find that the system formed by the last three equations is singular, and there will be no solution at all unless the constraint

$$
\frac{1}{1+2\gamma} B_{1,a}' + 4B_{2,a} = 0 \tag{3.8}
$$

holds. If (3.8) is assumed to hold, the solution will be of the form

$$
\begin{aligned}
u_1^a &= -\left(w_0^a\right)' - B_{1,a} \\
w_2^a &= \frac{\gamma\left(w_0^a\right)'' + \gamma B_{1,a}' - 2(1+\gamma)B_{2,a}}{2(1+\gamma)}.
\end{aligned}
$$

Then u_i^a and w_i^a can be determined for $2 < i \leq n+2$ as in (3.6) and (3.7). The terms with $n < i \leq n+2$ are needed here in the construction but they are dropped out naturally from the final result. In these equations, w_0^a is still not determined, but our aim is actually to find w_0^{a-2}. If the formulas for $B_{1,a}$ and $B_{2,a}$ are substituted into (3.8) and u_1^{a-2}, w_2^{a-2}, u_3^{a-2} and w_4^{a-2} are written in terms of w_0^{a-2} as presented above (set $a-2$ instead of a), one finds that only the choice

$$\begin{aligned} w_0^{a-2} &= -I_1^x[B_{1,a-2}] - 2\gamma I_2^x[B_{2,a-2}] \\ &\quad -6\frac{1+\gamma}{1+2\gamma} I_3^x[\tilde{B}_{1,a}] - 24(1+\gamma) I_4^x[\tilde{B}_{2,a}] \end{aligned}$$

satisfies the constraint (3.8). Here a tilde over $B_{\cdot,a}$ indicates that the first term is left out from the summation, i.e. the summation begins with $i=4$ or $i=5$. Now that w_0^{a-2} is known, all the remaining terms with superscript $a-2$ are also determined.

3. Raise a by two. Stop if $a > n$, otherwise go back to Step 2.

3.3 Asymptotic Convergence Rate of the n-model

In this final subsection, our goal is to estimate the relative asymptotic dimension reduction error $|||\underline{u}^{as,n} - \underline{u}^{n,as}|||/|||\underline{u}^{as,n}|||$ of the n-model. Here $\underline{u}^{n,as}$ satisfies (2.6) and the same kinematical constraints on Γ_s as $\underline{u}^{as,n}$, i.e., the same as $\underline{u}_f^n$. By the projection principle we have

$$|||\underline{u}^{as,n} - \underline{u}^{n,as}||| \leq |||\underline{u}^{as,n} - \underline{u}_f^n|||,$$

so what we need is a bound for $|||\underline{u}^{as,n} - \underline{u}_f^n|||$ and a lower bound for $|||\underline{u}^{as,n}|||$. We make use of the following truncation error estimates. These follow immediately of the algorithms presented above.

Lemma 3.1 *The asymptotic displacement field $\underline{u}_f^n = \sum_{i=0}^n \sum_{j=0,2,\ldots}^{n-2} \underline{u}_i^j t^j z^i$ constructed as above (membrane or bending case) satisfies Eqs. (3.1) through (3.4) with*

$$\begin{aligned} e_1 &= O(t^{n-1}) \qquad & b_1^{\pm} &= O(t^n) \\ e_2 &= O(t^{n-1}) \qquad & b_2^{\pm} &= O(t^n) \end{aligned}$$

in a pointwise sense.

We could sharpen these estimates by separating even and odd n:s, but this is unnecessary for our purposes.

To estimate $|||\underline{u}^{as,n} - \underline{u}_f^n|||$ we note first, integrating by parts, that

$$\begin{aligned}\mathcal{A}(\underline{u}^{as,n} - \underline{u}_f^n, \tilde{\underline{v}}) &= \int_\omega \sum_{i,j=1,3} (\tau_{ij}^{as,n} - \tau_{f\,ij}^n)\tilde{\varepsilon}_{ij} dx\, dz \\ &= -\int_{-1}^{1} b_1^+ \tilde{u}(x, +t/2) + b_2^+ \tilde{w}(x, +t/2)\, dx \\ &\quad + \int_{-1}^{1} b_1^- \tilde{u}(x, -t/2) + b_2^- \tilde{w}(x, -t/2)\, dx \\ &\quad + \int_\omega (e_1 \tilde{u} + e_2 \tilde{w})\; dx\, dz, \quad \tilde{\underline{v}} \in \mathcal{V}.\end{aligned}$$

Choosing here $\tilde{\underline{v}} = \underline{u}^{as,n} - \underline{u}_f^n$ we obtain

$$\begin{aligned}|||\underline{u}^{as,n} - \underline{u}_f^n|||^2 &\leq \Big(||b_1^\pm||_{L_2(\Gamma_l)} + ||b_2^\pm||_{L_2(\Gamma_l)}\Big) \cdot ||\underline{u}^{as,n} - \underline{u}_f^n||_{L_2(\Gamma_l)} \\ &\quad + \Big(||e_1||_{L_2(\omega)} + ||e_2||_{L_2(\omega)}\Big) \cdot ||\underline{u}^{as,n} - \underline{u}^n||_{L_2(\omega)} \\ &\leq C||\underline{u}^{as,n} - \underline{u}_f^n||_{1,2(\omega)} t^{n-1/2} \\ &\leq C|||\underline{u}^{as,n} - \underline{u}_f^n|||t^{n-3/2}\end{aligned}$$

Here we first used the Cauchy-Schwarz inequality, then the estimate

$$||u||_{L_2(\Gamma)} \leq Ct^{-1/2}||u||_{1,2(\omega)} \;\; \forall \underline{u} \in \mathcal{W},$$

which follows from the standard Trace theorem by a simple scaling argument, and finally the Korn inequality (2.2). In order to assure that $\underline{u}^{as,n} - \underline{u}_f^n \in \mathcal{V}$ we might have to add a rigid body motion, but this modification is not visible in the energy norm. Thus we have proved so far that the expansion $\underline{u}_f^n$ constructed above satisfies the estimate $|||\underline{u}^{as,n} - \underline{u}_f^n||| = O(t^{n-3/2})$. As we have pointed out, this estimate is not an optimal one. However, we can use the estimate to improve itself. By straightforward computation (based on the above algorithms) we can first estimate the strains and stresses for $\underline{u}_f^{n+N} - \underline{u}_f^n$ and get with help of these estimates

$$|||\underline{u}_f^{n+N} - \underline{u}_f^n||| = O(t^{n+1/2})$$

for any finite $N \geq 1$. Choosing here $N = 2$ and using the triangle inequality we conclude that actually

$$|||\underline{u}^{as,n} - \underline{u}_f^n||| = O(t^{n+1/2}).$$

Here we have chosen the conditions on Γ_s for both $\underline{u}^{as,n+2}$ and $\underline{u}^{as,n}$ according to $\underline{u}_f^{n+2}$. We need finally a lower bound for $|||\underline{u}^{as,n}|||$. From the expansions of $\underline{u}_f^n$ presented above we conclude that

$$|||\underline{u}_f^n|||^2 = \begin{cases} 48\frac{(1+\nu)(1+\gamma)}{E(1+2\gamma)}t^3||I_2^x[f]||_{L_2}^2 + O(t^5) & (\mathbf{B.1}) \\ 12\frac{(1+\nu)(1+\gamma)}{E(1+2\gamma)}t^3||I_1^x[f]||_{L_2}^2 + O(t^5) & (\mathbf{B.2}) \\ 4\frac{(1+\nu)(1+\gamma)}{E(1+2\gamma)}t||I_1^x[f]||_{L_2}^2 + O(t^3) & (\mathbf{M.1}) \\ \frac{(1+\nu)(1+\gamma)}{E(1+2\gamma)}t||f||_{L_2}^2 + O(t^3) & (\mathbf{M.2}) \end{cases}$$

Together with the convergence result, this shows that $|||\underline{u}_f^n|||/|||\underline{u}^{as,n}||| = O(1)$, except possibly when $n = 0$, or when $n = 1$ in the bending case. These cases make no exception, as is easily checked, so we come to the following convergence theorem:

Theorem 3.1 *The following estimate holds.*

$$\frac{|||\underline{u}^{as,n} - \underline{u}^{n,as}|||}{|||\underline{u}^{as,n}|||} \leq C(n,f) \cdot \begin{cases} \min\{1, t^{n-1}\} & \textit{(Bending case)} \\ t^n & \textit{(Membrane case)} \end{cases}$$

We have indicated here that the constant depends on n and f, but not on t.

4 The Edge Boundary Value Problem

In this chapter we will analyze in parallel $\underline{u}^{b,n}$ and its projection $\underline{u}^{n,b}$ according to (2.7).

Recall that $\underline{u}^{b,n}$ is the solution to the 2D elasticity problem where Γ_l is free of tractions and the boundary conditions on Γ_s are set so that $\underline{u}_f^n + \underline{u}^{b,n}$ satisfies the conditions of the original problem. Our aim is to first separate the boundary layer part from the other components of $\underline{u}^{b,n}$, and then to see how accurately different components are captured by the dimension reduction models. We begin with a lemma.

Lemma 4.1 *Consider the problem with any type of boundary conditions on Γ_s and with Γ_l free. Then if $\underline{\underline{\tau}}$ is the stress field corresponding to either the 2D model or any n-model, the following holds for all $-1 < x < 1$ and $0 \leq i \leq n$.*

$$\frac{\partial}{\partial x}\int_{-t/2}^{t/2} \tau_{11} z^i dz = i\int_{-t/2}^{t/2} \tau_{13} z^{i-1} dz, \quad \frac{\partial}{\partial x}\int_{-t/2}^{t/2} \tau_{13} z^i dz = i\int_{-t/2}^{t/2} \tau_{33} z^{i-1} dz.$$

Moreover, if one has stress boundary conditions $\tau_{11}(p,\cdot) = \overline{\tau}^p_{s1}$ or $\tau_{13}(p,\cdot) = \overline{\tau}^p_{s3}$ at a given end, $p = -1$ or $p = +1$, then for any i such that $0 \le i \le n$, the following identities hold for the corresponding stresses according to the n-model.

$$\int_{-t/2}^{t/2} \tau_{11}(p,z) z^i dz = \int_{-t/2}^{t/2} \overline{\tau}^p_{s1} z^i dz, \quad \int_{-t/2}^{t/2} \tau_{13}(p,z) z^i dz = \int_{-t/2}^{t/2} \overline{\tau}^p_{s3} z^i dz.$$

Proof. Consider in parallel the 2D and reduced variational formulations. Observe that

$$\underline{\tilde{u}}_1 = (v(x)z^i, 0) \in \mathcal{V}^n \subset \mathcal{V}, \quad \underline{\tilde{u}}_2 = (0, v(x)z^i) \in \mathcal{V}^n \subset \mathcal{V}$$

for any $v(x) \in H^1(-1,1)$ and for any $0 \le i \le n$ (modulo a possible rigid body motion). Substitute these candidates for $\underline{\tilde{u}}$ into the variational forms (2.1) and (2.3) and integrate once by parts with respect to x. In case of stress boundary conditions on Γ_s we obtain

$$\begin{aligned}
\int_{-1}^{1} \left[\int_{-t/2}^{t/2} \left(\tau_{11,1} z^i - i \tau_{13} z^{i-1} \right) dz \right] v(x) dx &= \int_{\Gamma_s} \left(\tau_{11} - \overline{\tau}^{\pm}_{s1} \right) z^i v(x) \cdot n_x \, dz, \\
\int_{-1}^{1} \left[\int_{-t/2}^{t/2} \left(\tau_{13,1} z^i - i \tau_{33} z^{i-1} \right) dz \right] v(x) dx &= \int_{\Gamma_s} \left(\tau_{13} - \overline{\tau}^{\pm}_{s3} \right) z^i v(x) \cdot n_x \, dz.
\end{aligned}$$

Note that this holds for other boundary conditions as well provided that one takes $v(p) = 0$ whenever a displacement component is prescribed at $x = p$. Since $v(x)$ is arbitrary, taking $v(\pm 1) = 0$ proves the first claim. The second claim then follows by taking $v(p) \neq 0$. □

As is well-known, the so called Saint-Venant's Principle holds in the problem of elastic strip. According to this principle, self-equilibrating stresses on Γ_s cause only exponentially (in scale t) decaying boundary layer terms to the solution of the 2D model. Let us define for notational convenience

$$A(x) = \int_{-t/2}^{t/2} \tau_{11} dz, \quad B(x) = \int_{-t/2}^{t/2} \tau_{13} dz, \quad C(x) = \int_{-t/2}^{t/2} \tau_{11} z dz.$$

The precise conditions for self-equilibrium may now be defined as follows.

Definition 4.1 *A stress distribution at x is called self-equilibrating if*

$$A(x) = B(x) = C(x) = 0.$$

Note that by Lemma 4.1, $A(x) = A$ and $B(x) = B$ must be constants and $C(x) = C(0) + Bx$ for any solution of the edge boundary value problem.

Theorem 4.1 (Saint-Venant's Principle) *Suppose that we are given a problem with self-equilibrating surface tractions $\overline{\tau}_{s1}^{\pm}$ and $\overline{\tau}_{s3}^{\pm}$ on Γ_s and with Γ_l free. Then both the 2D model and reduced n-model solutions (n arbitary) decay exponentially in the following sense:*

$$|||\underline{u}|||_\delta \leq Ce^{-k\delta/t}|||\underline{u}||| \tag{4.1}$$

with some positive constants C and k. Here $|||\cdot|||_\delta$ denotes the square root of deformation energy over the domain $\omega_\delta = \{(x,z)| -1+\delta < x < 1-\delta, -t/2 < z < t/2\}$.

Althought the theorem is well-known, cite [HK], we give a proof (based on variational methods) in Appendix C for the reader's convenience. We note also that Theorem 4.1 gives the rate of exponential decay only with respect to the parameter t. For a discussion concerning approximation of the parameter k, cite [HK], [H1],[H2].

For the unit tension, bending and flexure fields given in Appendix B we have

$$\begin{array}{lll} A^{UT} = 1, & B^{UT} = 0, & C^{UT}(0) = 0. \\ A^{UB} = 0, & B^{UB} = 0, & C^{UB}(0) = 1. \\ A^{UF} = 0, & B^{UF} = 1, & C^{UF}(0) = 0. \end{array}$$

Given the constraints A, B and $C(0)$ we can define an "interior" displacement field $\underline{u}^i$ as

$$\underline{u}^i = A\underline{u}^{UT} + C(0)\underline{u}^{UB} + B\underline{u}^{UF}.$$

If we substract $\underline{u}^i$ from the actual solution, the remaining part is seen to satisfy the conditions of self-equlibrium. Thus we may write

$$\underline{u}^{b,n} = \underline{u}^i + \underline{u}^e + \underline{u}^{RD}, \tag{4.2}$$

where $\underline{u}^e$ decays exponentially and $\underline{u}^{RD} = \sum_{i=1}^3 c_i \underline{u}^{RDi}$ is a rigid body motion. When considering dimensional reduction, we have to demand that the reduction order satisfies $n \geq 1$ in the membrane case and $n \geq 3$ in the bending case in order to quarantee that the unit solutions belong to $\mathcal{W}^n$ (see Appendix B). The splitting formula holds not only for surface traction conditions but for any type of boundary conditions. This is of course due to the fact that we can always consider any solution $\underline{u}$ (modulo a rigid body motion) as a solution to that surface traction problem where the given stresses are determined by $\underline{u}$ itself.

We are now ready to formulate the main result of this chapter. We are going to give the values of A, $C(0)$ and B and an estimate for the energy norm of $\underline{u}^e$ for all of the different types of boundary conditions considered for the 2D model and for any reduced models with $n \geq 1$ (membrane case) or $n \geq 3$ (bending case). The different combinations of the boundary conditions at the ends are treated one by one so that in each case, only one component at $x = -1$ is assumed to be non-homogeneous and the other three (one at $x = -1$ and two at $x = +1$) are assumed to be homogeneous. The general case then follows from these 32 cases by symmetry arguments and superposition.

Theorem 4.2 *For the 2D problem and for any reduced problems with $n \geq 1$ for the membrane case, $n \geq 3$ for the bending case, the values of A, $C(0)$ and B and the energy norm of $\underline{u}^e$ are as given or estimated in the tables of Appendices D and E.*

The assumptions made on the non-homogeneous boundary condition and the type of the three homogeneous conditions are given in the tables. Note that the results depend essentially on the type of the homogeneous conditions.

In order to prove the theorem, we need a number of auxiliary lemmas. The first one deals with relations between displacements and stresses.

Lemma 4.2 *In the 2D model and in any reduced models with $n \geq 1$ for the membrane case, $n \geq 3$ for the bending case, the following hold.*

$$\begin{aligned} A &= \frac{1}{2(1+\gamma)} \int_{\Gamma_s} \left[\gamma \tau_{13} z + \frac{E(1+2\gamma)}{1+\nu} u \right] \cdot n_x \, dz, \\ C(0) &= \frac{1}{2(1+\gamma)} \int_{\Gamma_s} \left[\frac{\gamma}{2} \tau_{13} z^2 + \frac{E(1+2\gamma)}{1+\nu} uz \right] \cdot n_x \, dz. \end{aligned}$$

Proof. To prove the second identity, we define

$$h(x) = \frac{1}{2(1+\gamma)} \left[\int_{-t/2}^{t/2} \frac{\gamma}{2} \tau_{13} z^2 + \frac{E(1+2\gamma)}{1+\nu} uzdz \right]$$

Using lemma 4.1 and the stress-displacement relations we get $h'(x) = \frac{1}{2}C(x) = \frac{1}{2}C(0) + \frac{1}{2}Bx$. Hence we have $h(1) - h(-1) = C(0)$ and the claim follows. The first identity follows in a similar manner. $\square$

We will make use of the complementary energy principle. In order to state it here we need first two definitons.

Definition 4.2 *By a statically admissible stress field we mean any stress tensor which satisfies the Euler equations and given stress boundary conditions (but is not necessarily derivable from any displacement field).*

Definition 4.3 *By a geometrically admissible displacement field we mean any displacement field which satisfies given displacement boundary conditions.*

Theorem 4.3 (Complementary energy principle) *Let us approximate a stress field $\underline{\underline{\tau}}$ of a 2D solution by*

$$\underline{\underline{\tau}}^A = \frac{1}{2}\left(\underline{\underline{\tau}}^S + \underline{\underline{\tau}}^D\right),$$

where $\underline{\underline{\tau}}^S$ is a statically admissible stress field and $\underline{\underline{\tau}}^D$ is obtained from a geometrically admissible displacement field by means of the stress-displacement relations. Then

$$|||\underline{\underline{\tau}} - \underline{\underline{\tau}}^A||| = \frac{1}{2}|||\underline{\underline{\tau}}^S - \underline{\underline{\tau}}^D|||.$$

Proof may be found e.g. in [No].

The energy norm is of course defined here as derived directly from the stresses with the help of (assumed) stress-strain relations, so displacements are not needed.

We will need sharp estimates for the inner products between the unit solutions and exponentially decaying boundary fields. The following lemma gives us estimates which are of order $\sqrt{t}$ better than the ones given straightly by the Cauchy-Schwarz inequality.

Lemma 4.3 *The following estimates hold for the inner products between the unit solutions and any displacement field $\underline{u}^e$ satisfying the assumptions of the Saint-Venant's Principle.*

$$\begin{aligned}
\mathcal{A}(\underline{u}^{UT}, \underline{u}^e) &\leq C|||\underline{u}^e|||, \\
\mathcal{A}(\underline{u}^{UB}, \underline{u}^e) &\leq Ct^{-1}|||\underline{u}^e|||, \\
\mathcal{A}(\underline{u}^{UF}, \underline{u}^e) &\leq Ct^{-1}|||\underline{u}^e|||.
\end{aligned}$$

Proof. Let us denote by $\mathcal{A}_{(a,b)}$ the part of $\mathcal{A}$ where the integration is carried out over the region where $a < x < b$. To prove the first claim, we proceed as

$$\begin{aligned}
\mathcal{A}(\underline{u}^{UT}, \underline{u}^{e}) &= \sum_{i=0}^{\lceil 1/t\rceil -1} \mathcal{A}_{(-1+it,-1+(i+1)t)}(\underline{u}^{UT}, \underline{u}^{e}) + \mathcal{A}_{(1-it,1-(i+1)t)}(\underline{u}^{UT}, \underline{u}^{e}) \\
&\leq \sum_{i=0}^{\lceil 1/t\rceil -1} \left(|||\underline{u}^{UT}|||_{(-1+it,-1+(i+1)t)} + |||\underline{u}^{UT}|||_{(1-it,1-(i+1)t)} \right) |||\underline{u}^{e}|||_{it} \\
&\leq C|||\underline{u}^{e}||| \sum_{i=0}^{\lceil 1/t\rceil -1} e^{-ki} \leq C|||\underline{u}^{e}|||.
\end{aligned}$$

If $1/t$ is not an integer then $-1+(i+1)t$ and $1-(i+1)t$ are replaced by 0 in the last term of the sum. The remainig two cases are treated similarly.$\square$

Proof of Theorem 4.2. Some of the values in the tables of Appendix D and E are given exactly and some with an error term. All the values which are given exactly and the relations $B = \pm C(0)$, $B = C(0) - \int_{-t/2}^{t/2} \overline{\tau}_{s1}^{-} z dz$ follow quite easily from the relation $C(x) = C(0) + Bx$ and Lemma 4.2.

Concerning the values with an error term we will first consider the 2D model only. The results for the reduced models follow then quite easily. Let us now turn our attention to those values for non-homogeneous displacement edge data which are not given exactly. Note that in some of the cases we have separated the "leading" term of the boundary condition due to its special role in the solution. Let us first analyze the problems where the boundary condition is taken purely as the leading term. We begin with estimating the energy of $\underline{u}^{e}$ by the complementary energy principle. This may be done by choosing $\underline{u}^{S}$ as a linear combination of the unit solutions (with coefficients as given in the table without the error term) and rigid body motions (with coefficients which make $\underline{u}^{S}$ satisfy the leading terms of kinematical boundary conditions). The stress field derived from this displacement field plays then the role of a statically admissible stress field $\underline{\underline{\tau}}^{S}$. After this is done, we define the geometrically admissible displacement field $\underline{u}^{D}$ as $\underline{u}^{S} + \underline{u}^{\tilde{e}}$, where the correction term corresponding to given displacement conditions is defined as

$$\begin{aligned}
\underline{u}^{\tilde{e}}(x,z) &= \left[\overline{\underline{u}}^{-}(z) - \underline{u}^{S}(-1,z)\right] \frac{1-x}{2} e^{-(1+x)/t} \\
&\quad + \left[\overline{\underline{u}}^{+}(z) - \underline{u}^{S}(+1,z)\right] \frac{1+x}{2} e^{-(1-x)/t}.
\end{aligned} \tag{4.3}$$

By the complementary energy principle we have

$$|||(A-A')\underline{u}^{UT}+(C(0)-C(0)')\underline{u}^{UB}+(B-B')\underline{u}^{UF}+\underline{u}^{e}-\frac{1}{2}\underline{u}^{\tilde{e}}||| = \frac{1}{2}|||\underline{u}^{\tilde{e}}|||.$$

The coefficients with primes are defined as the values (without correction) given in the tables. By straightforward computation we get for $|||\underline{u}^{\tilde{e}}|||$ the estimates given in the tables for $|||\underline{u}^{e}|||$. If we now look at the energy in the middle of the strip, say at $(-1/2 < x < 1/2)$, we may conclude by Saint-Venant's Principle that $\underline{u}^{e}$ is exponentially small and we have by the triangle inequality

$$\begin{aligned} A - A' &= O(t^{1/2}|||\underline{u}^{\tilde{e}}|||) \\ C(0) - C(0) &= O(t^{3/2}|||\underline{u}^{\tilde{e}}|||) \\ B - B' &= O(t^{3/2}|||\underline{u}^{\tilde{e}}|||). \end{aligned} \tag{4.4}$$

Thus we conclude again by the triangle inequality that $|||\underline{u}^{e}||| = O(|||\underline{u}^{\tilde{e}}|||)$. We improve next the bounds (4.4) by a factor $\sqrt{t}$, by making use of Lemma 4.3. First we form the inner product between $\underline{u}$ and the corresponding unit solution field to obtain

$$A = \left[\mathcal{A}(\underline{u},\underline{u}^{UT}) - \mathcal{A}(\underline{u}^{e},\underline{u}^{UT})\right]/|||\underline{u}^{UT}|||^2, \tag{4.5}$$

$$C(0) = \left[\mathcal{A}(\underline{u},\underline{u}^{UB}) - \mathcal{A}(\underline{u}^{e},\underline{u}^{UB})\right]/|||\underline{u}^{UB}|||^2, \tag{4.6}$$

$$B = \left[\mathcal{A}(\underline{u},\underline{u}^{UF}) - \mathcal{A}(\underline{u}^{e},\underline{u}^{UF})\right]/|||\underline{u}^{UF}|||^2. \tag{4.7}$$

We have used here the fact that $\mathcal{A}(\underline{u}^{UB},\underline{u}^{UF}) = 0$. The first terms in (4.5) trough (4.7) (corresponding to $\underline{u}^{e} = \underline{0}$) may in most cases be given simple expressions by partial integration. In this way we have obtained the leading terms of the coefficients (whenever given precisely) in the tables. Applying Lemma 4.3 in estimating the remainder terms in (4.5) through (4.7) we can now improve the bounds (4.4). In the cases where a relation $B = \pm C(0)$ is given, the inner product between $\underline{u}$ and $\underline{u}^{UB}$ cannot be derived directly. However, starting from the mentioned relation we obtain

$$C(0) = \left[\mathcal{A}(\underline{u},\underline{u}^{UB} \pm \underline{u}^{UF}) - \mathcal{A}(\underline{u}^{e},\underline{u}^{UB} \pm \underline{u}^{UF})\right]/\left(|||\underline{u}^{UB}|||^2 + |||\underline{u}^{UF}|||^2\right),$$

which may be evaluated utilizing the fact that for $\underline{u}^{UB} \pm \underline{u}^{UF}$ the stress component τ_{11} is identically zero at $x = \mp 1$.

For the remaining parts of the displacement boundary conditions (possible leading term subtracted) we utilize the same ideas choosing simply $\underline{u}^S = 0$.

Then we are left with non-homogeneous stress conditions. We write $\underline{u} = A'\underline{u}^{UT} + C(0)'\underline{u}^{UB} + B'\underline{u}^{UF} + \underline{\tilde{u}}$, where the coefficients with primes are the ones given in the tables. In order to estimate $|||\underline{\tilde{u}}|||$ we utilize again the complementary energy principle. In $\omega_{(-1,-1+t)}$, i.e., in the part of the strip where $-1 < x < -1+t$, we choose the statically admissible stress field $\underline{\underline{\tau}}^S$ as the solution to the problem with the stress conditions $\tilde{\tau}_{11}$, $\tilde{\tau}_{13}$ at $x = -1$ determined by $\underline{\tilde{u}}$ and with free boundary conditions on the remaining part of $\partial\omega_{(-1,-1+t)}$. It is important to note that this auxiliary problem is well-posed, i.e. the stress conditions at $x = -1$ satisfy the conditions for self-equilibrium. In $\omega_{(-1+t,1)}$ we may then choose $\underline{\underline{\tau}}^S = 0$. The Euler equations hold also at $x = -1+t$ (in the sense of distributions) due to the continuity of τ_{11} and τ_{13}. By a simple scaling argument we may deduce from standard stability results the estimate $|||\underline{\underline{\tau}}^S||| = O(\sqrt{t}(||\tilde{\tau}_{11}||_{L_2} + ||\tilde{\tau}_{13}||_{L_2}))$. The geometrically admissible displacement field is then defined as in (4.3). Finally we again improve the bounds for the error in the given values for A, $C(0)$ and B by a factor $\sqrt{t}$, using the relations (4.5) through (4.7). For the bending case with τ_{11} given, where (4.6) cannot be derived directly, we get with help of $B = C(0) - \int_{-t/2}^{t/2} \overline{\tau}_{s1}^{-} z dz$ the relation

$$C(0) = \frac{\mathcal{A}(\underline{u}, \underline{u}^{UB} + \underline{u}^{UF}) + |||\underline{u}^{UF}|||^2 \cdot \int_{-t/2}^{t/2} \overline{\tau}_{s1}^{-} z dz - \mathcal{A}(\underline{u}^e, \underline{u}^{UB} + \underline{u}^{UF})}{|||\underline{u}^{UB}|||^2 + |||\underline{u}^{UF}|||^2}$$

where the first term is seen to vanish by partial integration.

In some of the cases we have set some restrictions (R) for the given stress in order to quarantee the well posedness of the problem. However, the restrictions may always be satisfied by subtracting a suitable combination of the unit solutions from the original problem.

To see that the same results hold for the reduced models we observe that the formulas (4.5) through (4.7) are valid also in these cases. Thus all we need to know is that the field $\underline{u}^e$ satisfies the same estimates as in the 2D problem. This follows easily by the projection principle. □

Theorem 4.2 immediately gives us also the dimension reduction error, both globally and in the interior of the domain. Because the given values hold for both 2D and reduced models, the reduction error is at most of the same order as the error terms in the tables. In order to compare the different components we need to note only that $|||\underline{u}^{UT}||| \sim t^{-1/2}$ and $|||\underline{u}^{UB}||| \sim |||\underline{u}^{UF}||| \sim t^{-3/2}$. We see that the global relative reduction error (avoiding some special cases) is $O(\sqrt{t})$, due to the error made in the boundary layer. In all of the cases the reduction error in the interior part of the strip is either exponentially small (in cases where the unit-field component $\underline{u}^i$ is captured exactly) or of order $\sqrt{t}$ smaller than the global one.

Let us now discuss shortly the special cases excluded by Theorem 4.2 where the model order n is not high enough in order to capture the unit fields. We note first that for the membrane problem the model $n = 0$ fails in general asymptotically. An exception is the case $\gamma = 0$, for which Theorem 4.2 holds even with $n = 0$. For the bending case $n = 0$ fails asymptotically, and so does the linear model $n = 1$, except if $\gamma = 0$. Then the relative error of the far-field solution is of order $O(t)$, independently of the type of boundary conditions. The quadratic model $n = 2$ is the first one to converge in the general case $\gamma \neq 0$. Here the relative interior convergence rate is again $O(t)$ for all types of boundary conditions. We note that it is possible to construct asymptotically converging models also with $n < 2$ (e.g. the classical Timoshenko model, which may be obtained by eliminating the quadratic term from the 2-model). However, keeping only in the straightforward use of the energy principle, $n = 2$ is the simplest model to converge in the general case.

Let us finally join together the results of Chapters 3 and 4 in order to deduce asymptotic error estimates for dimension reduction applied to the original problem considered. Avoiding some special cases, the global relative reduction error is $O(\sqrt{t})$ in the energy norm, independently of the model order n. The interior convegence rate is either $O(t)$ (for those boundary conditions for which a correction term for A, $C(0)$ or B is given in the tables for Theorem 4.2) or as given by Theorem 3.1: $O(t^{n-1})$ for the bending case and $O(t^n)$ for the membrane case.

Thus it is seen that the model order n has in general no influence at all on the global asymptotic convergence rate, due to the true 2D behaviour of the boundary layer term. Even the interior asymptotic convergence rate is affected by n only for some types of boundary conditions. In order to get the full benefit from the usage of high-order models, one should use the 2D model in the boundary layer, say to a distance $\sim t \log t$ from the edges, and the n-model in the interior of the domain only. Such a model (which could be easily implemented e.g. to FEM) would give as global convergence rates the "optimal" ones: $O(t^{n-1})$ for the bending problem and $O(t^n)$ for the membrane problem.

A Asymptotic Fields

B.1 Bending Problem, $\overline{\tau}_{l1}^{\pm} = 0$, $\overline{\tau}_{l3}^{\pm} = \pm t^3 f$.

$$
\begin{aligned}
u_1 &= \frac{1+\nu}{E(1+2\gamma)}\left\{[-24(1+\gamma)I_3^x[f]] + t^2\left[-\frac{3(2+7\gamma)}{5}I_1^x[f]\right] + t^4\left[\frac{87+17\gamma}{2800}f'\right] + \cdots\right\} \\
u_3 &= \frac{1+\nu}{E(1+2\gamma)}\left\{[4(2+3\gamma)I_1^x[f]] + t^2\left[-\frac{1-\gamma}{10}f'\right] + \left[-\frac{244+331\gamma}{16800}f^{(3)}\right] + \cdots\right\} \\
u_5 &= \frac{1+\nu}{E(1+2\gamma)}\left\{\left[-\frac{3+5\gamma}{5}f'\right] + t^2\left[\frac{4+5\gamma}{200}f^{(3)}\right] + t^4\left[\frac{401+645\gamma}{336000}f^{(5)}\right] + \cdots\right\} \\
&\;\;\vdots
\end{aligned}
$$

$$
\begin{aligned}
w_0 &= \frac{1+\nu}{E(1+2\gamma)}\left\{[24(1+\gamma)I_4^x[f]] + t^2\left[-\frac{3(8+13\gamma)}{5}I_2^x[f]\right] + t^4\left[-\frac{227+297\gamma}{2800}f\right] + \cdots\right\} \\
w_2 &= \frac{1+\nu}{E(1+2\gamma)}\left\{[12\gamma I_2^x[f]] + t^2\left[\frac{3(5+7\gamma)}{10}f\right] + t^4\left[\frac{70-17\gamma}{5600}f''\right] + \cdots\right\} \\
w_4 &= \frac{1+\nu}{E(1+2\gamma)}\left\{[-(1+3\gamma)f] + t^2\left[-\frac{2+\gamma}{40}f''\right] + t^4\left[\frac{87+331\gamma}{67200}f^{(4)}\right] + \cdots\right\} \\
w_6 &= \frac{1+\nu}{E(1+2\gamma)}\left\{\left[\frac{2+5\gamma}{30}f''\right] + t^2\left[-\frac{1+5\gamma}{1200}f^{(4)}\right] + t^4\left[-\frac{244+645\gamma}{2016000}f^{(6)}\right] + \cdots\right\} \\
&\;\;\vdots
\end{aligned}
$$

$$
\begin{aligned}
\tau_{11} &= -24zI_2^x[f] - \frac{2z(3t^2-20z^2)}{5}f + \frac{z(87t^4-280t^2z^2-1680z^4)}{2800}f'' \\
&\quad + \frac{z(389t^6-3660t^4z^2+5040t^2z^4+4800z^6)}{252000} + \cdots \\
\tau_{13} &= \left(t^2-4z^2\right)\left(-3I_1^x[f] - \frac{t^2-20z^2}{40}f' + \frac{17t^4-280t^2z^2-560z^4}{22400}f^{(3)} + \cdots\right) \\
\tau_{33} &= z(3t^2-4z^2)f + \left(t^2-4z^2\right)^2\left(\frac{z}{40}f'' - \frac{z(17t^2+20z^2)}{22400}f^{(4)} + \cdots\right)
\end{aligned}
$$

B.2 Bending Problem, $\overline{\tau}_{l1}^{\pm} = t^2 f$, $\overline{\tau}_{l3}^{\pm} = 0$.

$$
\begin{aligned}
u_1 &= \frac{1+\nu}{E(1+2\gamma)}\left\{[-12(1+\gamma)I_2^x[f]] + t^2\left[-\frac{6+11\gamma}{10}f\right] + t^4\left[-\frac{53+123\gamma}{5600}f''\right] + \cdots\right\} \\
u_3 &= \frac{1+\nu}{E(1+2\gamma)}\left\{[2(2+3\gamma)f] + t^2\left[\frac{7+13\gamma}{60}f''\right] + \left[\frac{36+89\gamma}{33600}f^{(4)}\right] + \cdots\right\} \\
u_5 &= \frac{1+\nu}{E(1+2\gamma)}\left\{\left[-\frac{3+5\gamma}{10}f''\right] + t^2\left[-\frac{8+15\gamma}{1200}f^{(4)}\right] + t^4\left[-\frac{19+55\gamma}{672000}f^{(6)}\right] + \cdots\right\} \\
&\ \ \vdots
\end{aligned}
$$

$$
\begin{aligned}
w_0 &= \frac{1+\nu}{E(1+2\gamma)}\left\{[12(1+\gamma)I_3^x[f]] + t^2\left[-\frac{4+9\gamma}{10}I_1^x[f]\right] + t^4\left[-\frac{87+157\gamma}{5600}f'\right] + \cdots\right\} \\
w_2 &= \frac{1+\nu}{E(1+2\gamma)}\left\{[6\gamma I_1^x[f]] + t^2\left[\frac{5+11\gamma}{20}f'\right] + t^4\left[\frac{70+123\gamma}{11200}f^{(3)}\right] + \cdots\right\} \\
w_4 &= \frac{1+\nu}{E(1+2\gamma)}\left\{\left[-\frac{1+3\gamma}{2}f'\right] + t^2\left[-\frac{6+13\gamma}{240}f^{(3)}\right] + t^4\left[-\frac{53+89\gamma}{134400}f^{(5)}\right] + \cdots\right\} \\
w_6 &= \frac{1+\nu}{E(1+2\gamma)}\left\{\left[\frac{2+5\gamma}{60}f^{(3)}\right] + t^2\left[\frac{7+15\gamma}{7200}f^{(5)}\right] + t^4\left[\frac{36+55\gamma}{4032000}f^{(7)}\right] + \cdots\right\} \\
&\ \ \vdots
\end{aligned}
$$

$$
\begin{aligned}
\tau_{11} &= -12zI_1^x[f] - \frac{z(3t^2-20z^2)}{5}f' - \frac{z(159t^4-1960t^2z^2+5040z^4)}{16800}f^{(3)} \\
&\quad - \frac{z(4t^6-135t^4z^2+840t^2z^4-1200z^6)}{126000}f^{(5)} + \cdots \\
\tau_{13} &= -\frac{t^2-12z^2}{2}f + \left(t^2-4z^2\right)\left(-\frac{t^2-20z^2}{80}f'' - \frac{19t^4-560t^2z^2+1680z^4}{134400}f^{(4)} + \cdots\right) \\
\tau_{33} &= \left(t^2-4z^2\right)\left(\frac{z}{2}f' + \frac{z(t^2-4z^2)}{80}f^{(3)} + \frac{z(t^2-4z^2)(19t^2-60z^2)}{134400}f^{(5)} + \cdots\right)
\end{aligned}
$$

M.1 Membrane Problem, $\overline{\tau}_{l1}^{\pm} = \pm t f$, $\overline{\tau}_{l3}^{\pm} = 0$.

$$
\begin{aligned}
u_0 &= \frac{1+\nu}{E(1+2\gamma)}\left\{[-2(1+\gamma)I_2^x[f]] + t^2\left[-\frac{2+5\gamma}{12}f\right] + t^4\left[-\frac{1+31\gamma}{2880}f''\right] + \cdots\right\} \\
u_2 &= \frac{1+\nu}{E(1+2\gamma)}\left\{[(2+3\gamma)f] + t^2\left[\frac{1+3\gamma}{24}f''\right] + t^4\left[-\frac{28+27\gamma}{5760}f^{(4)}\right] + \cdots\right\} \\
u_4 &= \frac{1+\nu}{E(1+2\gamma)}\left\{\left[-\frac{3+5\gamma}{12}f''\right] + t^2\left[-\frac{\gamma}{288}f^{(4)}\right] + t^4\left[\frac{57+85\gamma}{69120}f^{(6)}\right] + \cdots\right\} \\
u_6 &= \frac{1+\nu}{E(1+2\gamma)}\left\{\left[\frac{4+7\gamma}{360}f^{(4)}\right] + t^2\left[-\frac{1+\gamma}{8640}f^{(6)}\right] + t^4\left[-\frac{86+143\gamma}{2073600}f^{(8)}\right] + \cdots\right\} \\
&\vdots
\end{aligned}
$$

$$
\begin{aligned}
w_1 &= \frac{1+\nu}{E(1+2\gamma)}\left\{[2\gamma I_1^x[f]] + t^2\left[\frac{3+5\gamma}{12}f'\right] + t^4\left[\frac{30+31\gamma}{2880}f^{(3)}\right] + \cdots\right\} \\
w_3 &= \frac{1+\nu}{E(1+2\gamma)}\left\{\left[-\frac{1+3\gamma}{3}f'\right] + t^2\left[-\frac{2+3\gamma}{72}f^{(3)}\right] + t^4\left[-\frac{1-27\gamma}{17280}f^{(5)}\right] + \cdots\right\} \\
w_5 &= \frac{1+\nu}{E(1+2\gamma)}\left\{\left[\frac{2+5\gamma}{60}f^{(3)}\right] + t^2\left[\frac{1+\gamma}{1440}f^{(5)}\right] + t^4\left[-\frac{28+85\gamma}{345600}f^{(7)}\right] + \cdots\right\} \\
&\vdots
\end{aligned}
$$

$$
\begin{aligned}
\tau_{11} &= -2I_1^x[f] - \frac{t^2-12z^2}{6}f' - \frac{t^4-120t^2z^2+720z^4}{2880}f^{(3)} \\
&\quad + \frac{23t^6-294t^4z^2+672z^6}{60480}f^{(5)} + \cdots \\
\tau_{13} &= 2zf + \left(t^2-4z^2\right)\left(\frac{z}{6}f'' + \frac{z(t^2-36z^2)}{2880}f^{(4)} - \frac{z(23t^4-6t^2z^2-24z^4)}{60480}f^{(6)} + \cdots\right) \\
\tau_{33} &= \left(t^2-4z^2\right)\left(\frac{1}{4}f' + \frac{t^2-4z^2}{96}f^{(3)} - \frac{(t^2+12z^2)(t^2-4z^2)}{23040}f^{(5)} + \cdots\right)
\end{aligned}
$$

M.2 Membrane Problem, $\overline{\tau}_{l1}^{\pm} = 0$, $\overline{\tau}_{l3}^{\pm} = f$.

$$
\begin{aligned}
u_0 &= \frac{1+\nu}{E(1+2\gamma)}\left\{[-\gamma I_1^x[f]] + t^2\left[\frac{1+\gamma}{24}f'\right] + t^4\left[\frac{14+29\gamma}{5760}f^{(3)}\right] + \cdots\right\}\\
u_2 &= \frac{1+\nu}{E(1+2\gamma)}\left\{\left[-\frac{1+\gamma}{2}f'\right] + t^2\left[-\frac{2+3\gamma}{48}f^{(3)}\right] + t^4\left[-\frac{13+27\gamma}{11520}f^{(5)}\right] + \cdots\right\}\\
u_4 &= \frac{1+\nu}{E(1+2\gamma)}\left\{\left[\frac{2+3\gamma}{24}f^{(3)}\right] + t^2\left[\frac{3+5\gamma}{576}f^{(5)}\right] + t^4\left[\frac{12+25\gamma}{138240}f^{(7)}\right] + \cdots\right\}\\
u_6 &= \frac{1+\nu}{E(1+2\gamma)}\left\{\left[-\frac{3+5\gamma}{720}f^{(5)}\right] + t^2\left[-\frac{4+7\gamma}{17280}f^{(7)}\right] + t^4\left[-\frac{11+23\gamma}{4147200}f^{(9)}\right] + \cdots\right\}\\
&\;\vdots
\end{aligned}
$$

$$
\begin{aligned}
w_1 &= \frac{1+\nu}{E(1+2\gamma)}\left\{[(1+\gamma)f] + t^2\left[-\frac{\gamma}{24}f''\right] + t^4\left[-\frac{15+29\gamma}{5760}f^{(4)}\right] + \cdots\right\}\\
w_3 &= \frac{1+\nu}{E(1+2\gamma)}\left\{\left[\frac{\gamma}{6}f''\right] + t^2\left[\frac{1+3\gamma}{144}f^{(4)}\right] + t^4\left[\frac{14+27\gamma}{34560}f^{(6)}\right] + \cdots\right\}\\
w_5 &= \frac{1+\nu}{E(1+2\gamma)}\left\{\left[-\frac{1+3\gamma}{120}f^{(4)}\right] + t^2\left[-\frac{2+5\gamma}{2880}f^{(6)}\right] + t^4\left[-\frac{13+25\gamma}{691200}f^{(8)}\right] + \cdots\right\}\\
&\;\vdots
\end{aligned}
$$

$$
\begin{aligned}
\tau_{11} &= \frac{t^2-12z^2}{24}f'' + \frac{7t^4-120t^2z^2+240z^4}{2880}f^{(4)}\\
&\quad + \frac{37t^6-1092t^4z^2+5040t^2z^4-4032z^6}{967680}f^{(6)} + \cdots\\
\tau_{13} &= \left(t^2-4z^2\right)\left(-\frac{z}{24}f^{(3)} - \frac{z(7t^2-12z^2)}{2880}f^{(5)} - \frac{z(37t^4-216t^2z^2+144z^4)}{967680} + \cdots\right)\\
\tau_{33} &= f + \left(t^2-4z^2\right)^2\left(-\frac{1}{384}f^{(4)} - \frac{(3t^2-4z^2)}{23040}f^{(6)} + \cdots\right)
\end{aligned}
$$

B Special Solutions

Rigid Body Motions

$$\begin{array}{lllllllll} u^{RD1} & = & 1 & u^{RD2} & = & 0 & u^{RD3} & = & z \\ w^{RD1} & = & 0 & w^{RD2} & = & 1 & w^{RD3} & = & -x \end{array}$$

Unit Tension Field

$$\begin{aligned} u^{UT} &= \tfrac{1+\nu}{E(1+2\gamma)t}\left[(1+\gamma)x\right] \\ w^{UT} &= \tfrac{1+\nu}{E(1+2\gamma)t}\left[-\gamma z\right] \end{aligned}$$

$$\begin{array}{llllll} \varepsilon_{11}^{UT} & = & \tfrac{1+\nu}{E(1+2\gamma)t}\left[1+\gamma\right] & \tau_{11}^{UT} & = & \tfrac{1}{t} \\ \varepsilon_{13}^{UT} & = & 0 & \tau_{13}^{UT} & = & 0 \\ \varepsilon_{33}^{UT} & = & \tfrac{1+\nu}{E(1+2\gamma)t}\left[-\gamma\right] & \tau_{33}^{UT} & = & 0 \end{array}$$

Unit Bending Field

$$\begin{aligned} u^{UB} &= \tfrac{1+\nu}{E(1+2\gamma)t^3}\left[12(1+\gamma)xz\right] \\ w^{UB} &= \tfrac{1+\nu}{E(1+2\gamma)t^3}\left[-6(1+\gamma)x^2-6\gamma z^2\right] \end{aligned}$$

$$\begin{array}{llllll} \varepsilon_{11}^{UB} & = & \tfrac{1+\nu}{E(1+2\gamma)t^3}\left[12(1+\gamma)z\right] & \tau_{11}^{UB} & = & \tfrac{1}{t^3}\left[12z\right] \\ \varepsilon_{13}^{UB} & = & 0 & \tau_{13}^{UB} & = & 0 \\ \varepsilon_{33}^{UB} & = & \tfrac{1+\nu}{E(1+2\gamma)t^3}\left[-12\gamma z\right] & \tau_{33}^{UB} & = & 0 \end{array}$$

Unit Flexure Field

$$\begin{aligned} u^{UF} &= \tfrac{1+\nu}{E(1+2\gamma)t^3}\left\{\left[3(1+2\gamma)t^2+6(1+\gamma)x^2\right]z-2(2+3\gamma)z^3\right\} \\ w^{UF} &= \tfrac{1+\nu}{E(1+2\gamma)t^3}\left[-2(1+\gamma)x^3-6\gamma xz^2\right] \end{aligned}$$

$$\begin{array}{llllll} \varepsilon_{11}^{UF} & = & \tfrac{1+\nu}{E(1+2\gamma)t^3}\left[12(1+\gamma)xz\right] & \tau_{11}^{UF} & = & \tfrac{1}{t^3}\left[12xz\right] \\ \varepsilon_{13}^{UF} & = & \tfrac{1+\nu}{Et^3}\left[\tfrac{3}{2}(t^2-4z^2)\right] & \tau_{13}^{UF} & = & \tfrac{1}{t^3}\left[\tfrac{3}{2}(t^2-4z^2)\right] \\ \varepsilon_{33}^{UF} & = & \tfrac{1+\nu}{E(1+2\gamma)t^3}\left[-12\gamma xz\right] & \tau_{33}^{UF} & = & 0 \end{array}$$

C The Saint-Venant's Principle

The following proof follows closely the original idea of [Tou]. Below we denote by $|||\underline{u}|||^2_{(a,b)}$ the deformation energy evaluated over the region where $a < x < b$. Let us begin with a lemma.

Lemma C.1 *There is a constant C such that for any $\underline{u} \in \mathcal{W}$ and for any a, $-1 \leq a \leq 1-t$, there exists a rigid body motion $\underline{u}^{RD}$ such that*

$$||\underline{u} + \underline{u}^{RD}||^2_{L_{2(a,a+t)}} \leq Ct^2 |||\underline{u}|||^2_{(a,a+t)}.$$

Proof. Scale to a t-independent region and apply the Korn inequality. □

Proof of the Saint-Venant's Principle. It clearly sufficies to prove the theorem in the case where the stress boundary conditions are homogeneous at $x = 1$. Let us denote by $U(\delta)$ the energy contained in the region where the distance from $x = -1$ is at least δ. Using the Cauchy-Schwarz inequality and the arithmetic-geometric mean inequality we have

$$\begin{aligned}
&\text{(C.1)} \quad & U(\delta) &= -\int_{-t/2}^{t/2} [\tau_{11} u + \tau_{13} w]_{x=-1+\delta} \, dz \\
&\text{(C.2)} \quad & &\leq \frac{1}{2} \int_{-t/2}^{t/2} \left[t\left(\tau_{11}^2 + \tau_{13}^2\right) + \frac{1}{t}\left(u^2 + w^2\right) \right]_{x=-1+\delta} dz.
\end{aligned}$$

We define $Q(\delta)$ as the mean value of $U(\delta)$ on the interval $(\delta, \delta + t)$:

$$\begin{aligned}
Q(\delta) &= \frac{1}{t} \int_{\delta}^{\delta+t} U(\delta') \, d\delta' \leq k \, |||\underline{u}|||^2_{(-1+\delta,-1+\delta+t)} \\
&= k \cdot [U(\delta) - U(\delta + t)] = -ktQ'(\delta),
\end{aligned}$$

where k is a positive constant. Observe that self-equilibrium leaves us free to add any rigid body motion to (C.1) and so to (C.2) also. Thus the inequality is justified by the Lemma C.1. Now from

$$\frac{Q'(\delta)}{Q(\delta)} \leq -\frac{1}{kt}$$

we have integrating over the interval $(0, \delta - t)$

$$Q(\delta - t) \leq e^{-(\delta-t)/kt} Q(0).$$

Thus

$$|||\underline{u}|||_\delta \leq Q(\delta - t) \leq e^{-(\delta-t)/kt} Q(0) \leq Ce^{-\delta/kt} |||\underline{u}|||.$$

□

D Theorem 4.2: Tables for the Membrane case

$\overline{u}^- = a + \tilde{u},\ \frac{1}{\sqrt{t}}\|\|\tilde{u}\|\|_{L_2} + \sqrt{t}\|\|\tilde{u}'\|\|_{L_2} = O(b)$			
-1	$+1$	A	$\|\|\|\underline{u}^e\|\|\|$
$\overline{w}^-$	$\overline{u}^+, \overline{w}^+$	$-a\frac{E(1+2\gamma)t}{2(1+\nu)(1+\gamma)} + O(at^2 + bt)$	$O(at + b)$
	$\overline{u}^+, \overline{\tau}_{13}^+$	$-a\frac{E(1+2\gamma)t}{2(1+\nu)(1+\gamma)} + O(at^2 + bt)$	$O(at + b)$
	$\overline{\tau}_{11}^+, \overline{w}^+$	0	$O(b)$
	$\overline{\tau}_{11}^+, \overline{\tau}_{13}^+$	0	$O(b)$
$\overline{\tau}_{13}^-$	$\overline{u}^+, \overline{w}^+$	$-a\frac{E(1+2\gamma)t}{2(1+\nu)(1+\gamma)} + O(at^2 + bt)$	$O(at + b)$
	$\overline{u}^+, \overline{\tau}_{13}^+$	$-\frac{E(1+2\gamma)}{2(1+\nu)(1+\gamma)} \int_{-t/2}^{t/2} \overline{u}^- \, dz$	$O(b)$
	$\overline{\tau}_{11}^+, \overline{w}^+$	0	$O(b)$
	$\overline{\tau}_{11}^+, \overline{\tau}_{13}^+$	0	$O(b)$

$\frac{1}{\sqrt{t}}\|\|\overline{w}^-\|\|_{L_2} + \sqrt{t}\|\|\overline{w}^{-\prime}\|\|_{L_2} = O(b)$			
-1	$+1$	A	$\|\|\|\underline{u}^e\|\|\|$
$\overline{u}^-$	$\overline{u}^+, \overline{w}^+$	$O(bt)$	$O(b)$
	$\overline{u}^+, \overline{\tau}_{13}^+$	$O(bt)$	$O(b)$
	$\overline{\tau}_{11}^+, \overline{w}^+$	0	$O(b)$
	$\overline{\tau}_{11}^+, \overline{\tau}_{13}^+$	0	$O(b)$
$\overline{\tau}_{11}^-$	$\overline{u}^+, \overline{w}^+$	0	$O(b)$
	$\overline{u}^+, \overline{\tau}_{13}^+$	0	$O(b)$
	$\overline{\tau}_{11}^+, \overline{w}^+$	0	$O(b)$
	$\overline{\tau}_{11}^+, \overline{\tau}_{13}^+$	0	$O(b)$

$\frac{1}{\sqrt{t}}\|\|\overline{\tau}_{11}^{-}\|\|_{L_2} = O(b)$, R $\Leftrightarrow \int_{-t/2}^{t/2} \overline{\tau}_{11}^{-} dz = 0$				
-1	$+1$		A	$\|\|\|\underline{u}^e\|\|\|$
$\overline{w}^{-}$	$\overline{u}^{+}, \overline{w}^{+}$		$\int_{-t/2}^{t/2} \overline{\tau}_{11}^{-} dz$	$O(bt)$
	$\overline{u}^{+}, \overline{\tau}_{13}^{+}$		$\int_{-t/2}^{t/2} \overline{\tau}_{11}^{-} dz$	$O(bt)$
	$\overline{\tau}_{11}^{+}, \overline{w}^{+}$	R	0	$O(bt)$
	$\overline{\tau}_{11}^{+}, \overline{\tau}_{13}^{+}$	R	0	$O(bt)$
$\overline{\tau}_{13}^{-}$	$\overline{u}^{+}, \overline{w}^{+}$		$\int_{-t/2}^{t/2} \overline{\tau}_{11}^{-} dz$	$O(bt)$
	$\overline{u}^{+}, \overline{\tau}_{13}^{+}$		$\int_{-t/2}^{t/2} \overline{\tau}_{11}^{-} dz$	$O(bt)$
	$\overline{\tau}_{11}^{+}, \overline{w}^{+}$	R	0	$O(bt)$
	$\overline{\tau}_{11}^{+}, \overline{\tau}_{13}^{+}$	R	0	$O(bt)$

$\frac{1}{\sqrt{t}}\|\|\overline{\tau}_{13}^{-}\|\|_{L_2} = O(b)$			
-1	$+1$	A	$\|\|\|\underline{u}^e\|\|\|$
$\overline{u}^{-}$	$\overline{u}^{+}, \overline{w}^{+}$	$O(bt^2)$	$O(bt)$
	$\overline{u}^{+}, \overline{\tau}_{13}^{+}$	$-\frac{\gamma}{2(1+\gamma)} \int_{-t/2}^{t/2} \overline{\tau}_{13}^{-} z dz$	$O(bt)$
	$\overline{\tau}_{11}^{+}, \overline{w}^{+}$	0	$O(bt)$
	$\overline{\tau}_{11}^{+}, \overline{\tau}_{13}^{+}$	0	$O(bt)$
$\overline{\tau}_{11}^{-}$	$\overline{u}^{+}, \overline{w}^{+}$	0	$O(bt)$
	$\overline{u}^{+}, \overline{\tau}_{13}^{+}$	0	$O(bt)$
	$\overline{\tau}_{11}^{+}, \overline{w}^{+}$	0	$O(bt)$
	$\overline{\tau}_{11}^{+}, \overline{\tau}_{13}^{+}$	0	$O(bt)$

æ

E Theorem 4.2: Tables for the Bending case

$\overline{u}^- = az + \tilde{u},\ \frac{1}{\sqrt{t}}\lVert\tilde{u}\rVert_{L_2} + \sqrt{t}\lVert\tilde{u}'\rVert_{L_2} = O(b)$				
-1	$+1$	$C(0)$	B	$\lvert\lvert\lvert\underline{u}^e\rvert\rvert\rvert$
$\overline{w}^-$	$\overline{u}^+, \overline{w}^+$	$-a\frac{E(1+2\gamma)t^3}{24(1+\nu)(1+\gamma)} + O(at^4 + bt^2)$	$a\frac{E(1+2\gamma)t^3}{8(1+\nu)(1+\gamma)} + O(at^4 + bt^2)$	$O(at^2 + b)$
	$\overline{u}^+, \overline{\tau}_{13}^+$	$-a\frac{E(1+2\gamma)t^3}{24(1+\nu)(1+\gamma)} + O(at^4 + bt^2)$	0	$O(at^2 + b)$
	$\overline{\tau}_{11}^+, \overline{w}^+$	$-a\frac{E(1+2\gamma)t^3}{16(1+\nu)(1+\gamma)} + O(at^4 + bt^2)$	$-C(0)$	$O(at^2 + b)$
	$\overline{\tau}_{11}^+, \overline{\tau}_{13}^+$	0	0	$O(b)$
$\overline{\tau}_{13}^-$	$\overline{u}^+, \overline{w}^+$	$-a\frac{E(1+2\gamma)t^3}{24(1+\nu)(1+\gamma)} + O(at^4 + bt^2)$	0	$O(at^2 + b)$
	$\overline{u}^+, \overline{\tau}_{13}^+$	$-\frac{E(1+2\gamma)}{2(1+\nu)(1+\gamma)}\int_{-t/2}^{t/2}\overline{u}^- z\,dz$	0	$O(b)$
	$\overline{\tau}_{11}^+, \overline{w}^+$	0	0	$O(b)$
	$\overline{\tau}_{11}^+, \overline{\tau}_{13}^+$	0	0	$O(b)$

$\overline{w}^- = a + \tilde{w},\ \frac{1}{\sqrt{t}}\lVert\tilde{w}\rVert_{L_2} + \sqrt{t}\lVert\tilde{w}'\rVert_{L_2} = O(b)$				
-1	$+1$	$C(0)$	B	$\lvert\lvert\lvert\underline{u}^e\rvert\rvert\rvert$
$\overline{u}^-$	$\overline{u}^+, \overline{w}^+$	$O(at^4 + bt^2)$	$-a\frac{E(1+2\gamma)t^3}{8(1+\nu)(1+\gamma)} + O(at^4 + bt^2)$	$O(at^2 + b)$
	$\overline{u}^+, \overline{\tau}_{13}^+$	$O(bt^2)$	0	$O(b)$
	$\overline{\tau}_{11}^+, \overline{w}^+$	$a\frac{E(1+2\gamma)t^3}{32(1+\nu)(1+\gamma)} + O(at^4 + bt^2)$	$-C(0)$	$O(at^2 + b)$
	$\overline{\tau}_{11}^+, \overline{\tau}_{13}^+$	0	0	$O(b)$
$\overline{\tau}_{11}^-$	$\overline{u}^+, \overline{w}^+$	$-a\frac{E(1+2\gamma)t^3}{32(1+\nu)(1+\gamma)} + O(at^4 + bt^2)$	$C(0)$	$O(at^2 + b)$
	$\overline{u}^+, \overline{\tau}_{13}^+$	0	0	$O(b)$
	$\overline{\tau}_{11}^+, \overline{w}^+$	0	0	$O(b)$
	$\overline{\tau}_{11}^+, \overline{\tau}_{13}^+$	0	0	$O(b)$

$\frac{1}{\sqrt{t}}\|\|\overline{\tau}_{11}^{-}\|\|_{L_2} = O(b)$, R $\Leftrightarrow \int_{-t/2}^{t/2} \overline{\tau}_{11}^{-} z dz = 0$					
-1	$+1$		$C(0)$	B	$\|\|\|\underline{u}^e\|\|\|$
$\overline{w}^{-}$	$\overline{u}^{+}, \overline{w}^{+}$		$\frac{1}{4}\int_{-t/2}^{t/2} \overline{\tau}_{11}^{-} z dz + O(bt^3)$	$C(0) - \int_{-t/2}^{t/2} \overline{\tau}_{11}^{-} z dz$	$O(bt)$
	$\overline{u}^{+}, \overline{\tau}_{13}^{+}$		$\int_{-t/2}^{t/2} \overline{\tau}_{11}^{-} z dz$	0	$O(bt)$
	$\overline{\tau}_{11}^{+}, \overline{w}^{+}$		$\frac{1}{2}\int_{-t/2}^{t/2} \overline{\tau}_{11}^{-} z dz$	$-\frac{1}{2}\int_{-t/2}^{t/2} \overline{\tau}_{11}^{-} z dz$	$O(bt)$
	$\overline{\tau}_{11}^{+}, \overline{\tau}_{13}^{+}$	R	0	0	$O(bt)$
$\overline{\tau}_{13}^{-}$	$\overline{u}^{+}, \overline{w}^{+}$		$\int_{-t/2}^{t/2} \overline{\tau}_{11}^{-} z dz$	0	$O(bt)$
	$\overline{u}^{+}, \overline{\tau}_{13}^{+}$		$\int_{-t/2}^{t/2} \overline{\tau}_{11}^{-} z dz$	0	$O(bt)$
	$\overline{\tau}_{11}^{+}, \overline{w}^{+}$	R	0	0	$O(bt)$
	$\overline{\tau}_{11}^{+}, \overline{\tau}_{13}^{+}$	R	0	0	$O(bt)$

$\frac{1}{\sqrt{t}}\|\|\overline{\tau}_{13}^{-}\|\|_{L_2} = O(b)$, R $\Leftrightarrow \int_{-t/2}^{t/2} \overline{\tau}_{13}^{-} dz = 0$					
-1	$+1$		$C(0)$	B	$\|\|\|\underline{u}^e\|\|\|$
$\overline{u}^{-}$	$\overline{u}^{+}, \overline{w}^{+}$		$O(bt^2)$	$\int_{-t/2}^{t/2} \overline{\tau}_{13}^{-} dz$	$O(b)$
	$\overline{u}^{+}, \overline{\tau}_{13}^{+}$	R	$-\frac{\gamma}{4(1+\gamma)}\int_{-t/2}^{t/2} \overline{\tau}_{13}^{-} z^2 dz$	0	$O(bt)$
	$\overline{\tau}_{11}^{+}, \overline{w}^{+}$		$-\int_{-t/2}^{t/2} \overline{\tau}_{13}^{-} dz$	$\int_{-t/2}^{t/2} \overline{\tau}_{13}^{-} dz$	$O(bt)$
	$\overline{\tau}_{11}^{+}, \overline{\tau}_{13}^{+}$	R	0	0	$O(bt)$
$\overline{\tau}_{11}^{-}$	$\overline{u}^{+}, \overline{w}^{+}$		$\int_{-t/2}^{t/2} \overline{\tau}_{13}^{-} dz$	$\int_{-t/2}^{t/2} \overline{\tau}_{13}^{-} dz$	$O(b)$
	$\overline{u}^{+}, \overline{\tau}_{13}^{+}$	R	0	0	$O(bt)$
	$\overline{\tau}_{11}^{+}, \overline{w}^{+}$	R	0	0	$O(bt)$
	$\overline{\tau}_{11}^{+}, \overline{\tau}_{13}^{+}$	R	0	0	$O(bt)$

æ

References

[Be] BENTHEM, J. P., A Laplace Transform Method for the Solution of Semi-Infinite and Finite Strip Problems in Stress Analysis. *Quart. J. Mech. Appl. Math. 16 (1963) 413-429.*

[Bo] BOGY, D. B., Solution of the Plane End Problem for a Semi-Infinite Strip. *Z.A.M.P. 26 (1975) 749-769.*

[Br] BRYANT, R. H., An Examination of the Edge Effect in a Cantilever Beam. *J. Engrg. Math. 7 (1973) 351-360.*

[Fa] FADLE, J., Die Selbstspannungs-Eigenwertfunktionen der quadratischen Scheibe. *Österr. Ing. Arch. 11 (1941) 125-149.*

[GS] GAYDON, F. A. AND SHEPHERD, W. M., Generalized Plane Stress in a Semi-Infinite Strip Under Arbitrary End Load. *Proc. Roy. Soc. Lond. A281 (1964) 184-206.*

[Go] GOODIER, J. N., On the Problems of the Beam and the Plate in the Theory of Elasticity. *Trans. Roy. Soc. Canada 32 (1938) 65-88.*

[Gr1] GREGORY, R. D., Green's Functions, Bi-Linear Forms, and Completeness of the Eigenfunctions for the Elastostatic Strip and Wedge. *J. of Elasticity 9 (1979) 283.*

[Gr2] GREGORY, R. D., The Semi-Infinite Strip $x \geq 0$, $-1 \leq y \leq 1$; Completeness of the Papkovich-Fadle Eigenfunctions when $\phi_{xx}(0,y)$, $\phi_{yy}(0,y)$ are Prescribed. *J. of Elasticity 10 (1980) 57-80.*

[Gr3] GREGORY, R. D., The Traction Boundary Value Problem for the Elastostatic Semi-Infinite Strip; Existence of Solution, and Completeness of the Papkovich-Fadle Eigenfunctions. *J. of Elasticity 10 (1980) 295-327.*

[GG] GREGORY, R. D. AND GLADWELL, I., The Cantilever Beam Under Tension, Bending or Flexure at Infinity. *J. of Elasticity 12 (1982) 317-343.*

[GW] GREGORY, R. D. AND WAN, F. Y. M., Decaying States of Plane Strain in a Semi-Infinite Strip and Boundary Conditions for Plate Theory. *J. of Elasticity 14 (1984), pp. 27-64.*

[Gu] GUPTA, G. D., An Integral Equation Approach to the Semi-Infinite Strip Problem. *J. Appl. Mech. 40 (1973) 948-954.*

[Gz1] GUSEIN-ZADE, M. I., On the Conditions of Decaying Solutions of the Two-Dimensional Problem of the Theory of Elasticity for a Semi-Infinite Strip. *PMM 29, No. 2 (1965) 393-399.*

[Gz2] GUSEIN-ZADE, M. I., On Necessary and Sufficient Conditions for the Existence of Decaying Solutions of the Plane Problem of the Theory of Elasticity for a Semistrip. *PMM 29, No. 4 (1965) 752-760.*

[H1] HORGAN, C. O., Recent Developments Concerning Saint-Venant's Principle: an Update. *Applied Mechanics Reviews, 42 (1989), pp. 295-303.*

[H2] HORGAN, C. O., Decay Estimates for the Biharmonic Equation with Applications to Saint-Venant Principles in Plane Elasticity and Stokes Flows. *Quarterly of Applied Math., 47 (1989), pp. 147-157.*

[HK] HORGAN, C. O. AND KNOWLES, J. K., Recent Developments Concerning Saint-Venant's Principle. *Advances in Applied Mechanics 23 (1983), pp. 179-269.*

[HP] HORGAN, C. O. AND PAYNE, L. E., On the Asymptotic Behavior of Solutions of Linear Second-Order Boundary-Value Problems on a Semi-Infinite Strip. *Archive for Rational Mechanics and Analysis, 124 (1993), pp. 277-303.*

[JL] JOHNSON, M. W. AND LITTLE, R. W., The Semi-Infinite Strip. *Quart. Appl. Math. 22 (1965) 335-344.*

[Lo] LOVE, A. E. H., A Treatise on the Mathematical Theory of Elasticity. *4th ed., Dover, New York (1944).*

[M] MATHÚNA, D., Mechanics, Boundary Layers and Function Spaces, *Birkhäuser 1989.*

[NH1] NEČAS, J. AND HLAVĂČEK, I., On Inequalities of Korn's Type. I. Boundary-Value Problems for Elliptic Systems of Partial Differential Equations, II. Applications to Linear Elasticity. *Archive for Rational Mechanics and Analysis, 36 (1970), pp. 305-334.*

[NH2] NEČAS, J. AND HLAVÁČEK, I., Mathematical Theory of Elastic and Elasto-Plastic Bodies: An Introduction. *Elsevier, Amsterdam, New York (1981).*

[No] NORDGREN, R. P., A Bound on the Error in Plate Theory. *Quart. Applied Mathematics, 28 (1971), pp. 587-595.*

[Pa] PAPKOVICH, P. R., Über eine Form der Lösung des biharmonischen Problems für das Rechteck. *C. R. (Doklady) Acad. Sci. USSR, 27 (1940) 337.*

[Sm] SMITH, R. T. C., The Bending of a Semi-Infinite Strip. *Austral. J. Sci. Res. A 5 (1952) 227-237.*

[SW] SCHWAB, C. AND WRIGHT, S., Boundary Layer Approximation in Hierarchical Beam and Plate Models. *Report 92-08, Department of Mathematics, University of Maryland, Baltimore County (1992).*

[Sp] SPENCE, D. A., Mixed Boundary Value Problems for the Elastic Strip; the Eigenfunction Expansion. *Technical Summary Report 1863, Mathematics Research Center, Madison (1978).*

[TG] TIMOSHENKO, S. P. AND GOODIER, J. N., Theory of Elasticity. *3rd ed., McGraw-Hill (1970).*

[Tor] TORVIK, P. J., The Elastic Strip with Prescribed End Displacements. *J. Appl. Mech. 38 (1971) 929-936.*

[Tou] TOUPIN, R. A., Saint-Venant's Principle. *Archive for Rational Mechanics and Analysis, 18 (1965), pp. 83-96.*

[Wa] WASHIZU, K., Variational Methods in Elasticity & Plasticity. *3rd ed., Pergamon Press (1982).*

An h-p-n Adaptive Finite Element Scheme for Shell Problems

O. Ovaskainen and J. Pitkäranta

Helsinki University of Technology, Institute of Mathematics,
P.O. Box 1000, FIN-02015 HUT, Finland

Abstract. We propose an adaptive finite element algorithm for shells which in addition to the usual $h-p$ adaption shows also adaptivity with respect to the order n of the dimension reduction. The idea of the algorithm is to adaptively capture and resolve the various length scales that may occur in shells. The algorithm presented in the paper is limited to axisymmetric problems, which reduces the $h-p$ -part of the problem to one dimension only. The performance of the algorithm is tested in some example cases where the shell is cylindrical. For comparison, we test the algorithm also when n is limited so that $n \leq k$ where $k = 1, 2$ or 3. Choosing $k = 2$ essentially corresponds to the classical shell models.

Subject classification. (AMS) 73C02, 73K15

1 Introduction

The standard approach to the problems of thin bodies in linear elasticity, like plates and shells, has been to apply a numerical method to a dimension reduction model. The accuracy of the model itself has thus set a lower bound for the error of the numerical solution, no matter how accurately the numerical computations have been made. The inaccuracy built in the model is often known only as an asymptotic (as the effective thickness of the body goes to zero) convergence rate estimate. Thus in real computations the correctness of the model used and hence also the usefulness of the results obtained may be quite questionable.

The classical shell models are based on low-order polynomial expansions through the thickness of the shell. In this work we study a hierarchic family of shell models of arbitrary order n from the point of view of an adaptive finite element scheme. Thus in addition to the usual $h-p$ -adaptivity along the midsurface of the shell, our scheme shows adaptivity also with respect to the model order n. When n is constant along the midsurface, we refer to the dimension reduction model as the *n-model*. The classical shell models are close to the 2-model [6], [7].

From the viewpoint of adaptive modelling, the main feature of shell deformations is their multi-scale character. When the thickness d of the shell is small, the deformation typically consists of a piecewise smooth, global component plus various local layers with characteristic length scales depending on d. The layers decay exponentially, often as damped oscillations, from line or point irregularities induced by the load or by the boundary conditions. In case of plates, layers occur typically in length scales proportional to d, which is the smallest scale in general. In shells, much wider layer scales arise from curvature effects. Depending on the geometry of the shell (elliptic, parabolic, hyperbolic) the layers may include scales proportional to $\sqrt{Rd}$, $\sqrt[3]{R^2d}$ or even $\sqrt[4]{R^3d}$, where R is a principal radius of curvature, see [4] (and the references therein). Hence the range of the layers of practical shells can be quite diverse. We should add that the variation in the relative strength (or amplitude) of the layers is even more diverse [6].

Due to the multi-scale "layered" character of shell deformations, the idea of adaptively capturing and resolving the various length scales arises very naturally in numerical shell modelling. Since the layer components are of local nature, and typically rather smooth in their characteristic length scales, an efficient adaptive algorithm should basically work in the two-stage "search-and-resolve" manner. In the (h,p,n) - setting this could go as follows.

First, when the (h,p)-discretization along the midsurface of the shell is coarse, the algorithm should work mainly in the h-p adaptive "search" mode where the model order parameter n is held fixed at a low value, say at $n=2$. Higher values of n are not needed at this stage, since all the relevant length scales can be located correctly already with low-order n-models [6].

Once the layer of a given length scale is properly located, the algorithm should pass to a "resolve" mode where parameter n is activated as well. The optimal value of n apparently depends both on the layer amplitude (which varies along the midsurface) and on the error tolerance. Most critically, however, the optimal n depends on the *effective thickness* of the shell defined as $t = d/D$, where D is the length scale to be resolved (possibly $D = D(d)$). This dependence arises simply because the accuracy of the n-model grows with powers of t when D is chosen as the length unit and other length scales are ignored, c.f. [5], [6].

We should add that in addition to layers, which may be considered more or less smooth in their characteristic length scales, shell deformations may also contain asymptotic irregularities of non-local algebraic type, see [4] and the references therein. The automatic resolution of such irregularities should basically follow the adaptive philosophy common in more standard elliptic problems, c.f. [1], [2], [3], [9], [10], [11]. We should note, however, that so far the theory of adaptive algorithms for elliptic problems is limited to problems with non-severe parametric dependence, so this theory does not extend to shells in any straightforward way. In particular, it may not be easy to find a posteriori error indicators for shells that are both simple, effective and reliable [8].

In this work we introduce an $h-p-n$ adaptive FE algorithm for axisymmetric shell problems and test its scale resolution ability in a simple model problem where the shell is cylindrical (see Section 2). In the model problem, the angular variation of the displacement field is trigonometric. This is factored out exactly, thus transforming the problem into a two-dimensional one. Hence the (h, p) FE discretization within a given n-model is one-dimensional, acting in the axial direction only.

The adaptive scheme is guided by three kinds of change-of-the-error indicators, Take, Drop and Split. These are of simple geometric nature (see Section 4.2). Take predicts how much the accuracy would improve if a new degree of freedom, or a set of d.o.f., were introduced. Similarly, Drop predicts how much the accuracy would degrade if a set of d.o.f. were dropped. Split indicates whether it pays off to split an element into two and simultaneously lower the degree p of the local FE space in such a way that the local d.o.f. density remains about the same. As the measure of accuracy we simply take the energy norm in these indicators. In this work we only demonstrate the performance of the algorithm proposed. A posteriori error estimation that would give a possibility of shooting at a given error tolerance are so far not attempted.

2 The Model Problem

As our model problem we consider a cylindrical shell of half-length H equal to the radius R (as measured to the middle surface) and with thickness d to be varied (Fig. 1). The shell is assumed to consist of homogeneous isotropic material with Young's modulus E and Poisson's ratio ν. Further, choosing $R = H$ as the length

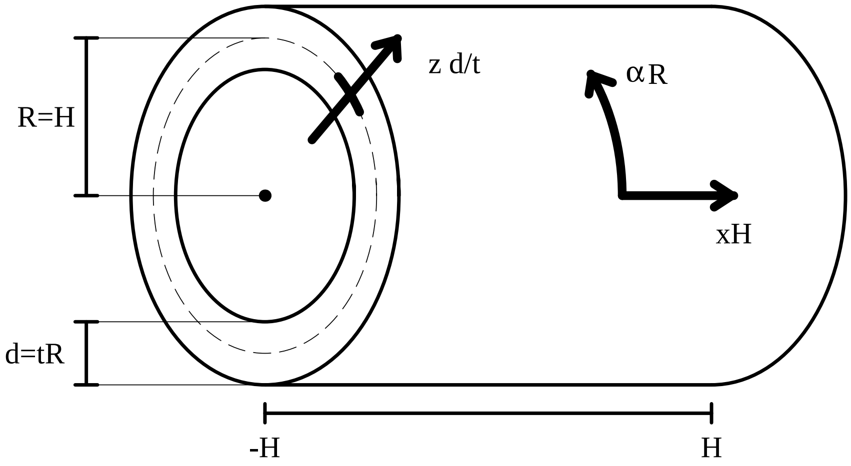

Figure 1: The shell of the model problem.

unit, the only parameter that essentially remains to be varied is the dimensionless thickness $t = d/R$.

In what follows, we use dimensionless variables choosing $R = H$ for the length unit. The dimensionless cylindrical coordinates, x (axial), α (angular), z (radial), are chosen in such a way that the shell occupies in these coordinates the region

$$\Omega = \{(x, \alpha, z) \,|\, -1 < x < 1,\ 0 \leq \alpha < 2\pi,\ -t/2 < z < t/2\}.$$

We assume that the shell is loaded by a normal pressure distribution that acts on the outer surface of the shell and varies as

$$p = P(x)\cos k\alpha\,, \qquad (1)$$

where k is an integer. In the computations that follow we choose in fact $\nu = 1/3$ and $k = 2$. The load amplitude $P(x)$ will be chosen to be one of the following.

Case 1. Discontinuous load:

$$P(x) = \begin{cases} P_0, & -1 < x \leq 1/2 \\ 0, & 1/2 < x < 1 \end{cases}$$

Case 2. Line load:

$$P(x) = P_0\,\delta_{1/2},\ \text{the delta distribution at } x = 1/2$$

(Here P_0=const.) We have chosen here the point of irregularity of the load ($x = 1/2$) so as to avoid any simplifying symmetry effects in the numerical computations. We assume a clamped support at the ends of the cylinder, i.e., all displacements vanish at $x = \pm 1$. This is known to lead to a membrane dominated energy state [7]. The exact deformation of the shell under the load (1) is assumed to obey the laws of 3D linear elasticity. Due to the special shape of the load, the displacement field is of the form

$$(U(x,z)\cos k\alpha,\ V(x,z)\sin k\alpha,\ W(x,z)\cos k\alpha), \tag{2}$$

so we have in fact a problem in 2D only, where the domain is

$$\omega = \{(x,z) \,|\, -1 < x < 1,\ -t/2 < z < t/2\}.$$

We denote by $\underline{U} = (U(x,z), V(x,z), W(x,z))$ the dimensionless displacement (amplitude) field, obtained by scaling the actual field by R. The energy of the shell may then be expressed as

$$\begin{aligned} \mathcal{F}(\underline{U}) &= F_0 \left\{ \frac{1}{2} \int_\omega \left[\frac{\nu}{(1+\nu)(1-2\nu)} (\mathrm{tr}\underline{\underline{\epsilon}})^2 + \frac{1}{1+\nu} \sum_{i,j=1}^{3} \epsilon_{ij}^2 \right] \cdot (1+z)\, dx\, dz \right. \\ & \qquad \left. - \int_{-1}^{1} W(x, \frac{t}{2}) \cdot Q(x) \cdot \left(1 + \frac{t}{2}\right) dx \right\}, \end{aligned} \tag{3}$$

where $F_0 = l\pi E R^3$ with $l = 2$ for $k = 0$ and otherwise $l = 1$, $Q(x) = P(x)/E$ is the dimensionless load amplitude, and the strain amplitudes ϵ_{ij} are given by

$$\begin{aligned} \epsilon_{11} &= \frac{\partial U}{\partial x} & \epsilon_{22} &= \frac{1}{r}(kV + W) \\ \epsilon_{12} &= \frac{1}{2}\left(-\frac{k}{r}U + \frac{\partial V}{\partial x}\right) & \epsilon_{23} &= \frac{1}{2}\left(\frac{\partial V}{\partial z} - \frac{1}{r}(V + kW)\right) \\ \epsilon_{13} &= \frac{1}{2}\left(\frac{\partial U}{\partial z} + \frac{\partial W}{\partial x}\right) & \epsilon_{33} &= \frac{\partial W}{\partial z} \end{aligned}$$

where $r = 1 + z$. The energy space $\mathcal{U}$ is defined as

$$\mathcal{U} = \{\underline{U} \in [H^1(\omega)]^3 \,|\, \underline{U}(\pm 1, \cdot) = 0\}.$$

The solution $\underline{U}^{3D}$ for the elastic problem is then defined to be the unique minimizer of (3) in $\mathcal{U}$.

We define here the energy norm $|||\cdot|||$ and the load functional $\mathcal{Q}$ for later use. To this end, rewrite (3) as $\mathcal{F}(\underline{U}) = \frac{1}{2}\mathcal{A}(\underline{U}, \underline{U}) - \mathcal{Q}(\underline{U})$, where $\mathcal{A}$ and $\mathcal{Q}$ represent the quadratic and linear parts of (3). The energy norm is then defined in terms of the quadratic part as

$$|||\underline{U}||| = \{\mathcal{A}(\underline{U}, \underline{U})\}^{1/2}.$$

By standard linear elastic theory we have for any $\underline{U} \in \mathcal{U}$

$$c||\underline{U}||_1 \le |||\underline{U}||| \le C||\underline{U}||_1,$$

where c, C are positive constants and $||\cdot||_1$ denotes the standard H^1-norm over ω. However, unlike in more standard elliptic problems where we would have $c \sim C \sim 1$, we have here $C \sim 1$ and $c = c(t) \sim t$, so the parametric dependence of the energy norm is severely non-uniform when t is small.

As to the behavior of the exact solution to these model problems, we note that the solution consists of three kinds of components [6]:

1. a global component (in length scale $D \sim 1$) which is uniformly smooth with respect to t on the subdomains $\omega_- = \{(x,z) \in \omega | -1 < x < \frac{1}{2}\}$ and $\omega_+ = \{(x,z) \in \omega | \frac{1}{2} < x < 1\}$,
2. boundary (or interior) layers in the length scale $D \sim \sqrt{t}$ at $x = -1$, $x = \frac{1}{2}$ and $x = 1$,
3. layers in the scale $D \sim t$ at $x = -1$, $x = \frac{1}{2}$ and $x = 1$.

The approximate n-model solutions ($n \geq 1$) behave qualitatively in the same way as the exact solution [6].

3 Dimension Reduction Models

The classical shell models are derived from low-order (usually of order 0 for W and of order 1 for U and V) polynomial expansions of the displacement field, and from similar expansions of the strain/stress fields, through the thickness of the shell. The accuracy of these models as compared with the 3D-model improves in general when the relative thickness of the shell decreases, but there is no guarantee on the performance of these models at moderate thicknesses. This uncertainty is avoided by assuming a system of hierarchic models, where the order of the polynomial expansion may vary in different parts of the domain. Our dimension reduction will be based on the straightforward use of the energy principle, so we need to expand the displacements only. In practice, this corresponds to using a 3D (here 2D) finite element approach with one layer of varying-order elements in the radial direction.

Since the expansion in the z-direction reduces our model problem to one dimension only, the computational domain in the FE scheme will be $I = \{x \in \mathbf{R} \,|\, -1 < x < 1\}$. Let us partition the domain into subintervals $I_k = \{x \in I \,|\, x_{k-1} < x < x_k\}$ for $k = 1, \ldots, N$, where $-1 = x_0 < x_1 < \cdots < x_N = 1$. Upon assigning an integer n_k to each subinterval I_k, we obtain a variable-order dimension reduction model for our problem by applying the energy principle and assuming that the displacement field is a polynomial of degree $\leq n_k$ on each I_k and continuous at the break points. We could in fact derive further models by assuming expansions of different orders in different displacement components. For simplicity, however, we do not consider such extension here. In the n-model we have $n_k = n$ for all k. The classical dimension reduction models for shells may be understood as simplifications of the 2-model [6].

4 The h-p-n Adaptive Finite Element Scheme

4.1 The Finite Element Method

In the finite element model the subintervals I_k act as the basis of our axial finite element approximation as well. On each interval the finite element solution is then assumed to be a polynomial of finite degree p_{ki} in x. The adaptive algorithm will allow different axial degrees for different terms in the expansion with respect to the z-coordinate, so the representation of the FE solution $\underline{U}^{FE}$ on I_k is of the form

$$\underline{U}^{FE}_{|I_k} = \sum_{i=0}^{n_k} \sum_{j=0}^{p_{ki}} \underline{a}_{kij} P_i(z) x^j \text{ for } k = 1, \ldots, N.$$

Here P_i is the i:th Legendre polynomial and $\underline{a}_{kij} = (a^1_{kij}, a^2_{kij}, a^3_{kij})$ includes the coefficients for $\underline{U}^{FE} = (U^{FE}, V^{FE}, W^{FE})$. In the numerical computations we used a basis polynomial system utilizing the Legendre polynomials also in the x-direction. Below we denote by $\phi_{kj}(x)$ the basis polynomials associated with the subinterval I_k. Here ϕ_{k0} and ϕ_{k1} are the usual linear shape functions, and the remaining ones are $\phi_{kj} = (x - x_{k-1})(x - x_k)P^k_{j-2}(x)$, $j \geq 2$, where P^k_j is the j:th (scaled) Legendre polynomial on I_k. The 2D vector basis polynomials $\underline{e}_s P_i(z)\phi_{kj}(x)$ (here $s = 1, 2, 3$ and $\underline{e}_s$ includes the standard unit vectors) which span the finite element space $\mathcal{U}^{FE}$ will be denoted by $\underline{\Phi}_l$ (with some index system $l = 1, \ldots, L$). We note that $\underline{U}^{FE}$ may be interpreted as the projection of the exact solution $\underline{U}^{3D}$ to the finite element space, so

$$|||\underline{U}^{3D} - \underline{U}^{FE}||| \leq |||\underline{U}^{3D} - \underline{V}||| \ \ \forall\, \underline{V} \in \mathcal{U}^{FE}.$$

4.2 Indicators

We will use three kinds of indicators for guiding the adaptive process. These are called Take, Drop and Split. Take indicates the expected best degrees of freedom that should be added to the FE space to improve the accuracy, whereas Drop shows those degrees of freedom which may be dropped out without decreasing the accuracy too much. Split indicates whether it pays off to split an interval into two and lower the (axial) order of the local FE space in such a way that the total number of d.o.f:s remains approximately the same. All of these indicators are based on the following simple derivation of geometric nature.

Let us consider at the same time the possibility of dropping the degrees of freedom $\{\underline{\Phi}_l\}_{l=1}^{L^d}$ from $\mathcal{U}^{FE}$ and adding a set of new degrees of freedom $\{\underline{\Psi}_l\}_{l=1}^{L^t}$ into the space. Let us denote this new FE space by $\tilde{\mathcal{U}}^{FE}$ and the corresponding solution by $\underline{\tilde{U}}^{FE}$. Next we define

$$\mathcal{U}^* = \{\underline{U} \in \mathcal{U} \mid \underline{U} = \underline{U}^{FE} - \sum_{l=1}^{L^d} b_l \underline{\Phi}_l + \sum_{l=1}^{L^t} c_l \underline{\Psi}_l\},$$

where b_l are the coefficients of the Φ_l in the FE solution $\underline{U}^{FE}$ and c_l are free variables. Clearly we have $\mathcal{U}^* \subset \tilde{\mathcal{U}}^{FE}$. Let us denote by $\underline{U}^*$ the minimizer of $|||\underline{U}^{3D} - \underline{U}|||$ in $\underline{U} \in \mathcal{U}^*$ and the minimizing coefficients by c_l^*. We note that in order to compute the coefficients c_l^*, a matrix of size $L^t \times L^t$ only must be inverted. We obtain by the projection principle and by a simple computation

$$\begin{aligned} |||\underline{U}^{3D} - \underline{\tilde{U}}^{FE}|||^2 &\leq |||\underline{U}^{3D} - \underline{U}^*|||^2 \\ &= |||\underline{U}^{3D} - \underline{U}^{FE}|||^2 + |||\sum_{l=1}^{L^d} b_l \underline{\Phi}_l|||^2 - |||\sum_{l=1}^{L^t} c_l^* \underline{\Psi}_l|||^2 \\ &=: |||\underline{U}^{3D} - \underline{U}^{FE}|||^2 + D^2 - T^2. \end{aligned}$$

Here D^2 and T^2 are the Drop and Take indicators and the Split indicator is simply $S = D^2 - T^2$. We note that these indicators may be interpreted as reliable (though not necessarily sharp) bounds for the increase or decrease in accuracy if the old FE system is replaced by the new one.

4.3 The Adaptive Algorithm

The algorithm consists of the following steps.

1. An initial mesh $\{I_k\}$ and the integers n_k and p_{ki} are specified.

2. The FEM-solution $\underline{U}^{FE}$ is computed.

3. Let the number of d.o.f. in $\mathcal{U}^{FE}$ be L. We try to find the $M \sim L/C_T$ most important new d.o.f. that should be added to the space. Here C_T is a constant given by the user. (In the numerical examples we chose $C_T = 2$.) The new d.o.f are chosen by computing the Take indicators T^2 for each additional set of $L^t = 3$ degrees of freedom when either 1) p_{ki} is replaced by $p_{ki} + 1$ for given k, i, or 2) n_k is replaced by $n_k + 1$ for given k, with $p_{k,n_k+1} = 2$. First we choose the L/C_T best ones of these and let T^2_{min} be the lowest value accepted. Then we continue to raise the values of p_{ki} and n_k further for the d.o.f. chosen so far and test if we get better indicators than T^2_{min}. (This time $L^t = 6$.) The search is continued with $L^t = 9$ etc. until no improvement is achieved. Finally we select $M \sim L/C_T$ degrees of freedom by combining the best of the tested sets.

4. The Drop indicators D^2 for decreasing each p_{ki} by 1 are computed. Those d.o.f:s for which the indicator is at most T^2_{min}/C_D are dropped. Here again, C_D is a constant given by the user. (We used the value $C_D = 20$.)

5. The Split indicators $S = T^2 - D^2$ are computed separately for each I_k. This time we test the effect of splitting the element I_k into two parts $[x_{k-1}, x^*]$ and $[x^*, x_k]$ and simultaneously lowering the orders of the polynomials in such a way that the number of d.o.f:s remains approximately the same. This is done by the following algorithm.

   (a) Let the recursion level r be $r = 1$. We make the initial choice $x_r^* = \frac{1}{2}(x_{k-1} + x_k)$.

   (b) Given x_r^* we drop the basis functions $\underline{e}_s P_i(z)\phi_{kj}(x)$ with $j \geq 2$ and replace by the corresponding basis functions on $[x_{k-1}, x_r^*]$ and $[x_r^*, x_k]$ with $j < p_{ki}/2$ rounded. Then we compute the Split indicator $S_r = T^2 - D^2$ for the splitting.

   (c) If S_1 is negative or zero, no splitting is done on I_k. If S_1 is positive, we use a recursive search to possibly find a better x^*. The recursive search is done by replacing x_r^* either by $x_r^* - d_k/2^{r+1}$ or $x_r^* + d_k/2^{r+1}$, where $d_k = x_k - x_{k-1}$ is the length of the interval I_k. With these choices we recompute the indicators $S = T^2 - D^2$. If either of these exceeds S_r, we pass to the next recursion level $r = 2$ and let the new x_r^* be the one of the two points tested that gave a larger indicator. The search is continued until $T^2 - D^2$ is not improved.

6. Return to step 2.

5 Numerical Examples

We now test the above adaptive algorithm in the model problems introduced in Chapter 2 (Cases 1 and 2), with the relative thickness of the shell chosen to be either $t = 0.1$ or $t = 0.01$. Let us first look at the convergence rates of the algorithm in these four problems. In Figs. 2-3 we show the $(\log_{10}, \log_{10})$ plots of the relative error $|||\underline{U}^{3D} - \underline{U}^{FE}|||/|||\underline{U}^{3D}|||$ with respect to the number of degrees of freedom in Case 1 (discontinuous load) and Case 2 (line load) at both values of t. (Here $|||\underline{U}^{3D}|||$ was computed approximately using high-order FEM.) The points in the figures indicate the steps of the adaptive algorithm. The effect of staying within a given n-model ($n_k \leq n$) is also shown in the figures.

At $t = 0.1$, the limitations of the low-order n-models are clearly seen in Figs. 2-3 a). At $t = 0.01$, the 2-model already performs reasonably well, and even the 1-model has improved. We note that due to the membrane-dominated nature of the deformation in our model problems [6], all n-models with $n \geq 1$ are asymptotically correct at $t = 0$ [5], [7]. In both Case 1 and Case 2, the

Case	n	$t = 0.1$	$t = 0.01$
1	1	25.4	6.7
	2	6.3	0.9
	3	3.1	–
2	1	36.5	21.7
	2	22.0	4.3
	3	18.6	–

Table 1: The relative error $|||\underline{U}^{3D} - \underline{U}^n|||/|||\underline{U}^{3D}|||$ of a few lowest n-models (%).

convergence rate of the general hierarchic model is somewhat faster at $t = 0.01$ than at $t = 0.1$, which apparently is due to the more 3D-like behavior of the solution at moderate values of t. When staying within a given n-model, the saturation is somewhat faster at $t = 0.1$ - apparently because of the more regular behavior of the exact n-model solution at larger values of t.

In Table 1 we show the relative error $|||\underline{U}^{3D} - \underline{U}^n|||/|||\underline{U}^{3D}|||$ of the lowest n-models. As noted earlier, the classical shell models are expected to be roughly as accurate as the 2-model. Since the 2-model shows here relative errors of order 6.3% in Case 1 and 22.0% in Case 2 at $t = 0.1$, it seems clear that the classical shell models are neither able to give accurate results (in the energy norm) for such moderately thick shells. On the other hand, the much better behavior of the 2-model at $t = 0.01$ indicates that the classical shell models would be acceptable as well.

In Figures 4 (Case 1) and 5 (Case 2) we show contour plots of the d.o.f. density given by the adaptive algorithm at $t = 0.1$. In Figs. 4-5 a) the total d.o.f density is plotted with respect to the number of iterations, whereas in Figs. 4-5 (b) we show how the final degrees of freedom are distributed over different degrees of the polynomials $P_i(z)$ in the radial direction.

From figures 4-5 (a) we observe that the algorithm basically works in the desired "search-and-resolve" manner: Once having captured the global (piecewise) smooth component of the solution, it concentrates on locating and resolving first the $\sqrt{t}$-scale and then the t-scale of the layers at $x = -1$, $x = \frac{1}{2}$ and $x = 1$. From figures b) we conclude that especially the t-scale behaves essentially 3 dimensionally: The highest degrees n_k ($n_k \geq 5$) appear only very close to points $x = -1$, $x = \frac{1}{2}$ and $x = 1$ where the t-scale component of the solution is significant. In Case 1, the irregularity caused by the discontinuity of the load is much weaker than the ones caused by the boundary conditions, and is actually not seen at all in Fig. 4 (b). In Case 2 the main irregularity of the solution is caused by the line load at $x = 1/2$. This is even stronger than the boundary irregularities in Case 1. It is apparently the strong irregularity at $x = \frac{1}{2}$ which mainly causes the much slower convergence rate in this Case 2 (Fig. 3) as compared with Case 1 (Fig. 2).

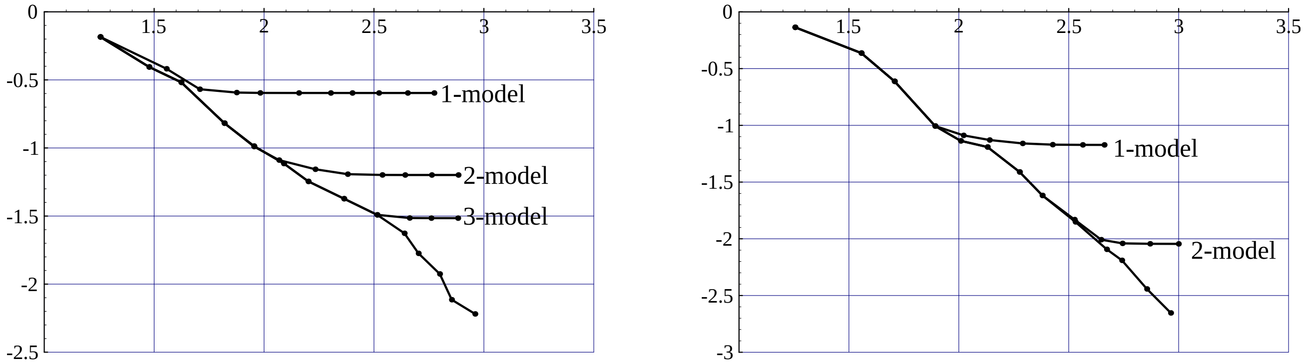

(a) (b)

Figure 2: Convergence of the adaptive algorithm in Case 1. Relative error in the energy norm. a) $t = 0.1$, b) $t = 0.01$

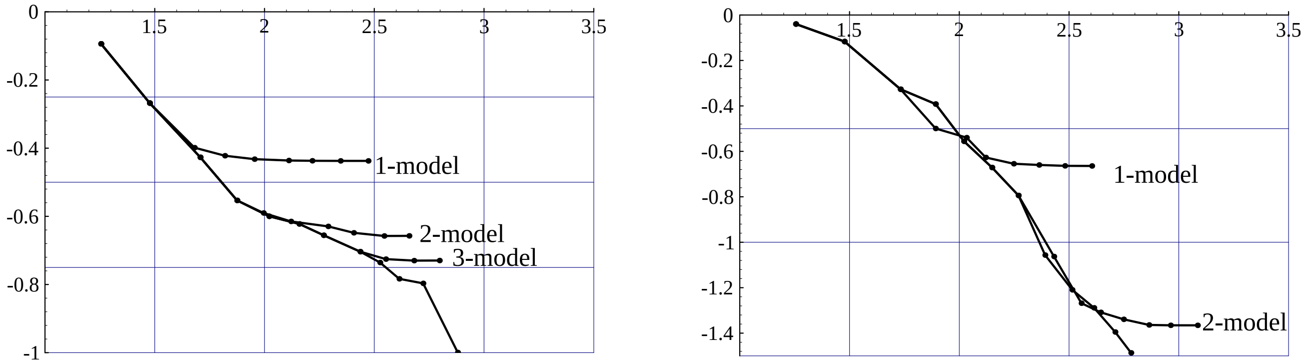

(a) (b)

Figure 3: Convergence of the adaptive algorithm in Case 2. Relative error in the energy norm. a) $t = 0.1$, b) $t = 0.01$

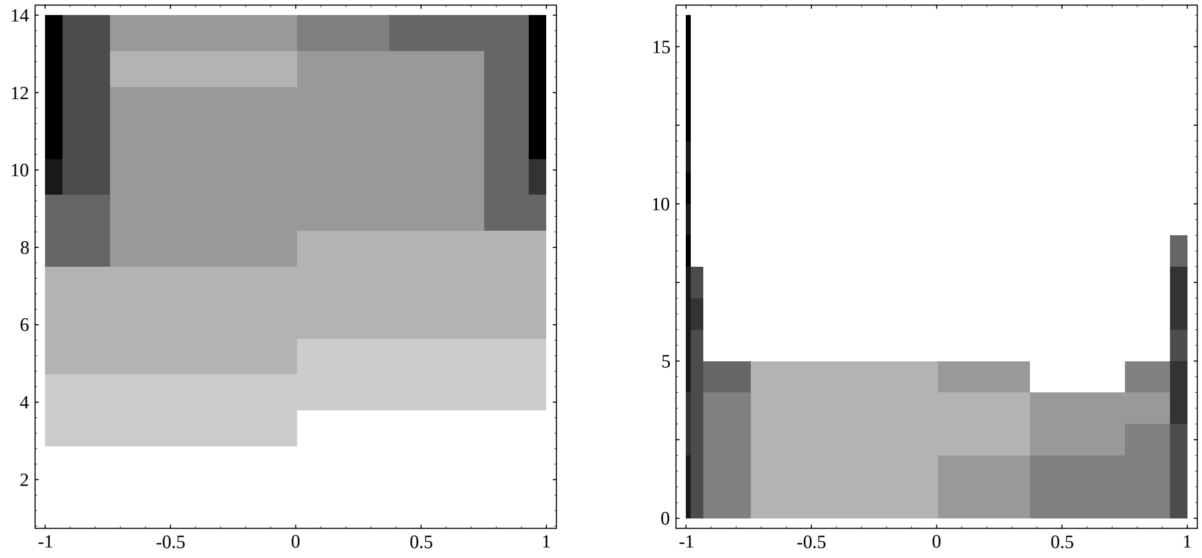

(a) (b)

Figure 4: Contour plots of the d.o.f. density in Case 1 at $t = 0.1$. a) Total d.o.f density with respect to the number of iterations. b) Final density of the axial d.o.f. with respect to the degree of the polynomials in the z-direction.

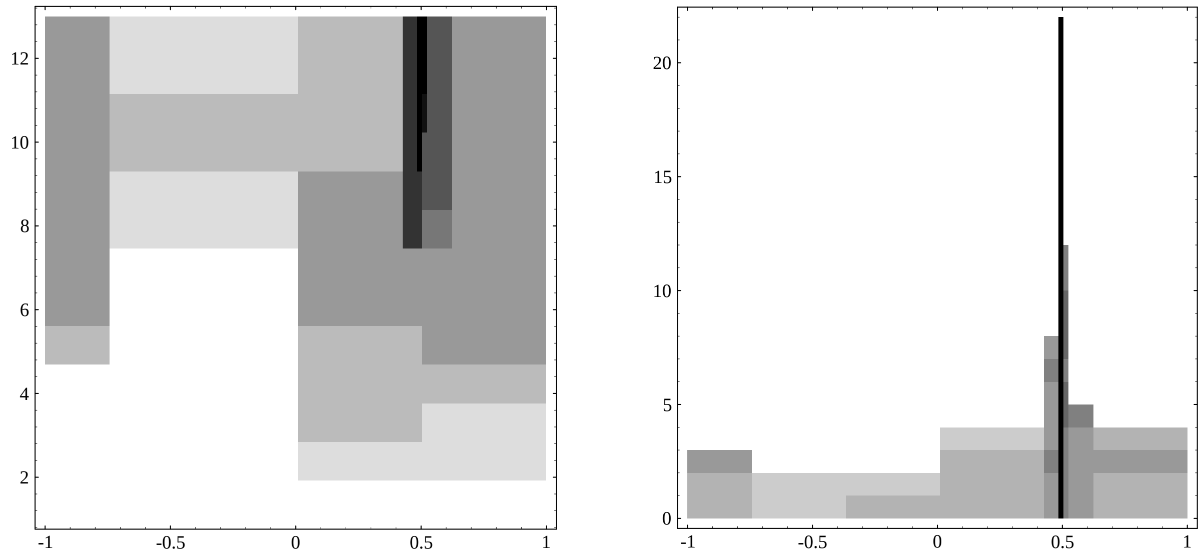

(a) (b)

Figure 5: Contour plots of the d.o.f. density in Case 2 at $t = 0.1$. a) Total d.o.f density with respect to the number of iterations. b) Final density of the axial d.o.f with respect to the degree of the polynomials in the z-direction.

References

[1] BABUŠKA, I. AND MILLER, A., *A-Posteriori Error Estimates and Adaptive Techniques for the Finite Element Method*, Techn. Rep. BN968, University of Maryland, Inst. for Phys. Sci. and Technol., 1981.

[2] ERIKSON, K. AND JOHNSON, C., *An Adaptive Finite Element Method for Linear Elliptic Problems*, Math. Comp. 50 (1988), pp. 361-383.

[3] ERIKSON, K. AND JOHNSON, C., *Adaptive Finite Element Methods for Parabolic Problems I: A Linear Model Problem*, SIAM J. Numer. Anal. 28 (1991), pp. 43-77.

[4] HAKULA, H., LEINO, Y. AND PITKÄRANTA, J., *Scale resolution, locking and high-order finite element modelling of shells*, Proc. of the International Conference on Spectral and High Order Methods (ICOSAHOM'95), to appear.

[5] OVASKAINEN, O. AND PITKÄRANTA, J., *An Energy Method Approach to the Problem of Elastic Strip*, Helsinki University of Technology, Institute of Mathematics, Research Report A328 (1994).

[6] PITKÄRANTA, J., LEINO, Y., OVASKAINEN, O. AND PIILA, J., *Shell Deformation States and the Finite Element Method: A Benchmark Study of Cylindrical Shells*, to appear in Comp. Meth. in Appl. Mech. and Engrg.

[7] PIILA, J. AND PITKÄRANTA, J., *Energy Estimates Relating Different Linear Elastic Models of a Cylindrical Shell. (I) The Membrane-Dominated Case*, SIAM J. Math. Anal. 24 (1993) pp. 1-22.

[8] STEIN, E., RUST, W. AND OHNIMUS, S., *h- and d-Adaptive FE Methods for Two-Dimensional Structural Problems Including Post-Buckling of Shells*, Comp. Meth. in Appl. Mech. and Engrg 101 (1992) pp. 315-354.

[9] ZENG, L. F. AND WIBERG, N.-E., *Adaptive h-p Procedures for High Accuracy Finite Element Analysis of Two-Dimensional Linear Elastic Problems*, Computers & Structures Vol 42, No.6 (1992), pp. 869-886.

[10] ZIENKIEWICZ, O. C. AND ZHU, J. Z., *A Simple Error Estimator and Adaptive Procedure for Practical Engineering Analysis*, Int. J. Numer. Meth. Engrg 24 (1987), pp. 333-357.

[11] ZIENKIEWICZ, O. C., ZHU, J. Z. AND GONG, G., *Effective and Practical h-p Version Adaptive Analysis Procedures for the Finite Element Method*, Int. J. Numer. Meth. Engrg 28 (1989), pp. 879-891.

Local A Posteriori Error Estimation on Thin Domains of Linear Elasticity: Theory and an Example

Otso Ovaskainen

Helsinki University of Technology, Institute of Mathematics,
P.O. Box 1000, FIN-02015 HUT, Finland

Abstract. We discuss the problem of a posteriori error estimation in the FE-approximation of parameter dependent thin body problems of linear elasticity. We consider a posteriori error estimation based directly on the energy and complementary energy (dual) principles. We summarize first the general theory in Hilbert spaces and transform it to the language of linear elasticity and finite element analysis. Then we apply the theory to the $2D$-elastic strip. Here we first derive results quantifying the more general theorems (in particular in terms of the thickness parameter of a thin body) and then illustrate the results by some numerical experiments.

Subject classification. (AMS) 73C02

1 Introduction

A posteriori error estimation has become an essential part of finite element analysis, especially along the success of adaptive modeling during the last decade. A posteriori error estimation is in general understood to mean the estimation of the error of the computed approximate solution using information from the approximate solution itself. In practice, however, a wide diversity of a posteriori error estimation approaches is obtained depending on how the information from the FE solution is actually used and in what sense the accuracy is measured.

In the context of thin bodies in linear elasticity, one can usually split the overall approximation procedure into two steps, where the first step corresponds to a *dimension reduction* and the second one consists of applying a finite element scheme to the dimensionally reduced problem. Even if the finite element scheme is applied directly to the original problem, the dimension reduction is often implicitly contained in the numerical model. This is the case, e.g., if a beam, plate or shell is discretized directly using a single layer of (2D or 3D) finite elements of a given degree.

In the present work the starting point, i.e., the "exact" model is considered to be that of standard 3D or 2D elasticity for an isotropic material. As an example case we consider the 2D problem of an elastic strip.

Let us denote, respectively, by $\underline{U}^{nD}$, $\underline{U}^{RD}$ and $\underline{U}^{FE}$ the displacement fields in a given nD elastic problem corresponding to the "exact" model, the dimension reduction model and the finite element model. (Here the dimension reduction may be implicitely contained in the FE model.) In this setting the *model error* is $\underline{e}^M := \underline{U}^{3D} - \underline{U}^{RD}$, the FE *approximation error* is $\underline{e}^A := \underline{U}^{RD} - \underline{U}^{FE}$ and the *total error* is $\underline{e} := \underline{U}^{3D} - \underline{U}^{FE}$. In the present work we are mainly interested in estimating $\underline{e}^A$ though some of the more abstract results (Sections 2 and 3) apply to $\underline{e}^M$ or $\underline{e}$ as well.

In the literature on adaptive finite element methods for elliptic problems, the main emphasis has so far been in the development of effective and reliable algorithms in thick body cases [2],[3],[4], [5],[6],[7],[8],[10],[11], [12],[13],[25],[27],[28]. In case of thin body problems, there also exists a considerable amount of work on adaptivity and a posteriori error estimation in many special cases [1],[9],[19],[20],[23],[26]. A lot of work has been done also on modeling the error estimation (estimates for $\underline{e}^M$), c.f. [14],[21],[22],[24] and the further references therein. However, the general behavior of adaptive FE error indicators in case of thin bodies appears still largely an unresolved issue. The estimators analyzed in this paper will be based on two well known principles of simple geometric nature, the *energy principle* and the *complementary energy principle*. The estimators will be considered only with respect to the *energy norm*, denoted here by $|||\cdot|||$. When the energy principle is used, the a posteriori error estimation is closely related to an adaptive finite element procedure, the idea of which is easily stated: Given a finite element solution u^1, compute another reference solution u^2 by solving a set of auxiliary local problems where the boundary conditions are of Dirichlet (kinematic) type and derived from u^1. Then use u^2 to control the adaptive algorithm. Some variation of this idea is usually applied in thick body problems, and experiments have also been made on model thin body problems [15], [17].

Information from the reference solution u^2 can also be used for obtaining both a lower and an upper bound for the error of u^1 in the energy norm. Such a posteriori bounds are usually quite efficient in thick body cases (c.f. [10]), but on thin bodies, the upper bound obtained in this way may be pessimistic. The question then arises: how pessimistic at most? This is one of the main issues considered here.

Another way of obtaining a reliable upper error bound for the finite element solution is to use the complementary energy principle in the a posteriori computation. Here the local boundary conditions are of Neumann type (stress conditions), so local equilibrium conditions are required. In practice, this forces one to first solve a global problem prior to the local computations. The global problem, however, is of relatively moderate size, see section 3.2 below.

Since the error estimators studied here are of geometric nature, they can be studied, and to some extent even analyzed, in a very general setting. We take the advantage of this by first presenting the main ideas in a general Hilbert space setting in Chapter 2. In Chapter 3 these ideas are translated in the language of 3D elasticity and finite element methods. Finally, in Chapter 4 we descend to an even more concrete level. Here we study the problem of 2-dimensional elastic strip where the critical parameter is the dimensionless thickness (t) of the domain, which is considered small. In practice, the thickness is typically small even compared with the finite element mesh spacing. As dimension reduction models, we consider the Timoshenko model for beam bending and the so called $2D.n$-model based on polynomial expansion and the energy principle. Some bounds for the quality of the a posteriori error indicators are derived here. We also study numerically, in a few example cases, how the (two kinds of) error indicators perform in practice.

The analysis of Chapters 2 and 3 remains on a general level, and our results here should be considered known. We have collected these ideas here to serve the reader who can otherwise find them mostly in a very scattered form in the wide adaptive literature.

2 Abstract Error Estimation in Hilbert Spaces

Let us be given two Hilbert spaces, the "displacement" space $\mathcal{U}$ and the "stress" space $\mathbf{\Sigma}$ with inner products $(\cdot,\cdot)_U$ and $(\cdot,\cdot)_\Sigma$, where

$$(u_1, u_2)_U = (Su_1, Su_2)_\Sigma$$

and $S : \mathcal{U} \to \mathbf{\Sigma}$ is a linear injection. The norm of $\mathcal{U}$ is denoted by $||\cdot||_U = \sqrt{(\cdot,\cdot)_U}$ and the norm of $\mathbf{\Sigma}$ by $||\cdot||_\Sigma = \sqrt{(\cdot,\cdot)_\Sigma}$. Let there also be given a bounded linear mapping $L : \mathcal{U} \to \mathbf{R}$, and let $u \in \mathcal{U}$ be such that

$$(u, v)_U = L\ v \quad \forall \quad v \in \mathcal{U}. \tag{2.1}$$

Let $\mathcal{U}^1$ be a subspace of $\mathcal{U}$. Our aim is to derive a posteriori error estimates for $||u - u^1||_U$, where $u^1 \in \mathcal{U}^1$ satisfies

$$(u^1, v)_U = L\ v \quad \forall \quad v \in \mathcal{U}^1. \tag{2.2}$$

Obviously u and u^1 are both uniquely defined and u^1 is the orthogonal projection of u onto $\mathcal{U}^1$. Let $\mathcal{U}^0 \subset \mathcal{U}^1$ (possibly $\mathcal{U}^0 = \mathcal{U}^1$) be another subspace of $\mathcal{U}$, let $\mathcal{U}^2$ be a 'residual' subspace such that

$$\mathcal{U} = \mathcal{U}^0 \oplus \mathcal{U}^2,$$

and let $u^2 \in \mathcal{U}^2$ be such that

$$(u^2, v)_U = L\ v - (u^1, v)_U \quad \forall \quad v \in \mathcal{U}^2. \tag{2.3}$$

Then u^2 is the projection of $u - u^1$ onto $\mathcal{U}^2$. Let us further define the angle between the spaces $\mathcal{U}^0$ and $\mathcal{U}^2$:

$$c = \sup_{v^0 \in \mathcal{U}^0, v^2 \in \mathcal{U}^2} \frac{(v^0, v^2)_U}{||v^0||_U\ ||v^2||_U} \quad \text{and} \quad K = \frac{1}{1 - c^2}. \tag{2.4}$$

We note that the supremum is achieved when v^2 is the projection of v^0 in (2.4):

$$(v^2, v)_U = (v^0, v)_U \ \ \forall\, v \in \mathcal{U}^2.$$

We will denote this projection operator by $\mathcal{P}_U \ : \ \mathcal{U}^0 \to \mathcal{U}^2$. Thus we have

$$c = \sup_{v^0 \in \mathcal{U}^0} \frac{||\mathcal{P}(v^0)||_U}{||v^0||_U}. \tag{2.5}$$

Then we have

Theorem 2.1 (The Energy Principle)

$$||u^2||_U^2 \le ||u - u^1||_U^2 \le K||u^2||_U^2$$

Proof. The first inequality is trivial. To derive the second one, let us define $w = u - u^1$. We may write (uniquely)

$$w - u^2 = w^0 + w^2, \text{ where } w^0 \in \mathcal{U}^0, \ w^2 \in \mathcal{U}^2.$$

Next we note that $(w, w^0) = 0$. It follows that

$$\begin{aligned} ||u - (u^1 + u^2)||_U^2 &= -(u^2, w^0)_U \\ &\le c\, ||u^2||_U ||w^0||_U. \end{aligned} \tag{2.6}$$

On the other hand, we have

$$\begin{aligned} ||u - (u^1 + u^2)||_U^2 &= ||w^0||_U^2 + ||w^2||_U^2 + 2(w^0, w^2)_U \\ &\ge ||w^0||_U^2 + ||w^2||_U^2 - 2c\, ||w^0||_U ||w^2||_U \end{aligned}$$

Thus we obtain

$$||w^2||_U^2 - 2c\, ||w^0||_U ||w^2||_U + ||w^0||_U^2 - ||u - (u^1 + u^2)||_U^2 \le 0. \tag{2.7}$$

Interpreted as a quadratic inequality for $||w^2||_U$, (2.7) must admit a real solution and thus the discriminant must be non-negative:

$$D = 4c^2||w^0||_U^2 - 4||w^0||_U^2 + 4||u - (u^1 + u^2)||_U^2 \ge 0.$$

This implies that

$$||w^0||_U^2 \le \frac{1}{1 - c^2}||u - (u^1 + u^2)||_U^2,$$

so by (2.6)

$$||u-(u^1+u^2)||_U^2 \le \frac{c^2}{1-c^2}||u^2||_U^2$$

and the second inequality of the theorem follows. $\square$

In practice one often deals with the situation where the spaces $\mathcal{U}^i \subseteq \mathcal{U}$ $(i=0,2)$ are composed as

$$\mathcal{U}^i = \left\{ \bigoplus_{k=1}^{N} \mathcal{U}_k^i \right\} \cap \mathcal{U}, \quad \mathcal{U} = \left\{ \bigoplus_{k=1}^{N} \mathcal{U}_k \right\} \cap \mathcal{U},$$

where $\mathcal{U}_k = \mathcal{U}_k^0 \oplus \mathcal{U}_k^2$ and $1 \le N \le \infty$. Let us also assume that for $u, v \in \mathcal{U}$, $(u,v)_U$ is decomposed in terms of the given inner products $(u_k, v_k)_{U_k}$ as

$$(u,v)_U = \sum_{k=1}^{N} (u_k, v_k)_{U_k},$$

where $u_k, v_k \in \mathcal{U}_k$. This notation relates to a finite element method where $\mathcal{U}_k$, $\mathcal{U}_k^i$ are local finite element spaces and $(\cdot,\cdot)_{U_k}$ is the contribution of the k:th element to the global inner product.

Lemma 2.1

$$c \le \max_k c_k,$$

where

$$c_k = \sup_{v_k^0 \in \mathcal{U}_k^0, v_k^2 \in \mathcal{U}_k^2} \frac{(v^0, v^2)_{U_k}}{||v^0||_{U_k}\ ||v^2||_{U_k}}$$

Proof.

$$\begin{aligned} c &= \sup_{v^0 \in \mathcal{U}^0, v^2 \in \mathcal{U}^2} \frac{(v^0, v^2)_U}{||v^0||_U\ ||v^2||_U} \le \sup_{v_k^0 \in \mathcal{U}_k^0, v_k^2 \in \mathcal{U}_k^2} \frac{\sum_{k=1}^N (v_k^0, v_k^2)_{U_k}}{||v^0||_U\ ||v^2||_U} \\ &\le \sup_{v_k^0 \in \mathcal{U}_k^0, v_k^2 \in \mathcal{U}_k^2} \frac{\sum_{k=1}^N c_k ||v_k^0||_{U_k} ||v_k^2||_{U_k}}{||v^0||_U\ ||v^2||_U} \le \max_k c_k \quad \square \end{aligned}$$

Thus in the finite element method, it suffices to compute the constant c_k (and the associated K_k) for the 'worst' element.

We note that in practical adaptive algorithms Theorem 2.1 is typically applied in a situation where $\mathcal{U}^1$ is finite dimensional and $\mathcal{U}$ is infinite-dimensional. Then $\mathcal{U}^2$ is infinite-dimensional as well and hence the upper bound of Theorem 2.1 (which is of the main interest) is not computable, even if K is. To obtain practical bounds, one then needs to replace $\mathcal{U}^2$ by some finite dimensional subspace. Unfortunately, the upper error bound obtained in such a way is no more reliable - only the lower bound is.

We derive next an alternative upper error bound for $||u-u^1||_U$ which is both reliable and computable. This is based on the (modified) complementary energy principle.

Let there be given another bounded linear functional $l : \mathcal{U} \to \mathbf{R}$ with the norm

$$||l||_{U^*} = \sup_{v\in\mathcal{U}} \frac{|lv|}{||v||_U},$$

and define

$$\mathbf{\Sigma}_{L,l} = \{\sigma \in \mathbf{\Sigma} \mid (\sigma, Sv)_\Sigma = Lv + lv \ \ \forall v \in \mathcal{U}\}. \tag{2.8}$$

When $l = 0$, $\mathbf{\Sigma}_{L,l}$ is referred to as the set of "statically admissible" stresses. We give this set the symbol $\mathbf{\Sigma}_{SA}$, i.e., $\mathbf{\Sigma}_{SA} = \mathbf{\Sigma}_{L,0}$.

Theorem 2.2 *Let $\sigma \in \mathbf{\Sigma}_{L,l}$. Then*

$$||u-u^1||_U^2 \le \left(\sqrt{||\sigma||_\Sigma^2 + ||l||_{U^*}^2} + ||l||_{U^*}\right)^2 - ||u^1||_U^2$$

Proof. Given $\sigma \in \mathbf{\Sigma}_{L,l}$, we have

$$\begin{aligned} ||\sigma - Su||_\Sigma^2 &= ||\sigma||_\Sigma^2 + ||u||_U^2 - 2Lu - 2lu \\ &= ||\sigma||_\Sigma^2 - ||u||_U^2 - 2lu, \end{aligned}$$

from which we get

$$||u||_U^2 - 2||l||_{U^*}||u||_U - ||\sigma||_\Sigma^2 \le 0.$$

This implies

$$||u||_U \le \sqrt{||\sigma||_\Sigma^2 + ||l||_{U^*}^2} + ||l||_{U^*}.$$

The theorem now follows, since

$$||u-u^1||_U^2 = ||u||_U^2 - ||u^1||_U^2 \quad \square$$

Corollary 2.1 (The Complementary Energy Principle) *For any* $\sigma \in \mathbf{\Sigma}_{SA}$

$$||u - u^1||_U^2 \leq ||\sigma||_\Sigma^2 - ||u^1||_U^2 \quad \Box$$

We note that the results of this section do not depend at all on the (bounded linear) mapping L.

3 Error Estimation in Linear Elasticity

In this section we will transform the theorems and notation given in the preceding section to the language of linear elasticity and finite element analysis. Thus, we are considering a body occupying a domain $\Omega \subset \mathbf{R}^n$, where $n = 1, 2, 3$, depending on whether we consider the full $3D$-theory or some lower dimensional theory. We will denote the displacement field by the symbols $\underline{U} = \{U_i\}_{i=1}^n$, $\underline{V} = \{V_i\}_{i=1}^n$, the strain tensor by the symbol $\underline{\underline{\varepsilon}} = \{\varepsilon_{ij}\}_{i,j=1}^n$ and the stress tensor by the symbol $\underline{\underline{\sigma}} = \{\sigma_{ij}\}_{i,j=1}^n$. The boundary $\Gamma = \partial\Omega$ will be splitted in two parts as $\Gamma = \overline{\Gamma}_u \cup \overline{\Gamma}_\tau$. Here Γ_u represents the part of the boundary with kinematical constraints (we consider here for simplicity only the case of clamped boundary on Γ_u, the generalization to arbitrary kinematical constraints would be quite straightforward), and Γ_τ the part of the boundary with given stress boundary conditions. Thus we require that the solution to the problem satisfies on Γ the following:

$$\underline{U} = \underline{0} \text{ on } \Gamma_u, \qquad \underline{\underline{\sigma}} \cdot \underline{n} = \underline{f} \text{ on } \Gamma_\tau,$$

where $\underline{f}$ is the given load on Γ_τ. The deformation energy of the body (which is a quadratic functional of $\underline{U}$) will be denoted by $\mathcal{A}(\underline{U}, \underline{U})$, the load potential (a linear functional of $\underline{U}$) by $\mathcal{Q}(\underline{U})$ (including both the body force $\underline{g}$ in Ω and the load $\underline{f}$ on Γ_τ), and the energy norm by $||| \cdot ||| = \sqrt{\mathcal{A}(\cdot, \cdot)}$. The energy space $\mathcal{U}$ may then be defined as

$$\mathcal{U} = \{\underline{U} \in \mathcal{W} \,|\, \underline{U} = 0 \text{ on } \Gamma_u\},$$

where $\mathcal{W}$ is a suitable Sobolev space depending on $\mathcal{A}$. In case the kinematical constraints on Γ_u leave free some rigid body motions $\underline{U}^R$ (where $|||\underline{U}^R||| = 0$), we assume that the load satisfies the corresponding equilibrium condition $\mathcal{Q}(\underline{U}^R) = 0$, and we shrink the energy space by imposing the constraint

$$\int_\Omega \underline{U}^R \cdot \underline{U} \, \mathrm{d}V = 0, \quad \underline{U} \in \mathcal{U}.$$

In case of (homogeneous and isotropic) nD linear elasticity with $n=2$ or $n=3$ we have

$$
\begin{aligned}
\mathcal{W} &= [H^1(\Omega)]^n \\
\mathcal{A}(\underline{U},\underline{V}) &= \int_\Omega \sum_{i,j=1}^{n} \sigma_{ij}(\underline{U})\cdot\varepsilon_{ij}(\underline{V})\,\mathrm{d}V, \qquad (3.9)\\
\mathcal{Q}(\underline{V}) &= \int_\Omega \underline{g}\cdot\underline{V}\,\mathrm{d}V + \int_{\Gamma_\tau} \underline{f}\cdot\underline{V}\,\mathrm{d}S.
\end{aligned}
$$

Here the strain tensor $\underline{\underline{\varepsilon}}(\underline{U})$ is defined as $\varepsilon_{ij} = \frac{1}{2}(U_{i,j}+U_{j,i})$ and the stress tensor $\underline{\underline{\sigma}}(\underline{U})$ by the linear Hooke's law as $\underline{\underline{\sigma}} = T\underline{\underline{\varepsilon}}$ with some symmetric tensor T depending on the material of the body. The stress space $\mathbf{\Sigma}$ is defined as

$$\mathbf{\Sigma} = \{\underline{\underline{\sigma}} \in \mathcal{H} \mid \sigma_{ij} = \sigma_{ji}\}, \text{ where } \mathcal{H} = [L_2(\Omega)]^{n^2},$$

and the inner product of $\mathbf{\Sigma}$ as

$$(\underline{\underline{\sigma}},\underline{\underline{\tau}})_\Sigma = (T^{-1}\underline{\underline{\sigma}},\underline{\underline{\tau}})_\mathcal{H}.$$

Referring to the notation of section 2 we have the obvious analogies $\mathcal{A}(\underline{U},\underline{V}) \sim (u,v)_U$, $\mathcal{Q}(\underline{V}) \sim Lv$, $T\underline{\underline{\varepsilon}}(\underline{U}) \sim Su$, etc.

3.1 The Energy Principle

In this section we discuss the use of Theorem 2.1 in finite element analysis. To this end, consider a situation where we have first solved the elasticity problem in some finite element space (denoted by $\mathcal{U}^1$) and would then like to approximate the error $|||\underline{U}-\underline{U}^1|||$, where $\underline{U}^1$ is the finite element solution and $\underline{U}$ the exact solution to the problem. However, as we are restricted to finite computations also in the error estimation, we have to take $\underline{U}^2$ in (2.3) to be a finite element solution of higher order. So let us assume, that we have originally solved the problem in a subspace $\mathcal{U}^1 \subset \mathcal{U}$ spanned by the basis functions $\{\underline{\varphi}_i^G\}_{i=1}^{N_1}$, $\{\underline{\varphi}_i^L\}_{i=1}^{N_2}$. Here we have separated the degrees of freedoms of the space $\mathcal{U}^1$ to two groups: to the "global" ones (the $\underline{\varphi}_i^G$), and to the "local" ones (the $\underline{\varphi}_i^L$). By a local basis function we mean here a function $\underline{\varphi}_i^L$ such that $\mathrm{supp}(\underline{\varphi}_i^L) \subset \Omega_\nu$ for some ν, where $\{\Omega_\nu\}_{\nu=1}^m$ is a given partition of Ω into disjoint subdomains. The latter is usually the finite element partition itself, but some other possibilities could be used.

In the above notation, the space $\mathcal{U}^2$ is defined by inserting a set of new degrees of freedom $\{\underline{\phi}_i\}_{i=1}^{N_3}$ to $\mathcal{U}^1$. These are assumed to be of the local type, i.e., $\mathrm{supp}(\underline{\phi}_i) \subset \Omega_\nu$ for some $\nu = \nu(i)$. As to the definition of $\mathcal{U}^0$ (which affects K, see (2.4)), there are various possibilities. For example:

1. Choose $\mathcal{U}^0 = \mathcal{U}^1$ and let $\mathcal{U}^2$ be the space spanned by the $\underline{\phi}_i$.

2. Choose $\mathcal{U}^0$ to be the space spanned by the $\underline{\varphi}_i^G$ and let $\mathcal{U}^2$ be the space spanned by the $\underline{\varphi}_i^L$ and the $\underline{\phi}_i$.

In both of these cases, the space $\mathcal{U}^2$ and thus also the computation needed for the error estimate given by $|||\underline{U}^2|||$ are local. If the set $\{\underline{\varphi}_i^L\}_{i=1}^{N_2}$ is empty in the original space $\mathcal{U}^1$, there is obviously no difference between the two options. Otherwise, let $\underline{U}_k^2$ be the solution to the local problem (2.3), where $k = 1, 2$ corresponds to the cases $1, 2$ above. Respectively, let K_k be the constant K in (2.4) representing the angle between the spaces $\mathcal{U}^0$ and $\mathcal{U}^2$ in the two cases. By Theorem 2.1, we obtain easily the following.

$$|||\underline{U}_1^2|||^2 \leq |||\underline{U}_2^2|||^2 \leq |||\underline{\tilde{U}} - \underline{U}^1|||^2 \leq \min_{k=1,2} K_k |||\underline{U}_k^2|||^2,$$

where $\underline{\tilde{U}}$ is the "exact" solution corresponding to $\tilde{\mathcal{U}} = \mathcal{U}^0 \oplus \mathcal{U}^2$. Thus the choice between options 1 and 2 should depend on which choice leads to the better estimate.

3.2 The Complementary Energy Principle

In order to utilize the Complementary Energy Principle (Corollary 2.1), we must find a statically admissible stress field $\underline{\underline{\sigma}} \in \mathbf{\Sigma}_{SA}$ approximating (if possible) the actual stress field of the problem. This may be difficult - then one has to use more general Theorem 2.2 and try to find a field $\underline{\underline{\sigma}}$ for which the functional l is small. For the sake of simplicity, we consider here the case $\underline{\underline{\sigma}} \in \mathbf{\Sigma}_{SA}$ only.

By partial integration, we have the following characterization of $\mathbf{\Sigma}_{SA}$ in an nD elastic problem ($n = 2, 3$):

$$\mathbf{\Sigma}_{SA} = \left\{ \underline{\underline{\sigma}} \in \mathbf{\Sigma} \,|\, \underline{\mathrm{div}\, \underline{\underline{\sigma}}} = \underline{g} \text{ in } \Omega,\ \underline{\underline{\sigma}} \cdot \underline{n} = \underline{f} \text{ on } \Gamma_\tau \right\}.$$

When constructing such a $\underline{\underline{\sigma}}$, one would in general like to use the information given by the finite element solution $\underline{U}^1$, in order to localize the computations needed for the error estimate. An obvious idea for such a localization is to compute the stresses of

$\underline{U}^1$ at the intersubdomain boundaries and use them as boundary values for $\underline{\underline{\sigma}}$. However, there are two problems in this approach. First of all, the boundary values of the stresses computed from $\underline{U}^1$ are in general discontinuous causing δ-distributions to appear in $\underline{\operatorname{div}}\,\underline{\underline{\sigma}}$. This problem may be avoided by averaging. But, the more severe problem is that the local problems are not solvable unless the boundary stresses are in equilibrium. In order to guarantee this, we have to construct the field $\underline{\underline{\sigma}}$ in two steps.

Step 1.
First, we construct an auxiliary stress field $\underline{\underline{\sigma}}^*$ in such a way that i) $\underline{\underline{\sigma}}^* \cdot \underline{n}$ is continuous on Ω, and ii) the stress boundary conditions given by $\underline{\underline{\sigma}}^*$ are in equilibrium in each element locally. Among such stress fields, we may, e.g., choose the one minimizing $|||\underline{\underline{\sigma}}^* - \underline{\underline{\sigma}}(\underline{U}^1)|||$. In practice $\underline{\underline{\sigma}}^*$ can be constructed as follows. First let $\mathbf{\Sigma}^*$ be a finite dimensional subspace of $\mathbf{\Sigma}$ such that for any $\underline{\underline{\sigma}}^* \in \mathbf{\Sigma}^*$, $\underline{\underline{\sigma}}^*$ satisfies i) and $\underline{\underline{\sigma}}^* \cdot \underline{n} = \underline{0}$ on Γ_τ. Further let $\mathcal{U}^* \subset [L_2(\Omega)]^n$ be the space of discontinuous displacement fields $\underline{U}^*$ on Ω such that $\underline{U}^*|_{\Omega_\nu}$ is a rigid body motion on Ω_ν for each ν. Then the task is to find $(\underline{\underline{\sigma}}^*, \underline{U}^*) \in \mathbf{\Sigma}^* \times \mathcal{U}^*$ satisfying

$$(3.10a) \qquad (\underline{\underline{\sigma}}^*, \underline{\underline{\tau}})_{\mathbf{\Sigma}} - \int_\Omega \underline{U}^* \cdot \underline{\operatorname{div}}\,\underline{\underline{\tau}}\,\mathrm{d}V = (\underline{\underline{\sigma}}(\underline{U}^1), \underline{\underline{\tau}})_{\mathbf{\Sigma}} \text{ for all } \underline{\underline{\tau}} \in \mathbf{\Sigma}^*,$$

$$(3.10b) \qquad \int_\Omega \underline{div}\,\underline{\underline{\sigma}}^* \cdot \underline{v}\,\mathrm{d}V = \int_\Omega \underline{g} \cdot \underline{v}\,\mathrm{d}V + \int_{\Gamma_\tau} \underline{f} \cdot \underline{v}\,\mathrm{d}S \text{ for all } \underline{v} \in \mathcal{U}^*.$$

Note that in this formulation, $\underline{U}^*$ appears as a Lagrange multiplier for imposing the constraint ii). Note also that (3.10b) couples adjacent subdomains, so (3.12) has to be solved as a global system. In practice, (3.10a) is solved most efficiently by first condensing $\underline{\underline{\sigma}}^*$. The remaining global system then has size $3(n-1)m$ (n=2,3), where m is the number of the subdomains Ω_ν.

For the above system to be solvable, the space $\mathbf{\Sigma}^*$ needs to be large enough compared with $\mathcal{U}^*$. The weakest condition of solvability is:

$$(3.11) \qquad \int_\Omega \underline{U}^* \cdot \underline{\operatorname{div}}\,\underline{\underline{\tau}}\,\mathrm{d}V = 0 \ \ \forall\, \underline{\underline{\tau}} \in \mathbf{\Sigma}^*$$
$$\Rightarrow \ \underline{U}^* = \underline{U}^R = \text{ rigid body motion on } \Omega \text{ satisfying } \underline{U}^R = \underline{0} \text{ on } \Gamma_u.$$

Note that the requirement $\underline{U}^* \in \mathcal{U}$ together with (3.11) implies $\underline{U}^* = \underline{0}$. In the case where the kinematical constraints remove all global rigid body motions, a necessary condition for (3.11) to hold is that $\dim(\mathbf{\Sigma}^*) \geq 3(n-1)m$. For stronger versions of the (stability) condition (3.11), and the related convergence analysis of mixed finite element methods, the reader is referred to [18] (and to the further references therein).

Step 2.
The second step is to construct a stress field $\underline{\underline{\sigma}} \in \mathbf{\Sigma}_{SA}$ by local computations on each Ω_ν using $\underline{\underline{\sigma}}^* \cdot \underline{n}$ as a stress boundary condition on intersubdomain boundaries. Thus on each Ω_ν, we wish to find a (sufficiently large) set of stresses $\underline{\underline{\sigma}}$ such that

$$\left\{ \begin{array}{rcll} \underline{\mathrm{div}\,\underline{\underline{\sigma}}} & = & \underline{g} & \text{on} \quad \Omega_\nu \\ \underline{\underline{\sigma}} \cdot \underline{n} & = & \underline{f} & \text{on} \quad \partial\Omega_\nu \cap \Gamma_\tau \\ \underline{\underline{\sigma}} \cdot \underline{n} & = & \underline{\underline{\sigma}}^* \cdot \underline{n} & \text{on} \quad \partial\Omega_\nu \setminus \Gamma_\tau \end{array} \right. \tag{3.12}$$

Among such stresses we simply minimize $|||\underline{\underline{\sigma}}|||$ (locally on each Ω_ν). Note that by (3.10b), the constraints in (3.12) are in local equilibrium. In practice one may need to approximate $\underline{g}$ and $\underline{f}$ in (3.12), e.g. by a polynomial expansion. The constraint $\underline{\underline{\sigma}} \in \mathbf{\Sigma}_{SA}$ is then violated, but Theorem 2.2 is still applicable.

4 The Elastic Strip

In this section we analyze the problem of two-dimensional elastic strip. This is a $2D$ elastic problem on a domain

$$\Omega = \{(x, z) \in (-H/2, H/2) \times (-t/2, t/2)\}$$

where t/H is small. The bilinear form $\mathcal{A}$ is defined as in (3.9). We set

$$\mathcal{A}(\underline{U}, \underline{V}) = \int_\Omega \Sigma_{i=1,3} \sigma_{ij}(\underline{U}) \varepsilon_{ij}(\underline{V})\, dx\, dz, \tag{4.13}$$

where the stress tensor $\underline{\underline{\sigma}} = (\sigma_{ij})_{i,j=1,3}$, and the strain tensor $\underline{\underline{\varepsilon}} = (\varepsilon_{ij})_{i,j=1,3}$ are related to the displacement field

$$\underline{U} \in \mathcal{U}^{2D} = \{\underline{U} = (u, w) \in [H^1(\Omega)]^2\}$$

as

$$\begin{array}{ll} \varepsilon_{11} = u_{,x} & \sigma_{11} = \frac{E}{1+\nu}\left[\gamma(\varepsilon_{11} + \varepsilon_{33}) + \varepsilon_{11}\right] \\ \varepsilon_{13} = \frac{1}{2}(u_{,z} + w_{,x}) & \sigma_{13} = \frac{E}{1+\nu}\varepsilon_{13} \\ \varepsilon_{33} = w_{,z} & \sigma_{33} = \frac{E}{1+\nu}\left[\gamma(\varepsilon_{11} + \varepsilon_{33}) + \varepsilon_{33}\right]. \end{array} \tag{4.14}$$

Here $E > 0$ is the Young's modulus and ν the Poisson's ratio of the (homogeneous and isotropic) material, and

$$\gamma = \begin{cases} \nu/(1-2\nu) & \text{(plane strain)} \\ \nu/(1-\nu) & \text{(plane stress).} \end{cases}$$

We assume that ν is fixed to some value $0 \leq \nu < 1/2$, i.e., we do not consider here the case $\nu \to 1/2$ of nearly incompressible material. The Euler equations, i.e., the equilibrium conditions for the stresses are

$$\begin{aligned} \sigma_{11,x} + \sigma_{13,z} &= 0 \\ \sigma_{13,x} + \sigma_{33,z} &= 0 \end{aligned} \tag{4.15}$$

Here we have assumed that the body force $\underline{g}$ is zero.

In the elastic strip problem, it is always possible to split the problem into two parts, namely to *membrane* and *bending* parts. This is done simply by considering the symmetric and antisymmetric parts of the displacement fields in the z-direction separately. In the membrane case we study the symmetric part of the component u and antisymmetric part of the component w, and in the bending case vice versa. As is easily seen, this splitting is orthogonal with respect to the inner product $\mathcal{A}$, so the two problems are independent once the external load is split orthogonally as well (c.f.[16]).

We will first show that it is not possible to obtain a finite error constant K for the comparison made between the linear model in the x-direction and the full $2D$-model.

Theorem 4.1 *Suppose*

$$\begin{aligned} \mathcal{U}^0 &= \{\underline{U} \in \mathcal{U}^{2D} \,|\, \underline{U}(x,z) = \underline{f}_1(z) + \underline{f}_2(z)x\} \\ \mathcal{U}^2 &= \{\underline{U} \in \mathcal{U}^{2D} \,|\, \underline{U}(\pm H/2, \cdot) = 0\} \end{aligned}$$

Then $K = \infty$.

Proof. Choose

$$\underline{U}^0 = \begin{pmatrix} \cos(2k\pi z/t) \\ 0 \end{pmatrix}$$

and let $\underline{U}^2$ be the projection of $\underline{U}^1$ to

$$\left\{ \underline{U} = \begin{pmatrix} a(x)\cos(2k\pi z/t) \\ b(x)\sin(2k\pi z/t) \end{pmatrix} \,|\, a(\pm H/2) = b(\pm H/2) = 0 \right\}.$$

By a simple computation we see that

$$\frac{\mathcal{A}(\underline{U}^1,\underline{U}^2)}{|||\underline{U}^1|||\,|||\underline{U}^2|||} = \frac{Hk^2\pi(20H\pi + \sinh(2k\pi/t))}{(2kt+20t^2)\sinh^2(2k\pi/t)} \to \infty \;\text{ as } k \to \infty. \qquad \square$$

A finite value $K = K(n, H, t)$ is obtained if the displacement field is restricted to be a polynomial of degree n in z, i.e.,

$$\mathcal{U} = \mathcal{U}^{2D.n} = \left\{ \underline{U} \in \mathcal{U}^{2D} \,|\, \underline{U} = \sum_{i=0}^{n} (u_i(x)z^i, w_i(x)z^i) \right\}. \tag{4.16}$$

This corresponds to the $2D.n$ dimension reduction problem [16]. The case $n = 2$ will be discussed in section 4.2 below. We first consider a simpler dimension reduction model, the so called Timoshenko model.

4.1 The Timoshenko Beam Model

In order to concretize the usage of the theorems derived in the preceding section, we start with the simplest thin body problem, the 1-dimensional Timoshenko beam problem with clamped boundary. In this problem we are looking for the displacement field satisfying

$$\mathcal{A}(\underline{U}, \underline{\tilde{U}}) = \mathcal{Q}(\underline{\tilde{U}}) \;\; \forall\, \underline{\tilde{U}} \in \mathcal{U}.$$

The Timoshenko model describes the bending of the elastic strip as a beam. It may be seen as a simplification of the $2D.2$-model where $u(x, z) = -z\theta(x)$, w is independent of z and the bilinear form $\mathcal{A}$ in (3.9) is defined as

$$\mathcal{A}(\underline{U}, \underline{\tilde{U}}) = \frac{Et^3}{12}\int_{-H/2}^{H/2} \theta'\tilde{\theta}'\,\mathrm{d}x + \frac{E\alpha t}{12}\int_{-H/2}^{H/2} (\theta - w')(\tilde{\theta} - \tilde{w}')\,\mathrm{d}x.$$

Here α is a parameter depending on the shape of the cross section and on the material of the beam but independent of t. For example, for a beam of rectangular cross section and consisting of homogeneous isotropic material with Poisson's ratio ν, one has $\alpha = 5/(1+\nu)$. Assuming clamped boundaries at $x = \pm H/2$ we have

$$\underline{U} \in \mathcal{U} = \left\{ \underline{U} = (w, \theta) \in [H^1(-H/2, H/2)]^2 \,|\, \underline{U}(\pm H/2) = 0 \right\}.$$

Finally, the load potential

$$\mathcal{Q}(\underline{U}) = \int_{-H/2}^{H/2} f \cdot w \;\mathrm{d}x$$

corresponds to the stress boundary conditions $\sigma_{31}(x, \pm t/2) = 0$, $\sigma_{33}(x, \pm t/2) = \pm f(x)$ in the original problem.

We consider here the use of the energy principle (Theorem 2.1 and Lemma 2.1) only. Let us assume that we are solving the above problem by the finite element method by subdividing the interval $(-H/2, H/2)$ into N subintervals of length h_k, $k = 1, \ldots, N$. Let $\mathcal{U}^0 = \mathcal{U}^1$ be the space of continuous piecewise linear functions associated to this subdivision, and let $\mathcal{U}^2$ be the subspace of $\mathcal{U}$ consisting of functions that vanish at the endpoints of each subinterval. Let $\underline{U}$, $\underline{U}^1$ and $\underline{U}^2$ be the corresponding solutions for these spaces, as defined in section 2 in the abstract setting.

Theorem 4.2

$$|||\underline{U}^2|||^2 \leq |||\underline{U} - \underline{U}^1|||^2 \leq K|||\underline{U}^2|||^2,$$

where

$$K = 1 + \frac{\alpha \max_k h_k^2}{12t^2}.$$

Proof. We apply Lemma 2.1, so it suffices to consider only one of the subintervals, the length of which will be denoted by h. In order to apply the energy principle, we have to calculate the angle c between the spaces

$$\begin{aligned} \mathcal{U}^0 &= \{\underline{U} \in \mathcal{U} \mid \underline{U} = \underline{a} + \underline{b}x\}, \\ \mathcal{U}^2 &= \{\underline{U} \in \mathcal{U} \mid \underline{U}(\pm h/2) = 0\}. \end{aligned}$$

Here $\mathcal{U}$ is defined as above with h replacing H. As the problem here is 1-dimensional, it is possible to compute the projection $\mathcal{P}_{\mathcal{A}}(\underline{U}^0)$ in (2.5) for any $\underline{U}^0 \in \mathcal{U}^0$ analytically. To this end, we define

$$\underline{U}_1^0 = (1, 0), \quad \underline{U}_2^0 = (0, 1), \quad \underline{U}_3^0 = (x, 0), \quad \underline{U}_4^0 = (0, x).$$

Clearly this forms a basis of $\mathcal{U}^0$, so it suffices to compute $\underline{U}_i^2 = \mathcal{P}_{\mathcal{A}}(\underline{U}_i^0)$ for each i. But this is equivivalent to solving $D_j(\underline{U}_i^2) = D_j(\underline{U}_i^0)$, $j = 1, 2$, where D_1, D_2 are the differential operators in the Euler equations of the problem:

$$D_1(\underline{U}) = -t^3\theta'' + \alpha t(\theta - w'), \quad D_2(\underline{U}) = \alpha t(\theta' - w'').$$

We obtain

$$\begin{aligned}
\underline{U}_1^2 &= (0,0) \\
\underline{U}_2^2 &= \left(\frac{x(h^2-4x^2)}{2(h^2+12t^2/\alpha)}, \frac{3(h^2-4x^2)}{2(h^2+12t^2/\alpha)}\right) \\
\underline{U}_3^2 &= -\underline{U}_2^2 \\
\underline{U}_4^2 &= \left(\frac{h^2-4x^2}{8}, 0\right)
\end{aligned}$$

and then by easy computation,

$$c^2 = \max_{a_i} \frac{||\sum_{i=1}^4 a_i \underline{U}_i^2||^2}{||\sum_{i=1}^4 a_i \underline{U}_i^0||^2} = \frac{h^2}{h^2+12t^2/\alpha},$$

from which we obtain the K given in the theorem by the relation

$$K = \frac{1}{1-c^2}. \quad \square$$

In Fig. 1 we demonstrate the use of Theorem 4.2 by a numerical example where we first solve the problem with linear elements (giving the solution $\underline{U}^1$) and then estimate the error in $\underline{U}^1$ as compared with the solution $\underline{U}$ given by quadratic elements. This corresponds to choosing $\mathcal{U}^0 = \mathcal{U}^1$ as above and $\mathcal{U}$ to be the space of continuous piecewise quadratic functions. When applying Theorem 2.1 we choose here the value of K as given by Theorem 4.2 - note that also in this way we get a reliable (though not necessarily sharp) upper bound for the error. Taking $H=1$, $\nu = 1/3$, $h_k = 1/10$ for $k = 1, \ldots, 10$, and letting t vary in the range $t \in [10^{-4}, 1]$ we obtain the error $E := |||\underline{U} - \underline{U}^1|||^2/|||\underline{U}|||^2$, the lower bound $EP := |||\underline{U}^2|||^2$ and the upper bound $K \cdot EP$, as shown in Fig. 1. As seen from this $(\log_{10} \cdot, -\log_{10} t)$-picture, there occurs numerical locking in the problem: the relative error approaches 1 as $t \to 0$. From the picture, the rate of EP is seen to be $\sim t^2$, so the actual numerical locking is not predicted by EP. Instead the upper bound is rather sharp, indicating that the value of K used is only a mild overestimate.

4.2 The 2D.2-model

We show first that Theorem 4.1 is improvable when $\mathcal{U}^0$ is restricted to be a subspace of $\mathcal{U}^{2D.2}$

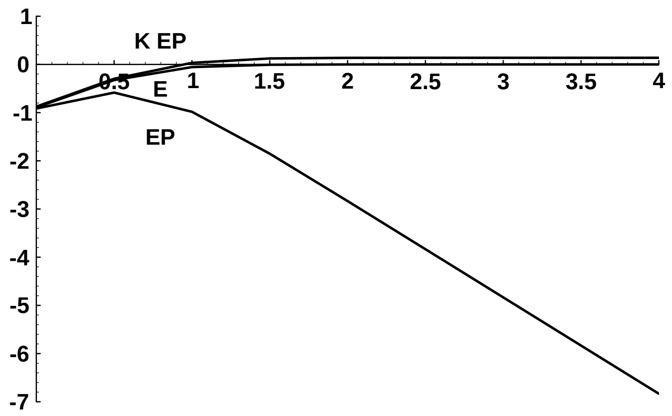

Figure 1: True relative error and the estimated lower and upper bounds for the model problem.

Theorem 4.3 *Suppose*

$$\begin{aligned}\mathcal{U}^0 &= \{\underline{U} \in \mathcal{U}^{2D.2} \,|\, \underline{U}(x,z) = \underline{f}_1(z) + \underline{f}_2(z)x\} \\ \mathcal{U}^2 &= \{\underline{U} \in \mathcal{U}^{2D} \,|\, \underline{U}(\pm h/2, \cdot) = 0\}\end{aligned}$$

Then

$$K = \begin{cases} \mathcal{O}(1 + \frac{h}{t}) & \textit{in the membrane case,} \\ \mathcal{O}(1 + \frac{h^2}{t^2}) & \textit{in the bending case.} \end{cases}$$

and the estimates can not be improved even if $\mathcal{U}^2 \subset \mathcal{U}^{2D.2}$.

Proof. When considering separately the membrane and bending cases, the space $\mathcal{U}^0$ is originally 6-dimensional. However, some of the displacement fields in $\mathcal{U}^0$ are rigid body motions $\underline{U}^R$ for which $|||\underline{U}^R||| = 0$. In the membrane case there is one such rigid body motion, $\underline{U}^{R1} = (1,0)$, and in the bending case there are two, $\underline{U}^{R2} = (0,1)$ and $\underline{U}^{R3} = (z,-x)$. After excluding the rigid body motions we may thus write $\underline{U}^0 = \sum_{i=1}^d a_i \underline{U}_i^0$, where $d = 5$ in the membrane case and $d = 4$ in the bending case. Let us then define $\underline{U}^2 = \mathcal{P}_{\mathcal{A}}(\underline{U}^0) = \sum_{i=1}^d a_i \mathcal{P}_{\mathcal{A}}(\underline{U}_i^0)$, where $\mathcal{P}_{\mathcal{A}} : \mathcal{U}^0 \to \mathcal{U}^2$ is the projection operator as in (2.5), now in the sense of the inner product (4.13). Then it is easy to see that

$$c^2 = \max_{\underline{a} \in \mathbf{R}^d} \frac{|||\underline{U}^2|||^2}{|||\underline{U}^0|||^2} = \max_{\underline{a} \in \mathbf{R}^d} \frac{\underline{a}^T M^2 \underline{a}}{\underline{a}^T M^0 \underline{a}},$$

where $\underline{a} = \{a_i\}_{i=1}^d$, and M^0 and M^2 are the following (nonsingular) $d \times d$ matrices:

$$M^0_{ij} = \mathcal{A}(\underline{U}^0_i, \underline{U}^0_j)\ ,\ M^2_{ij} = \mathcal{A}(\mathcal{P}(\underline{U}^0_i), \mathcal{P}(\underline{U}^0_j)).$$

Thus the supremum may be computed as the largest eigenvalue of the matrix $(M^0)^{-1}M^2$. However, as the problem here is not one-dimensional (if we do not assume $\mathcal{U}^2 \subset \mathcal{U}^{2D.2}$), it is not possible to compute the projections $\mathcal{P}(\underline{U}^0_i)$ exactly. The problem may be avoided, e.g. by using the complementary energy principle. First, we find stress fields $\underline{\underline{\sigma}}$ satisfying (4.15) such that

$$\begin{aligned} \sigma_{13}(\cdot, \pm t/2) &= 0, \\ \sigma_{33}(\cdot, \pm t/2) &= 0. \end{aligned} \tag{4.17}$$

It is easy to see (by the complementary energy principle) that for any such stress field $\underline{\underline{\tau}}$ (which may depend on $\underline{a}$) we have

$$c^2 = \max_{\underline{a} \in \mathbf{R}^d} \frac{|||\underline{U}^2|||^2}{|||\underline{U}^0|||^2} \le \max_{\underline{a} \in \mathbf{R}^d} \frac{|||\underline{\underline{S}}\,(\underline{U}^0) - \underline{\underline{\tau}}|||^2}{|||\underline{U}^0|||^2}, \tag{4.18}$$

where $\underline{\underline{S}}(\underline{U}^0)$ is the stress field associated to $\underline{U}^0$ according to (4.14). In Appendix A we give some complementary fields $\underline{\underline{\sigma}} = \underline{\underline{\tau}}_i$ satisfying both(4.15) and (4.17). The idea is to choose enough stress fields $\underline{\underline{\tau}}_i$ in such a way that the space they span is able to capture the main characteristics of the stress fields $S(\underline{U}^0_i)$. Most of the fields given in the appendix are needed to approximate the $\underline{\underline{S}}(\underline{U}^0_i)$ as $t/h \to 0$, but some also to ensure that K does not grow as $h/t \to 0$.

With the fields $\underline{\underline{\tau}}_i$ from the appendix available, we define $\underline{\underline{\tau}}$ to be the linear combination of the $\underline{\underline{\tau}}_i$ that minimizes (4.18). We note that the coefficients of the linear combination are again linear combinations of a_i. After a rather tedious computation (made here symbolically with MATHEMATICA) we obtain matrices M^0 and M^2 leading to the estimates given in the theorem.

Finally, to see that the estimates can not be improved, we give a counterexample. First, for the membrane case, assume $t < h/2$ and set

$$\begin{aligned} \underline{U}^0 &= (\ 0\ ,\ z\ ) \\ \underline{U}^2 &= (\ 0\ ,\ \phi(x) z\ )\ , \end{aligned}$$

where

$$\phi(x) = \begin{cases} \frac{1}{t}\left(\frac{x}{h} + \frac{1}{2}\right), & -h/2 \le x \le -h/2 + t, \\ 1, & -h/2 + t < x < h/2 - t, \\ \frac{1}{t}\left(\frac{1}{2} - \frac{x}{h}\right), & h/2 - t \le x \le h/2. \end{cases}$$

Then $\underline{U}^2 \in \mathcal{U}^{2D.2}$ and we get

$$K \geq \frac{24(1+\gamma)+(t/h)(1-32(1+\gamma))}{16(1+\gamma)+1-(t/h)24(1+\gamma)} \cdot \frac{h}{t}\,.$$

Thus $K = \mathcal{O}(1+h/t)$ is optimal for the membrane case. In the bending case, the choice

$$\begin{aligned} \underline{U}^0 &= (\ z\ ,\ 0\ ) \\ \underline{U}^2 &= \left(-6z\left(\frac{x^2}{h^2}-\frac{1}{4}\right)\ ,\ 2\frac{x}{h}\left(\frac{x^2}{h^2}-\frac{1}{4}\right) \right) \end{aligned}$$

leads to

$$K \geq 1 + \frac{h^2}{2(1+\gamma)t^2}\,,$$

showing the optimality of the estimate in that case. $\square$

In finite element analyses, the space $\mathcal{U}^2$ is always finite dimensional. If we also restrict the space $\mathcal{U}^2$ so that $\mathcal{U}^2 \subset \mathcal{U}^{2D.2}$, we may improve the previous results so as to obtain uniform estimates with respect to t and h. In the membrane case we do not need any further assumptions.

Theorem 4.4 *Consider the membrane case with*

$$\begin{aligned} \mathcal{U}^0 &= \{\underline{U} \in \mathcal{U}^{2D.2} \mid u_0, w_1, u_2 \in \mathcal{P}^1(-h/2,h/2) \textit{ in } (4.16)\} \\ \mathcal{U}^2 &= \Bigg\{\underline{U} \in \mathcal{U}^{2D.2} \mid u_0, w_1, u_2 \textit{ in } (4.16) \textit{ are of the form} \\ &\qquad \sum_{i=1}^{N} a_i\phi_i(x),\ \textit{ where } \phi_i(\pm h/2) = 0,\ i = 1\ldots N \Bigg\}, \end{aligned}$$

where the (fixed) basis functions ϕ_i are independent of t and depend on h as $\phi_i(x) = \tilde{\phi}_i(x/h)$, where the $\tilde{\phi}_i$ are h-independent functions defined on $(-1/2, 1/2)$. Then $K < \infty$ is independent of t and h.

Proof. As we already know that $K = \mathcal{O}(1+h/t)$, we may assume here that $t/h \to 0$. We note also that it suffices to consider the case $h = 1$, as we may scale the original variables (x, h) to $(x/h, 1)$. This change of variables just multiplies the inner product $\mathcal{A}$ by $1/h$, and thus does not affect the angle we are studying. Also, the functions ϕ_i will transform to $\tilde{\phi}_i$, which are assumed independent of t and h. Now, suppose the assertion of the theorem is not true. Then there is a sequence

$\{t^k, \underline{U}^{0,k}, \underline{U}^{2,k}\}_{k=1}^{\infty}$ such that $|||\underline{U}^{0,k}||| = |||\underline{U}^{2,k}||| = 1$ and $\lim_{k\to\infty} \mathcal{A}(\underline{U}^{0,k}, \underline{U}^{2,k}) = 1$, that is, $\lim_{k\to\infty} |||\underline{U}^{0,k} - \underline{U}^{2,k}||| = 0$. It is clear that this condition also implies $\lim_{k\to\infty} ||\varepsilon_{ij}(\underline{U}^{0,k} - \underline{U}^{2,k})||_\Omega = 0$ separately for all the strains ε_{ij}. To simplify the notation, we will drop the superscript k in the remaining part of the proof (the limit will always mean $k \to \infty$). We use the following inner product and norm symbols.

$$\begin{aligned} (u, v)_x &= \int_{-h/2}^{h/2} u \cdot v \, \mathrm{d}x \ , \ \ ||u||_x^2 \ = \ (u, u)_x, \\ (u, v)_\Omega &= \int_\Omega u \cdot v \, \mathrm{d}x \, \mathrm{d}z \ , \ \ ||u||_\Omega^2 \ = \ (u, u)_\Omega. \end{aligned}$$

In the membrane case, $\varepsilon_{11} = u_0' + u_2' z^2$. By the assumptions made on the spaces $\mathcal{U}^0$ and $\mathcal{U}^2$, it is easy to see that $\left(\varepsilon_{11}(\underline{U}^0), \varepsilon_{11}(\underline{U}^2)\right)_\Omega = 0$, which gives us by the previous analysis $||\varepsilon_{11}(\underline{U}^i)||_\Omega \to 0$ for both $i = 0, 2$. Next, as $\varepsilon_{33} = w_1$, we must have $\sqrt{t}||w_1^0 - w_1^2||_x \to 0$. However, as the spaces $\mathcal{U}^i$ are finite dimensional and $\mathcal{U}^0 \cap \mathcal{U}^2 = \{\underline{0}\}$, this implies $\sqrt{t}||w_1^i||_x \to 0$ for $i = 0, 2$, that is, $||\varepsilon_{33}(\underline{U}^i)||_\Omega \to 0$. Finally, we have $\varepsilon_{13} = (u_2 + w_1'/2)z$. By the assumptions made it is easy to see that we have $||\,(w_1^i)'\,||_x \leq C||w_1^i||_x$ for $i = 0, 2$ where C is independent of t. Then since $\sqrt{t}||w_1^i||_x \to 0$, we conclude that

$$\frac{t^3}{12}||u_2^0 - u_2^2||_x^2 \to 0.$$

By the argument used above for ε_{33}, this implies $||\varepsilon_{13}(\underline{U}^i)||_\Omega \to 0$ for $i = 0, 2$. But then $|||\underline{U}^i||| \to 0$, a contradiction since we assumed $|||\underline{U}^i||| = 1$. $\square$

In the bending case, we have to add some additional constraints to the space $\mathcal{U}^2$ in order to get t-independent estimates. Indeed, just observe that the example field $\underline{U}^2$ given in the proof of Theorem 4.3 satisfies $\underline{U}^2(x, z) = \tilde{\underline{U}}^2(x/h, z)$ with $\tilde{\underline{U}}^2$ independent of t and h. Sufficient constraints that guarantee t-independent estimates will be given in the next theorem. It turns out that while restricting the space $\mathcal{U}^2$ we may simultaneously loosen the space $\mathcal{U}^0$ by adding some new degrees of freedom here.

Theorem 4.5 *Consider the bending case with*

$$\mathcal{U}^0 = \left\{\underline{U} \in \mathcal{U}^{2D.2} \,|\, u_1, w_2 \in \mathcal{P}^2(-h/2, h/2),\ w_0 \in \mathcal{P}^3(-h/2, h/2) \ \mathit{in}\ (4.16)\right\}$$

and

$$\mathcal{U}^2 = \{\underline{U} \in \mathcal{U}^{2D.2} \quad | \quad u_0, w_1, u_2 \text{ in (4.16) are of the form } \sum_{i=1}^{N} a_i\phi_i(x),$$
$$\text{where } \phi_i(\pm h/2) = 0, \text{ and}$$
$$\int_{-h/2}^{h/2} u_1 \ dx = \int_{-h/2}^{h/2} w_2 \ dx = \int_{-h/2}^{h/2} (u_1 + w_0')x \ dx$$
$$= \int_{-h/2}^{h/2} (u_1 + w_0')x^2 \ dx = 0\},$$

where the (fixed) basis functions ϕ_i are independent of t and depend on h as $\phi_i(x) = \tilde{\phi}_i(x/h)$, where the $\tilde{\phi}_i$ are h-independent functions defined on $(-1/2, 1/2)$. Then $K < \infty$ is independent of t and h.

Proof. We use the same notation as in the membrane case and again argue by contradiction. In the bending case, $\varepsilon_{11} = u_1'z$, so we have also in this case $(\varepsilon_{11}(\underline{U}^0), \varepsilon_{11}(\underline{U}^2))_\Omega = 0$ implying $||\varepsilon_{11}(\underline{U}^i)||_\Omega \to 0$. By the same reasoning as in the membrane case, $\varepsilon_{33} = 2w_2z$ implies $t^{3/2}||w_2^i|| \to 0$, that is, $||\varepsilon_{33}(\underline{U}^i)||_\Omega \to 0$. Finally, as $\varepsilon_{13} = u_1 + w_0' + {w_2}'z^2$, we obtain

$$\begin{aligned}
||\varepsilon_{13}(\underline{U}^0 - \underline{U}^2)||_\Omega^2 \ \geq \ & t||(u_1^0 + (w_0^0)') - (u_1^2 + (w_0^2)')||_x^2 + \frac{t^5}{80}||\,(w_2^0)' - (w_2^2)'\,||_x^2 \\
& -\frac{t^3}{12}||(u_1^0 + (w_0^0)') - (u_1^2 + (w_0^2)')||_x||\,(w_2^0)' - (w_2^2)'\,||_x \\
\geq \ & \frac{3t}{4}||(u_1^0 + (w_0^0)') - (u_1^2 + (w_0^2)')||_x^2 + \frac{t^5}{180}||\,(w_2^0)' - (w_2^2)'\,||_x^2,
\end{aligned}$$

from which we may conclude that both terms of the last row must approach zero. But as the constrains in spaces $\mathcal{U}^0$ and $\mathcal{U}^2$ imply

$$\int_{-1/2}^{1/2} (u_1^0 + (w_0^0)')\,(u_1^2 + (w_0^2)')\ \mathrm{d}x = \int_{-1/2}^{1/2} (w_2^0)'\ (w_2^2)'\ \mathrm{d}x = 0,$$

we conclude that also $||\varepsilon_{13}(\underline{U}^i)||_\Omega \to 0$ for $i = 0, 2$, which is a contradiction. $\square$

We note that the conditions for the space $\mathcal{U}^2$ may always be satisfied by adding a suitable combination of bubbles from the space $\mathcal{U}^0$ as additioned degrees of freedom of space $\mathcal{U}^2$. Thus it is actually sufficient that the space $\mathcal{U}^0$ is as given in the theorem and $\mathcal{U}^2$ is any sufficiently large finite dimensional space (based on some functions $\tilde{\phi}_i$).

4.3 Numerical Experiments in 2D

We study here some examples illustrating both the Energy Principle (Theorem 2.1) and the Complementary Energy Principle (Corollary 2.1) in case of the elastic strip. In the numerical computations, we have chosen $\nu = 1/3$, $\gamma = \nu/(1-\nu)$ (corresponding to a plane stress state) and we let t vary from 10^{-1} to 10^{-5}. Furthermore, we choose $H = 1$ and discretize the $[-1/2, 1/2]$ using 12 elements. First we have splitted the interval $[-1/2, 1/2]$ to 10 subintervals using uniform subdivision, and then added one element of length $h = t$ at both ends of the strip. The small elements at the ends are designed so as to capture the main part of the boundary layer present in this problem. We assume the $2D.2$-model and consider two different loads, one leading to a membrane state and the other to a bending state.

1. In the membrane case we choose the load functional so that it corresponds to the stress conditions $\tau_{33}(\cdot, \pm t/2) = 1$, $\tau_{13}(\cdot, \pm t/2) = 0$. The approximate solution $\underline{U}^1$ (the error of which is estimated) is computed using the piecewise linear finite element method within the $2D.2$-model.

2. In the bending case we choose the load so that it corresponds to the boundary conditions $\tau_{33}(\cdot, \pm t/2) = \pm 1$, $\tau_{13}(\cdot, \pm t/2) = 0$. In this case we study finite element methods of three different orders (p), with the space $\mathcal{U}^1$ consisting of either piecewise linear $(p = 1)$, quadratic $(p = 2)$ or quartic $(p = 4)$ polynomials in x. (The $2D.2$-model is again assumed.)

Let us now shortly discuss the procedures used for the evaluation of the Energy and Complementary Energy Principles.

1. Concerning the Energy Principle, we have chosen $\mathcal{U}$ to consist of polynomials of degree $p+2$ in the x-direction. In addition, we have raised the model order in $\mathcal{U}$ from $n = 2$ to $n = 4$ locally on each subinterval by adding polynomial bubbles (= polynomials vanishing at the end points) of the form $\phi(x)z^3$ and $\phi(x)z^4$ (with ϕ of degree $p+2$ at most). Note that with this choice, $\underline{U} \in \mathcal{U}$ is still only quadratic in z at the grid points, so we are not truly comparing with the $2D.4$-model. Indeed if we added the continuous piecewise linear parts to the higher-order terms as well, problem (2.3) would become non-local and hence impractical for adaptive applications. In each of the cases, we will use choice 2 of section 3.1, thus the space $\mathcal{U}^0$ will be spanned by the continuous piecewise linear basis functions only and the space $\mathcal{U}^2$ by the local bubble functions completing the linear space $\mathcal{U}^0$ to the total space $\mathcal{U}$. In the figures

we will show the relative lower error bound $EP := |||\underline{U}^2|||^2/|||\underline{U}^{2D}|||^2$ as given by the Energy Principle (Theorem 2.1).

2. Concerning the Complementary Energy Principle, we have applied the procedure of section 3.2 as follows.

   (a) The auxiliary stress field $\underline{\underline{\sigma}}^*$ in (3.12) is constructed as a linear combination of piecewise polynomials of order p in the x-direction and of order 2 in the z-direction. Condition (3.11) then holds, as is easily checked.

   (b) The local stress field component σ_{13} is first chosen to be an arbitrary polynomial of degree $p+2$ in the x-direction and of degree 4 in the z-direction. Within this choice, the stress components σ_{ii}, $i = 1, 3$, are then determined from the Euler equations (4.15), up to arbitrary integration constants. Finally, the local (stress) boundary conditions as implied by the conditions of the original problem and by the auxiliary stress field $\underline{\underline{\sigma}}^*$ are imposed by the method of Lagrange multipliers. Finally, the degrees of freedom that are left free are determined by minimizing $|||\underline{\underline{\sigma}}|||$.

   In the figures we show the relative upper error bound $CEP := (|||\underline{\underline{\sigma}}|||^2 - |||\underline{U}^1|||^2)/|||\underline{U}^{2D}|||^2$, as given by the Complementary Energy Principle (Corollary 2.1).

For comparison, we also show the true relative error $E := |||\underline{U}^{2D} - \underline{U}^1|||^2/|||\underline{U}^{2D}|||^2$. As the "true" solution $\underline{U}^{2D}$ we have used a high-order FE approximation of the solution corresponding to $2D.n$-model with $n = 6$. By the two energy principles, the relation $EP \leq E \leq CEP$ will always hold. All the pictures are shown again in a $(\log_{10} \cdot, -\log_{10} t)$ scale.

The membrane case is numerically easy. From Fig. 2 we see that the finite element solution computed with linear elements ($p = 1$) is converging to the true solution as $t \to 0$, with rate $E \sim t$. By Theorem 4.4, K is independent of t in the membrane case already with linear elements. This is confirmed by Fig. 2 which shows that also $EP \sim t$. As we see, EP gives an excellent error estimate in this case. Also CEP behaves like $CEP \sim t$ giving a reasonable upper bound for the error in the case studied.

The bending case is numerically more demanding. With linear elements (Fig. 3) the finite element method locks so that the relative error $E \to 1$ as $t \to 0$. By Theorem 4.3 we have in this case $K = \mathcal{O}(1 + \frac{h^2}{t^2})$. This is also what we see from the picture: $E/EP \sim t^{-2}$. The upper bound for the error given by CEP finds the right t-behavior of the solution in this case (we note that although we always know that $E \leq 1$ in the finite element method, it is in general not guaranteed that also $CEP \leq 1$).

When we raise the degree of the elements to be quadratic (Fig. 4), we get rid of the locking problem in the bending case. We also note that EP gives a t-independent estimate already in this case, although in the general case it is guaranteed by Theorem 4.5 only at $p \geq 3$. CEP gives an excellent upper bound for the error in this case.

The case $p = 3$ behaves qualitatively as the case $p = 2$. With $p = 4$ (Fig. 5) we see that the finite element solution converges to the true one as $t \to 0$. The convergence rate here is $E \sim t$. As predicted by Theorem 4.5, we have $EP \sim E$ independently of t. Also CEP is able to follow the right convergence rate, although the estimate given by EP is quantitatively better in this case.

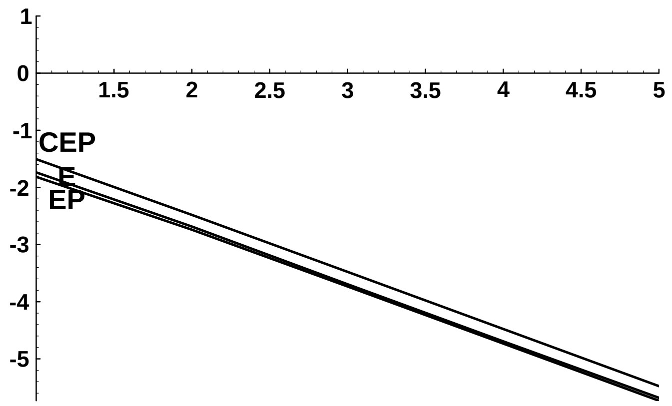

Figure 2: The Membrane Case. $p = 1$ (linear elements).

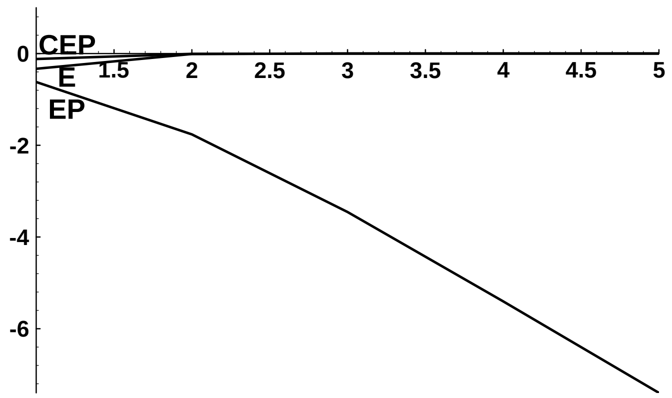

Figure 3: The Bending Case. $p = 1$ (linear elements).

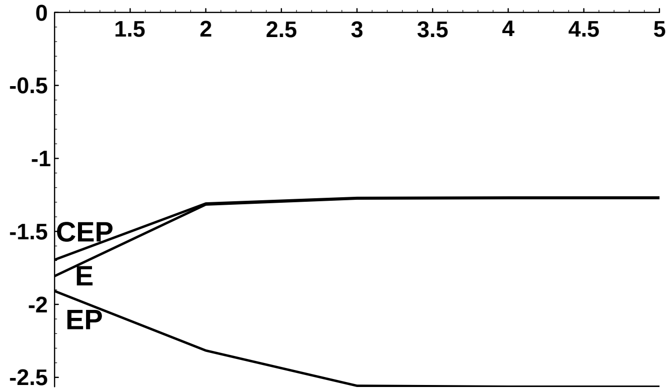

Figure 4: The Bending Case. $p = 2$ (quadratic elements).

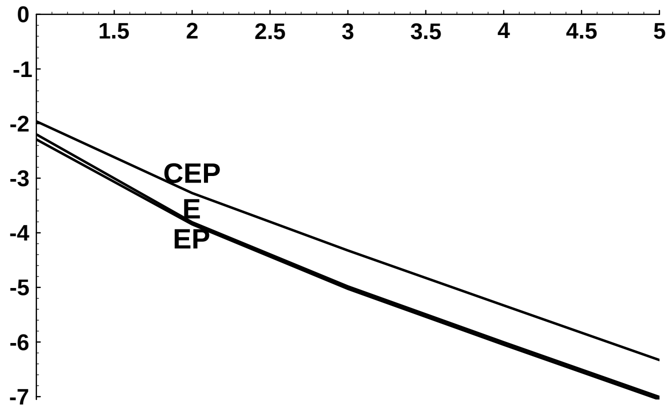

Figure 5: The Bending Case. $p = 4$ (quartic elements).

A Complementary Fields for Theorem 4.3

Notation:

$$I^x[f(x,z)] = \int_0^x f(x',z)\ \mathrm{d}x'\ ,\ I^z[f(x,z)] = \int_0^z f(x,z')\ \mathrm{d}z'$$

The Membrane case:

i	τ_{11}	τ_{13}	τ_{33}
1	1	0	0
2	$-I^x[\tau_{13,z}]$	$-I^x[\tau_{33,z}]$	$(4z^2-t^2)^2 x\cosh(x/t)$
3	$-I^x[\tau_{13,z}]$	$(4z^2-t^2)z\cosh(x/t)$	$-I^z[\tau_{13,x}] - t^3\sinh(x/t)/16$
4	$-I^x[\tau_{13,z}]$	$-I^x[\tau_{33,z}]$	$(4z^2-t^2)^2 z^2\cosh(x/t)$
5	$-I^x[\tau_{13,z}] + t^2(12z^2-t^2)$	$(4z^2-t^2)xz\cosh(x/t)$	$-I^z[\tau_{13,x}]$

The Bending case:

i	τ_{11}	τ_{13}	τ_{33}
1	z	0	0
2	$-8xz$	$4z^2-t^2$	0
3	$-I^x[\tau_{13,z}]$	$-I^x[\tau_{33,z}]$	$(4z^2-t^2)^2 z\cosh(x/t)$
4	$-I^x[\tau_{13,z}]$	$-I^x[\tau_{33,z}]$	$(4z^2-t^2)^2 xz\cosh(x/t)$
5	$2xz - 16xz^3/t^2$	$(4z^2-t^2)z^2/t^2$	0

References

[1] ACHCHAB, B. AND MAITRE, J. F., *Estimate of the Constant in Two Strengthened C.B.S. Inequalities for F.E.M. Systems of 2D Elasticity: Application to Multilevel Methods and a Posteriori Error Estimators*, Numer. Linear Algebra Appl. 3, No. 2, 147-159 (1996).

[2] AINSWORTH, M., ODEN, J. T, AND WU, W., *A Posteriori Error Estimation for $h-p$ Approximations in Elastostatics*, Appl. Numer. Math. 14, No. 1-3, 23-54 (1994).

[3] BABUŠKA, I., DURAN, R. AND RODRIGUEZ, R., *Analysis of the Efficiency of an a Posteriori Error Estimator for Linear Triangular Finite Elements*, SIAM J. Numer. Anal. 29, No. 4, 947-964 (1992).

[4] BABUŠKA, I., KELLY D. W., DE S GAGO, J. P. AND ZIENCIEWICZ, O. C., *A Posteriori Error Analysis and Adaptive Processes in the Finite Element Method - Part I. Error Analysis*, Int. J. Numer. Methods Engrg 19 (1983) 1593-1619.

[5] BABUŠKA, I. AND MILLER, A., *A-Posteriori Error Estimates and Adaptive Techniques for the Finite Element Method*, Techn. Rep. BN968, University of Maryland, Inst. for Phys. Sci. and Technol., 1981.

[6] BABUŠKA, I. AND MILLER, A., *A Feedback Finite Element Method with a Posteriori Error Estimation. I: The Finite Element Method and Some Basic Properties of the a Posteriori Error Estimator*, Comput. Methods Appl. Mech. Eng. (to appear).

[7] BABUŠKA, I., STROUBOULIS, T., UPADHYAY, C. S., GANGARAJ, S. K. AND COPPS, K., *Validation of a Posteriori Error Estimators by Numerical Approach*, Int. J. Numer. Methods Eng. 37, No. 7, 1073-1123 (1994).

[8] BÄHMANN, P. L. , SHEPHARD M. S. AND FLAHERTY, J. E., *A Posteriori Error Estimation for Triangular and Tetrahedral Quadratic Elements Using Interior Residuals*, Int. J. Numer. Methods Eng. 34, No. 3, 979-996 (1992).

[9] BECKERS, P., ZHONG, H. AND MAUNDER, E., *Numerical Comparison of Several a Posteriori Error Estimators for 2D Stress Analysis*, Rev. Eur. Elem. Finis 2, No. 2, 155-178 (1993).

[10] ERIKSON, K. AND JOHNSON, C., *An Adaptive Finite Element Method for Linear Elliptic Problems*, Math. Comp. 50 (1988), pp. 361-383.

[11] ERIKSON, K. AND JOHNSON, C., *Adaptive Finite Element Methods for Parabolic Problems I: A Linear Model Problem*, SIAM J. Numer. Anal. 28 (1991), pp. 43-77.

[12] KELLY, D. W. AND ISLES, J. D., *Procedures for Residual Equilibration and Local Error Estimation in the Finite Element Method*, Commun. Appl. Numer. Methods 5, No. 8, 497-505 (1989).

[13] MUECKE, R. AND WHITEMAN, J. R., *A Posteriori Error Estimates and Adaptivity for Finite Element Solutions in Finite Elasticity*, Int. J. Numer. Methods Eng. 38, No. 5, 775-795 (1995).

[14] NORDGREN, R. P., *A Bound on the Error in Plate Theory*, Quart. Applied Mathematics, 28 (1971) pp. 587-595.

[15] ODEN, J. AND CHO, J. R., *Local A Posteriori Error Estimation of Hierarchical Models for Plate- and Shell-Like Structures*, Texas Insitute for Computational and Applied Mathematics, The University of Texas at Austin, TX 78712 (1995).

[16] OVASKAINEN, O. AND PITKÄRANTA, J., *An Energy Method Approach to the Problem of Elastic Strip*, to appear in SIAM J. Math. Anal.

[17] OVASKAINEN, O. AND PITKÄRANTA, J., *An h-p-n Adaptive Finite Element Scheme for Shell Problems*, Advances in Engrg. Software, 26 No. 3 (1996), 201-208.

[18] PITKÄRANTA, J. AND STENBERG, R., *Analysis of Some Mixed Finite Element Methods for Plane Elasticity Equations*, Math. Comput. 41, 399-423 (1983).

[19] PLANK, L., STEIN, E. AND BISCHOFF, D., *Accuracy and Adaptivity in the Numerical Analysis of Thin-Walled Structures*, Comput. Methods Appl. Mech. Eng. 82, No. 1-3, 223-256 (1990).

[20] RIEDER, G., *A Posteriori Dual Bounds for FEM in Elasticity: a Classroom Example*, Z. Angew. Math. Mech. 73, No. 4-5, T389-T391 (1993).

[21] SCHWAB, C. AND WRIGHT, S., *Boundary Layer Approximation in Hierarchical Beam and Plate Models*, Report 92-08, Department of Mathematics, University of Maryland, Baltimore County (1992).

[22] SCHWAB, C., *A-Posteriori Modeling Error Estimation for Hierarchihc Plate Models*, Numer. Math. 74, No. 2, 221-259 (1996).

[23] STEIN, E., RUST, W. AND OHNIMUS, S., *h- and d-Adaptive FE Methods for Two-Dimensional Structural Problems Including Post-Buckling of Shells*, Comp. Meth. in Appl. Mech. and Engrg 101 (1992) pp. 315-354.

[24] VOGELIUS, M. AND BABUSKA, I., *On a Dimensional Reduction Method. III: A Posteriori Error Estimation and an Adaptive Approach*, Math. Comput. 37, 361-384 (1981).

[25] YANG, J. D., KELLY, D. W. AND ISLES, J. D., *A Posteriori Pointwise Upper Bound Error Estimates in the Finite Element Method*, Int. J. Numer. Methods Eng. 36, No. 8, 1279-1298 (1993).

[26] ZENG, L. F. AND WIBERG, N. E., *Adaptive h-p Procedures for High Accuracy Finite Element Analysis of Two-Dimensional Linear Elastic Problems*, Computers & Structures Vol 42, No.6 (1992), pp. 869-886.

[27] ZIENKIEWICZ, O. C. AND ZHU, J. Z., *A Simple Error Estimator and Adaptive Procedure for Practical Engineering Analysis*, Int. J. Numer. Meth. Engrg 24 (1987), pp. 333-357.

[28] ZIENKIEWICZ, O. C., ZHU, J. Z. AND GONG, G., *Effective and Practical h-p Version Adaptive Analysis Procedures for the Finite Element Method*, Int. J. Numer. Meth. Engrg 28 (1989), pp. 879-891.

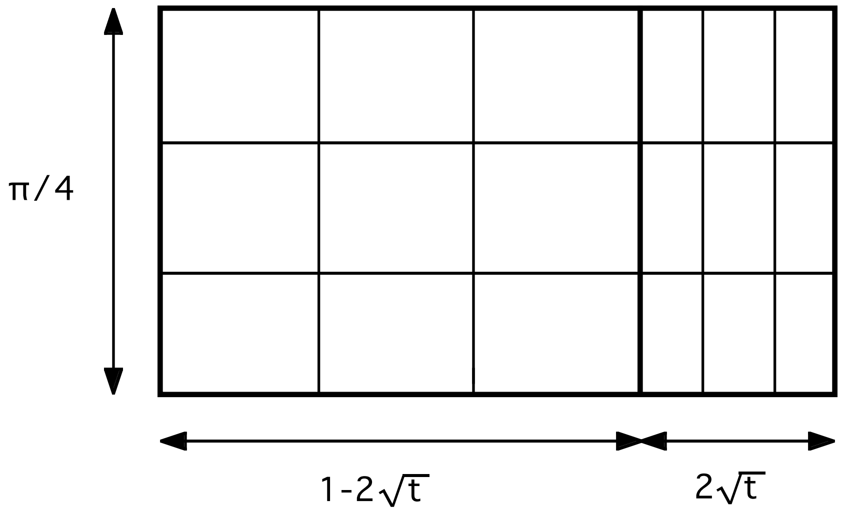

π/4
1-2√t
2√t